5-2017

Co-Optimization of Gas-Electricity Integrated Energy Systems Under Uncertainties

Linquan Bai
University of Tennessee, Knoxville, lbai3@vols.utk.edu

To the Graduate Council:

I am submitting herewith a dissertation written by Linquan Bai entitled "Co-Optimization of Gas-Electricity Integrated Energy Systems Under Uncertainties." I have examined the final electronic copy of this dissertation for form and content and recommend that it be accepted in partial fulfillment of the requirements for the degree of Doctor of Philosophy, with a major in Electrical Engineering.

Fangxing (Fran) Li, Major Professor

We have read this dissertation and recommend its acceptance:

Yilu Liu, Kevin Tomsovic, Mingzhou Jin

Accepted for the Council:
Dixie L. Thompson

Vice Provost and Dean of the Graduate School

(Original signatures are on file with official student records.)

Co-Optimization of Gas-Electricity Integrated Energy Systems Under Uncertainties

A Dissertation Presented for the

Doctor of Philosophy

Degree

The University of Tennessee, Knoxville

Linquan Bai

May 2017

DEDICATION

This dissertation is dedicated to my beloved parents, wife, and son whose love, patience and encouragement make it possible for me to finish my Ph. D. study and this work.

ACKNOWLEDGEMENTS

I would like to express my thanks to those who helped me with various aspects of conducting research and writing this dissertation.

First and foremost, I would like to express my deepest gratitude to my major advisor, Dr. Fangxing (Fran) Li for his continuous guidance and persistent help for this dissertation and all other research works during my Ph.D. study at the University of Tennessee at Knoxville (UTK).

I would like to thank Dr. Yilu Liu, Dr. Kevin Tomsovic, Dr. Mingzhou Jin for their time and efforts in serving as the members of my dissertation committee.

I would like to thank all the professors and friends in the Center for Ultra-Wide-Area Resilient Electric Energy Transmission (CURENT) who create a loving and friendly atmosphere for conducting research.

Last but not least, this dissertation not only represents my work, but it is also a milestone representing four year of works at the University of Tennessee at Knoxville (UTK).

ABSTRACT

In the United States, natural gas-fired generators have gained increasing popularity in recent years due to low fuel cost and emission, as well as the needed large gas reserves. Consequently, it is worthwhile to consider the high interdependency between the gas and electricity networks. In this dissertation, several co-optimization models for the optimal operation and planning of gas-electricity integrated energy systems (IES) are proposed and investigated considering uncertainties from wind power and load demands.

For the coordinated operation of gas-electricity IES: 1) an interval optimization based coordinated operating strategy for the gas-electricity IES is proposed to improve the overall system energy efficiency and optimize the energy flow. The gas and electricity infrastructures are modeled in detail and their operation constraints are fully considered. Then, a demand response program is incorporated into the optimization model, and its effects on the IES operation are investigated. Interval optimization is applied to address wind power uncertainty in IES. 2) a stochastic optimal operating strategy for gas-electricity IES is proposed considering N-1 contingencies in both gas and electricity networks. Since gas pipeline contingencies limit the fuel deliverability to gas-fired units, N-1 contingencies in both gas and electricity networks are considered to ensure that the system operation is able to sustain any possible power transmission or gas pipeline failure. Moreover, wind power uncertainty is addressed by stochastic programming. 3) a robust scheduling model is proposed for gas-electricity IES with uncertain wind power considering both gas and electricity N-1 contingencies. The proposed method is robust against wind power uncertainty to ensure that the system can sustain possible N-1 contingency event of gas pipeline or power transmission. Case studies demonstrate the effectiveness of the proposed models.

For the co-optimization planning of gas-electricity IES: a two-stage robust optimization model is proposed for expansion co-planning of gas-electricity IES. The proposed model is solved by the column and constraint generation (C&CG) algorithm. The locations and capacities of new gas-fired generators, power transmission lines, and gas pipelines are optimally determined, which is robust against the uncertainties from electric and gas load growth as well as wind power.

Keywords: Co-optimization, coordinated operation, expansion planning, gas and electricity integrated energy systems, interval optimization, robust optimization, stochastic optimization.

TABLE OF CONTENTS

CHAPTER 1 Introduction 1

1.1 General Introduction 1

1.2 Dissertation Outline 4

1.3 Contributions 5

CHAPTER 2 Interval Optimization based Operating Strategy for Gas-Electricity Integrated Energy Systems 6

2.1 Introduction 6

2.2 Nomenclature 9

2.3 Gas-Electricity Integrated Energy System Modeling 11

2.3.1 Natural Gas network model 11

2.3.2 Electricity Network Model 14

2.3.3 Incentive Demand Response 16

2.4 Optimization Model for IES Considering Demand Response 18

2.4.1 Deterministic Optimization Model for IES Coordinated Operation 18

2.4.2 Interval optimization model for IES coordinated operation 19

2.5 Case Study and Results 22

2.5.1 Six-bus Electricity Network with Seven-node Natural Gas Network 22

2.5.2 IEEE 118-Bus System with 14-node Gas Network 34

2.6 Conclusions 36

CHAPTER 3 Stochastic Optimal Scheduling for Integrated Energy Systems Considering Gas-Electricity N-1 Contingencies and Wind Power Uncertainty 37

3.1 Introduction 37

3.2 Nomenclature 39

3.3 Nominal IES Operation Considering N-1 Contingencies In Gas and Electricity Networks 42

3.3.1 Deterministic Optimal Scheduling Model for IES 42

3.3.2 Modeling N-1 Contingencies 45

3.3.3 Linearization of the Gas Network Model 48

3.4 Stochastic Optimal Scheduling Model for IES Considering N-1 Contingencies and Wind Uncertainty 49

3.4.1 Stochastic Programming 49

3.4.2 Stochastic Optimization Model of IES Operation 51

3.5 Case Studies 51

3.5.1 Six-bus Electricity Network with Seven-node Gas Network 52

3.5.2 IEEE 118-bus System with 14-node Gas Network 60

3.6 Conclusions 62

CHAPTER 4 Robust Scheduling for Wind Integrated Energy Systems Considering Gas Pipeline and Power Transmission N-1 Contingencies 64

4.1 Introduction 64

4.2 Modeling of Gas Pipeline and Power Transmission N-1 Contingencies in Gas-Electric Networks 65

4.3 Robust Scheduling Model 66

4.4 Case Studies 68

CHAPTER 5 Robust Expansion Co-planning for Integrated Gas and Electricity Energy Systems Considering Wind Power and Load Uncertainties 71
5.1 Introduction 71
5.2 Nomenclature 73
5.3 Linearized Gas Network Model 75
5.3.1 Gas Wells 76
5.3.2 Gas Pipeline 76
5.3.3 Gas Compressor 77
5.3.4 Gas Flow Nodal Balance 77
5.3.5 Linearization of Gas Network Model 77
5.4 Mixed Integer Linear Programming for Expansion Co-planning of IES ... 79
5.5 Two-stage Robust Optimization Model for Expansion Co-planning of IES82
5.6 Solution Methodology 83
5.6.1 Sub-problem 84
5.6.2 Master Problem 85
5.6.3 Column and Constraint Generation Algorithm 86
5.7 Case Studies 87
5.8 Conclusions 91
CHAPTER 6 Conclusion 93
6.1 Main Contributions and Conclusion 93
6.2 Future Research Work 94
LIST OF REFERENCES 96
APPENDIX 115

List of Abbreviations 116

Publications during Ph.D. Study 118

VITA 121

LIST OF TABLES

Table 2.1 Pressure at each node of gas network in Case 0 for 1-24 h 27

Table 2.2 Comparison results of the cases 28

Table 2.3 Electricity DR prices at each load node in Case 1-DR1 30

Table 2.4 Comparison results of the DR cases 31

Table 2.5 Intervals of the operating costs of IES 33

Table 3.1 Comparison of the optimization results of *Case* 1-4 56

Table 3.2 Optimization results of *Scenarios* 1-5 in Case 5 60

Table 3.3 Optimization results of *Scenarios* 1-5 in IEEE 118 bus with 14-node IES 61

Table 3.4 Computational time of Case 1-5 62

Table 4.1 Percentage increase in expected cost under different uncertainty levels with 20% wind power penetration 69

Table 4.2 Percentage increase in expected cost with different wind penetrations under 20% uncertainty level 69

Table 4.3 Computational time of robust model 70

Table 5.1 Load blocks in base year 88

Table 5.2 Candidate power transmission line data 89

Table 5.3 Optimal planning schemes of Case 1-5 in the P6G7IES system 90

Table 5.4 Computational time of Case 1-5 91

LIST OF FIGURES

Figure 2.1 Six-bus electricity network coupled with a seven-node gas network..... 23

Figure 2.2 Wind power forecast data with 20% uncertain interval 24

Figure 2.3 Base electricity load and residential gas load..... 24

Figure 2.4 Optimal output of each unit in Case 0 25

Figure 2.5 Gas production of gas wells in Case 0..... 26

Figure 2.6 Gas volume in gas storage in Case 0 26

Figure 2.7 Power output of Unit 1 in Case 0-3 28

Figure 2.8 Power output of Unit 1 under different DR Cases 29

Figure 2.9 Power output of Unit 1 under different DR cases 30

Figure 2.10 Sensitivity analysis of price elasticity of demand response 32

Figure 2.11 Power output of Unit 1 under 20% wind power uncertainty..... 34

Figure 2.12 System configurations of the IEEE 118-bus with 14-node gas network IES..... 35

Figure 2.13 Operating cost intervals of IES system under 20% wind power uncertainty 35

Figure 3.1 Six-bus electricity network coupled with a seven-node gas network..... 53

Figure 3.2 Wind power forecast..... 53

Figure 3.3 Total electricity load and residential gas load 54

Figure 3.4 Comparison of unit dispatch with and without wind power..... 55

Figure 3.5 Comparison of unit dispatch in Case 1-4 56

Figure 3.6 Power flow of Branch 1-4 in Case 1-4 58

Figure 3.7 Gas flow of Pipeline 2-5 in Case 1-4..... 58

Figure 3.8 Pressures at node 2 in gas network in Case 1-4..... 59

Figure 3.9 Wind power scenarios 60

Figure 3.10 IEEE 118-bus system with 14-node gas network IES..... 61

Figure 5.1 System topology of the P6G7IES system..... 88

CHAPTER 1

INTRODUCTION

1.1 General Introduction

In the United States, natural gas-fired generators have gained increasing popularity in recent years due to low fuel cost and emission, as well as the proven large gas reserves. According to the US Energy Information Administration [1], the natural gas demand in the power industry in 2013 is 8.2 Tcf, which is projected to increase to 9.4 Tcf by 2040 in the reference case. Gas-fired units are expected to be the largest natural gas consumer. Consequently, the interdependency between the gas network and power system is increased dramatically. In this work, the two energy sectors will be combined as the gas-electricity integrated energy system (IES). We focus on studying the co-optimization problems of the gas-electricity IES in the presence of renewable uncertainties.

The gas-electricity coordination problem in terms of planning, scheduling and market is of interest to both industry and academia. Long and medium term planning of gas-electricity integrated energy systems have been studied in [2]. In [2], a detailed gas network model and DC power flow model are used for the expansion planning of gas-electricity integrated energy systems. A long-term co-optimization planning model is proposed in [3] for natural gas and electricity transportation infrastructures with security constraints. In [4], a multi-area and multi-stage expansion planning model of gas-electricity integrated energy systems is introduced with the considerations of natural gas flow limits.

For the coordinated operation of combined gas-electricity networks, studies on the single-time and multi-time period operational optimization were investigated in [5], [6]. As for a single

time period snapshot, a combined natural gas and electricity optimal power flow is presented in [5]. The AC power flow model and steady-state nonlinear gas flow equations are adopted in the optimal power flow model to optimize total social welfare. Similarly, an integrated natural gas and electricity optimal power flow is presented in [6] with the objective of minimizing the sum of generating cost and gas supply cost. Multi-time period optimal operation is discussed in [7]–[11]. In [7], a security constrained unit commitment problem is solved considering the operation constraints of coupling natural gas networks. Based on the concept of energy hub, an optimal power flow framework was studied in [8] with multiple energy carriers. A multi-time period combined gas and electricity network optimization model was developed and demonstrated on the Great Britain network in [9]. A multi-period generalized network flow model of the U.S. integrated energy system was presented in [10] for an integrated energy system including coal network, gas network and electricity network considering the economic interdependencies between the subsystems. And the simulation results were presented in [11].

In today's deregulated electricity and natural gas network, a utility that supplies both electricity and natural gas [12] should take into account the impact of the gas market and electricity market in the economic dispatch of gas-electricity integrated energy systems. The gas-fired generating units generate power to the electricity network and meanwhile consume natural gas provided by the gas network. They participate in both electricity and gas markets. According to electricity and gas prices, gas-fired generators can decide to use the gas and sell electricity in the power market or sell the gas in the gas market rather than producing electricity power [13]. Through the linkage of gas-fired generators, the locational marginal prices (LMP) in the electricity market are tightly interacting with the gas price in the gas market. The impact of natural-gas

network and market on the electricity market is of great interest to independent system operators (ISOs).

In recent years, demand response [14]–[16] attracts much attention for its great potential to integrated energy system operation. In the electricity sector, a lot of work on demand response has been studied in the power system market and operation. Incentive demand response has been proven to be effective in improving system operation. The impact of price-based demand response on market clearing and the LMP of power system has been analyzed in [15]. However, only a few works considered the demand response model in the optimal operation of the combined gas-electricity network. The hourly economic demand response is incorporated in the coordinated stochastic day-ahead scheduling model of power systems with natural gas network constraints [16]. Usually in the electricity network, a DC power flow model is adopted which is a linear system model. But the gas network model is a strong non-convex model that needs to be carefully addressed. From the perspective of the solution algorithm, most existing literatures tend to use heuristic or non-linear optimization techniques for solving the integrated energy system model, which takes a long computational time.

This dissertation proposes various co-optimization models for the gas-electricity IES under uncertainties. The co-optimization models of optimal operation and planning of gas electricity IES are built. In terms of system modeling, the gas network is modeled in detail and linearization technique is studied to linearize the nonconvex models of gas pipelines and gas compressors. The demand response and system contingencies are incorporated into the co-optimization models. Interval optimization, stochastic optimization and robust optimization are applied to solve the proposed models with uncertainties, in terms of solving algorithms. The impact of wind power and load demand uncertainties, power transmission N-1 contingency, gas pipeline N-1 contingency,

and coordinated demand response on the system operation are investigated. Case studies demonstrate the effectiveness of the proposed models. The detailed organization of this dissertation is presented in the following subsection.

1.2 Dissertation Outline

This work focuses on proposing various co-optimization models of gas-electricity IES operation and planning in the presence of various uncertain factors in the integrated energy systems. The interdependency between natural gas and electricity networks is fully considered.

Chapter 2 proposes an interval optimization based coordinated operating strategy for the gas-electricity integrated energy system considering demand response and wind power uncertainty. The gas network is modeled in detail. Then a demand response program is incorporated into the optimization model and its effects on the IES operation are investigated.

Chapter 3 proposes a stochastic optimal operating strategy for gas-electricity integrated energy systems considering N-1 contingencies in both gas and electricity networks, in addition to wind uncertainty.

Chapter 4 proposes a robust scheduling model for wind integrated energy systems with the considerations of both gas pipeline and power transmission N-1 contingencies.

Chapter 5 proposes a two-stage robust expansion co-planning model for gas-electricity integrated energy systems considering the uncertainties of wind power, electric load, and gas load.

Chapter 6 concludes this work and provides suggestions for future work in the co-optimization of gas-electricity integrated energy systems.

1.3 Contributions

The contributions of this work are listed as followed.

- This work proposes an interval optimization based coordinated operating strategy for the gas-electricity integrated energy system considering demand response and wind power uncertainty.
- This work proposes a stochastic optimal operating strategy for gas-electricity integrated energy systems considering N-1 contingencies in both gas and electricity networks, in addition to wind uncertainty.
- This work proposes a robust scheduling model for wind integrated energy systems with the considerations of both gas pipeline and power transmission N-1 contingencies.
- This work proposes a two-stage robust optimization model for expansion co-planning of gas-electricity integrated energy systems considering uncertainties of wind power, electric load and gas load growth.

CHAPTER 2

INTERVAL OPTIMIZATION BASED OPERATING STRATEGY FOR GAS-ELECTRICITY INTEGRATED ENERGY SYSTEMS

2.1 Introduction

Today's power system is evolving towards a modern and clean smart grid with increasing penetration of renewable energy. To address the emerging technologies introduced into modern power systems, tremendous work has been done in the area of wide-area measurement system [17]–[20], voltage stability monitoring and assessment [21]–[24], voltage regulation and control [25]–[29], oscillation study [30]–[32], high-performance computing [33]–[35], wind power generation and control [36]–[39], photovoltaics (PV) generation system control [40]–[43], reactive power optimization [44], [45], demand response and electric vehicle (EV) [46]–[49], energy storage [50]–[55], microgrid operation [56]–[60], smart distribution network operation [61]–[64], communication system [65]–[67], etc. Another important transform that attracts our attention in a broader energy perspective is that power system is increasingly tightly-coupled with natural gas transportation system. It is worthwhile to reveal and investigate the interdependency between the two energy sectors.

In recent years, the interdependency between natural gas and electricity power energy systems are dramatically increasing with more natural gas utilized for electricity generation. In the United States, the natural gas consumption by electric power sector has increased from 32% in 2007 to 39% in 2009 [68]. Gas-fired power plants provide a linkage between natural gas and electricity networks. Compared to traditional coal-fired generators, gas-fired generators are preferred for its competitive fuel cost, lower pollutant emissions and fast response to fluctuating

renewable energy [69]. In New England ISO (ISO-NE), more than 50% of electricity is now generated from natural gas, compared to only 15% in 2000, with even more growth in the use of natural gas-fired generation anticipated going forward [70]. Natural gas transmission could affect the security and the economics of power transmission. For the highly interdependency between the two energy sectors, natural gas and electricity networks are regarded as an integrated energy system (IES) [10].

Extensive research has been conducted to address the coordinated planning and operation in the gas and electricity network. In [2], a combined gas and electricity network expansion planning model is proposed to minimize gas and electricity operational cost and network expansion cost simultaneously. A co-optimization planning model is proposed in [3] considering the long-term interdependency of natural gas and electricity infrastructures under security constraints. A long-term multi-area, multi-stage model integrated expansion planning of electricity and natural gas systems are presented in [4]. As for short-term economic dispatch, an operating strategy is proposed in [71] to coordinate the electricity and natural gas in Great Britain considering the uncertainty in wind power forecasts. The impact of gas network on power security and economic dispatch are investigated in [7], [72], [73]. In [7], [72], integrated optimization model is proposed to incorporate the natural gas network constraints into the optimal solution of security-constrained unit commitment. [73] proposes a security constrained optimal power and natural gas flow under N-1 contingencies.

With the integration of variable and uncertain renewable energy, the coordination of IES is facing new challenges. The uncertainties are not considered in the above model so that a small perturbation in the wind power data may lead to non-optimality or even infeasibility. Stochastic programming [71], [74], [75] and robust optimization [76]–[80] are usually used to deal with wind

uncertainties. Several works have investigated the effect of wind power uncertainty on system operation. In [71], stochastic optimization is adopted in the optimization model to deal with wind power uncertainty, in which a large number of wind forecast scenarios are generated and a scenario reduction algorithm is applied. [74], [75] applied stochastic optimization to the unit commitment problem with a number of wind power scenarios. However, stochastic optimization requires the probability distribution of wind power, which is not easy to be accurately obtained in practice. In addition, it is time consuming to generate a large number of scenarios [76]. A robust optimization approach is proposed in [77] to analyze the interdependency of the IES considering wind power uncertainty. In this work, the wind power uncertainty is actually addressed based on scenario analysis with introducing a penalty coefficient for reducing variance. [76] and [78] applied robust optimization to unit commitment problem considering wind power uncertainty. [79] proposes a look-ahead robust scheduling model for wind-thermal system considering natural gas congestion, but the constraints of the gas pipelines are considered in a simplified manner. Actually, robust optimization is usually considered to be too conservative due to the fact it always tries to find the worst-case scenario solutions which happen at a very low probability. In addition, due to the non-convex constraints of the pipeline and compressor model in the gas network, the robust optimization model for IES becomes difficult to solve.

In this chapter, interval optimization [81], [82] is introduced to address wind power uncertainty, wherein the wind power is represented as interval numbers. In the interval mathematics, all the uncertain information will be maintained in the solving process, which is also easy to implement in engineering applications. The interval optimization minimizes the operating cost interval rather than the worst-case scenarios in robust optimization [81]. Also, it has better computational performance than stochastic optimization [82]. Furthermore, demand response has

been recognized as an effective means to enhance power system operation [83], [84], but few literatures considered demand response in the IES.

Therefore, this work proposes an interval optimization based operating strategy for gas-electricity integrated energy systems considering demand response and wind uncertainty. With the objective of operating cost minimization, the multi-period power and gas flow are optimally determined. The gas and electricity networks are modeled in detail and security operation constraints are imposed. Then an incentive-based demand response program is incorporated into the proposed model and its effects on IES operation are analyzed. With the consideration of wind power uncertainty, the proposed model is solved by interval optimization. Finally, a multi-scenario case study verifies the proposed method.

2.2 Nomenclature

$Q_{w,t}$	Production of gas well *w* at time *t*.
$Q_{w,max}$	Maximum production of gas well *w*.
$Q_{w,\min}$	Minimum production of gas well *w*.
f_{mn}	Gas flow from node *m* to node *n*.
π_m	Pressure of gas node *m*.
C_{mn}	Flow factor of pipeline *m*-*n*.
$H_{j,t}$	Horsepower of compressor *j* at time *t*.
$Q_{d,t}$	Gas load *d* at time *t*.
$Q_{f,t}$	Gas consumption of gas-fired unit *f at t*.
$P_{d,t}$	Electric load *d* at time *t*.
$P_{c,t}$	Power consumption of compressor *c*.
RU_g	Ramp up limit of unit *g*.

RD_g Ramp down limit of unit g.

$P_{l,\max}$ Power flow limit of line j.

$R_{k,t}$ Spinning reserve of unit k at time t.

$Q_{r,t}$ Responsive gas load r at time t.

$C_{g,r,t}$ Incentive price to gas load r at time t.

$K_{g,r}$ Elasticity of gas load r.

φ_g Proportion of gas DR participation.

$\Delta Q_{n,t}$ Unserved gas load n at time t.

$R_{j,\max}$ Maximum compression ratio of j.

$R_{j,\min}$ Minimum compression ratio of j.

$Q_{s,t}$ Capacity of storage s at time t.

$Q_{s,\max}$ Maximum capacity of storage s.

$Q_{s,\min}$ Minimum capacity of storage s.

IR_S Hourly inflow limit of storage s.

OR_S Hourly outflow limit of storage s.

$P_{w,t}$ Wind power w at time t.

$P_{g,t}$ Generator g output at time t.

$P_{g,\max}$ Maximum output of generator g.

$P_{g,\min}$ Minimum output of generator g.

GSF Generation shift factor.

$R_{t,\min}$ Required system reserve at time t.

$P_{r,t}$ Responsive electric demand r at time t.

$K_{e,r}$ Incentive price to electricity load r at t.

$K_{e,r}$ Elasticity of electricity load r.

φ_e Proportion of electric DR participation.

$\Delta P_{i,t}$ Unserved electric load i at time t.

2.3 Gas-Electricity Integrated Energy System Modeling

2.3.1 Natural Gas network model

The natural gas network is composed of gas well, gas pipeline, compressor, gas storage and gas loads. Natural gas is produced at gas wells and transmitted through pipelines propelled by compressors then delivered to the gas load sites. The gas storage provides a buffer to coordinate the usage of gas during multiple periods. The steady state mathematical models of each component are presented below.

2.3.1.1 Gas Wells

Natural gas is injected from gas wells, which are commonly located at remote sites. The gas suppliers are modeled as positive gas injections at the gas well nodes. In each period, upper and lower limits are imposed on the available production of gas suppliers limited by the physical characteristics and long-term, mid-term gas contracts.

$$Q_{w,\min} \le Q_{w,t} \le Q_{w,\max}, w \in A_{GW} \tag{2.1}$$

where $Q_{w,\max}$ and $Q_{w,\min}$ are the maximum and minimum gas supply of gas well w, A_{GW} is the set containing all the gas well.

2.3.1.2 Gas Pipelines

The gas flow through the pipeline is driven by the pressure difference between the two ends of a pipeline. Meanwhile, the physical factors, such as the length, diameter, operating temperature, altitude drop, and the friction of pipelines, also affect the gas flow.

The gas flow from node m to node *n*, f_{mn} (kcf/hr) is expressed as

$$f_{mn} = \text{sgn}(\pi_m, \pi_n) C_{mn} \sqrt{\left|\pi_m^2 - \pi_n^2\right|}$$
$$\text{sgn}(\pi_m, \pi_n) = \begin{cases} 1 & \pi_m \geq \pi_n \\ -1 & \pi_m < \pi_n \end{cases} \quad (2.2)$$

where π_m and π_n are the pressures at node m and n respectively; sgn(π_m,π_n) indicates the direction of the gas flow, when it is 1, the gas flows from node *m* to *n*. C_{mn} is a constant related to the physical characteristic of each pipeline, given by

$$C_{mn} = 3.2387 \frac{T_0}{\pi_0} \sqrt{\frac{D_{mn}^5}{L_{mn} G F_{mn} Z_a T_{mn}}} \quad (2.3)$$

where T_0 is the standard temperature, 520° R; π_0 is the standard pressure, 14.65 psia; D_{mn} is the internal diameters of pipeline between nodes m and n, inch; *G* is the gas specific gravity (air = 1.0, gas = 0.6); F_{mn} is the friction factor of the pipeline; Z_a is the average gas compressibility factor; and T_{mn} is the average gas temperature. According to [5], F_{mn} varies as a function of the diameter D_{mn},

$$F_{mn} = \frac{0.032}{D_{mn}^{1/3}} \quad (2.4)$$

2.3.1.3 Gas Compressors

During the transmission of gas in pipelines, the gas compressor stations are installed to provide pressure for the gas flow to overcome friction. The gas flow from node *m* to node *n* through the compressor *j*, f_{mn} is expressed as

$$f_{mn} = \text{sgn}(\pi_m, \pi_n) \frac{H_j}{k_{j2} - k_{j1} [\frac{\max(\pi_m, \pi_n)}{\min(\pi_m, \pi_n)}]^{\alpha}} \quad (2.5)$$

where k_{j1}, k_{j2}, and α are empirical parameters related to the compressor properties, H_j represents

the power of compressor j, subject to the physical bound of the compressor.

$$H_{j,\min} \le H_j \le H_{j,\max} \tag{2.6}$$

where $H_{j,\max}$ and $H_{j,\min}$ are the maximum and minimum allowed pressure of the compressor.

The compression ratio between the outlet node and inlet node is subject to the following constraint:

$$R_{j,\min} \le \frac{\max(\pi_m, \pi_n)}{\min(\pi_m, \pi_n)} \le R_{j,\max} \tag{2.7}$$

where $R_{j,\max}$, and $R_{j,\min}$ are the maximum and minimum allowed compressor ratio.

The gas compressor must consume horsepower H_j to produce pressure. If the compressor node is coupled with an electricity node, the power will be supplied by the electricity network. In this case, H_j is regarded as an electricity load and will be addressed in the power flow. Otherwise, the compressor will consume natural gas directly from gas flow to provide H_j, expressed as

$$Q_c(H_j) = c_j + b_j H_j + a_j H_j^2 \tag{2.8}$$

where a_j, b_j, and c_j are the coefficients of the gas consumption of the compressor j.

2.3.1.4 Gas Storage

Gas storage facilities provide a buffer to coordinate the gas flow during multi-period horizon. The gas storage level, gas withdrawal and injection amount are subject to the capacity of the storage and in-flow and out-flow rates limit.

$$Q_{s,\min} \le Q_{s,t} \le Q_{s,\max} \tag{2.9}$$

$$-IR_s \le dQ_{s,t} = \left(Q_{s,t} - Q_{s,t-1}\right) \le OR_s \tag{2.10}$$

where $Q_{s,max}$ and $Q_{s,min}$ are the maximum and minimum operating storage capacity. IR_s and OR_s are the inflow and outflow rate limit of the storage.

2.3.1.5 Gas Load

The natural gas load includes residential, commercial and industrial loads. The gas-fired generators are taking an increasing share of the overall gas demand. The gas load could be regarded as negative gas injections at the gas load nodes, denoted as $Q_{d,t}$, $d \in A_{GD}$, A_{GD} is the set of gas load.

2.3.1.6 Gas Flow Nodal Balance

At each node in the gas network, the total natural gas flow injection to a node is equal to zero:

$$\boldsymbol{Q}_{inj} = \boldsymbol{I}_{nw} \cdot \boldsymbol{Q}_w - \boldsymbol{I}_{ns} \cdot d\boldsymbol{Q}_s - \boldsymbol{I}_{nf} \cdot \boldsymbol{Q}_f - \boldsymbol{I}_{nd} \cdot \boldsymbol{Q}_d - \boldsymbol{I}_{np} \boldsymbol{f} - \boldsymbol{I}_{nc} F_c(\boldsymbol{H}_c) = -\boldsymbol{\Delta Q} \qquad (2.11)$$

where $\boldsymbol{I}_{nw}$, $\boldsymbol{I}_{ns}$, $\boldsymbol{I}_{nf}$, $\boldsymbol{I}_{nr}$, $\boldsymbol{I}_{np}$ and $\boldsymbol{I}_{nc}$ are the incidence matrices of gas wells, storages, gas-fired units, gas load, pipe lines and compressors, respectively. $\boldsymbol{\Delta Q}$ is the unserved gas load. Note that each incidence matrix $\boldsymbol{I}$ has a dimension of (number of nodes) by (number of components), while each gas quantity matrix $\boldsymbol{Q}$ has a dimension of (number of components) by (time horizon).

2.3.2 Electricity Network Model

A DC power flow model is adopted in this paper to represent the power flow in electricity network. In the electricity sector, the operation constraints are provided as follows.

1) Power flow nodal injection

$$\boldsymbol{P}_{inj} = \boldsymbol{I}_{lw} \cdot \boldsymbol{P}_w + \boldsymbol{I}_{lg} \cdot \boldsymbol{P}_g - \boldsymbol{I}_{ld} \cdot \boldsymbol{P}_d - \boldsymbol{I}_{lc} \cdot \boldsymbol{P}_c + \boldsymbol{\Delta P} \qquad (2.12)$$

where $\boldsymbol{P}_w$ is wind output, $\boldsymbol{P}_g$ is the thermal generator output (including gas-fired generators), $\boldsymbol{P}_d$ is the electrical load, and $\boldsymbol{P}_c$ is the power consumption of the gas compressor. $\boldsymbol{\Delta P}$ is the potential load shedding.

2) Power generation constraints: the output power of a thermal generator is kept within its physical limits

$$P_{g,\min} \le P_{g,t} \le P_{g,\max} \tag{2.13}$$

where $P_{g,max}$ and $P_{g,min}$ are the maximum and minimum power generation of the thermal unit g.

3) Ramping up and down constraints: the ramping up and down rates of a thermal generator are subjected to its physical limits

$$P_{g,t} - P_{g,t-1} \le RU_g \tag{2.14}$$

$$P_{g,t-1} - P_{g,t} \le RD_i \tag{2.15}$$

where RU_g and RD_g are the maximum ramping up and down rates of the thermal unit g.

4) Power transmission constraints: each transmission line in the electricity network has a maximum capacity. GSF is the generation shift factor with a dimension of (number of lines) by (number of buses), while $\boldsymbol{PL}_{max}$ has a dimension of (number of lines) by (time horizon).

$$-\boldsymbol{P}_{\boldsymbol{L}\max} \le \boldsymbol{GSF} \cdot \boldsymbol{P}_{\boldsymbol{inj}} \le \boldsymbol{P}_{\boldsymbol{L}\max} \tag{2.16}$$

5) Spinning reserve constraints: spinning reserve is needed to maintain the balance between generation and demand at all times. Traditionally, spinning reserve is usually equal to the capacity of the largest generator or a certain percentage of the peak load to address load forecasting errors. Wind power uncertainty is represented by uncertainty bounds, which are actually interval numbers, and addressed by interval mathematics in this paper. The uncertainty of wind power is addressed in the power balancing constraint in (2.12) through interval numbers. For deterministic model, additional spinning reserve is required for the wind power uncertainty. However, in this paper, the impact of wind power uncertainty is addressed through interval numbers. For each specific wind power scenario within the wind power uncertainty bounds, there is a corresponding optimal solution that dispatches the output power of thermal generators.

Thus, the uncertainties of wind forecasts are taken into account implicitly through the interval numbers of wind power [85], [86]. The optimal scheduling of system operation based on the interval mathematics is able to deal with the wind power variations within the uncertainty bounds. Therefore, the spinning reserve in this model only needs to address the load forecasting errors in a traditional way. 10% of the maximum load is set as the spinning reserve requirement to address the load uncertainty.

$$\sum_{k} R_{k,t} \geq R_{t,\min} \tag{2.17}$$

where $R_{k,t}$ is the spinning reserve of thermal unit k at time t, and $R_{t,min}$ is the reserve requirement of the system at time t.

It can be seen that the gas-fired generators serve as the power source in electricity network and natural gas load in gas network meanwhile. So, the gas-fired generators are the components that link the two sectors together. The model of gas-fired generators is represented by a quadratic function of output power with respect to the fuel consumption as expressed in (2.18).

$$P_{g,i}(Q_{ng,i}) = k_{2,i}Q_{ng,i}^2 + k_{1,i}Q_{ng,i} + k_{0,i} \quad \forall i \in N_{NG} \tag{2.18}$$

where N_{NG} is the set of gas network nodes. $k_{2,i}$, $k_{1,i}$, and $k_{0,i}$ are the fuel consumption coefficients of the gas-fired generator i. and $Q_{ng,i}$ is the amount of natural gas supplied to the gas-fired generator i.

2.3.3 Incentive Demand Response

To evaluate the effects of demand response of residential consumers on electricity and natural gas demand, two incentive demand response programs are designed as linear functions with respect to the compensation price provided by utilities. At different nodes, the prices for demand response are different. The incentive prices for gas and electricity loads at each node are

taken as the decision variables in the optimization model, which could provide a reference for the utilities. The response from the consumers is modeled as a linear function of the compensation price. When the compensation is high, more consumers are willing to participate into the demand response.

$$Q_r = f(C_{g,r}) = K_{g,r} \cdot C_{g,r} \tag{2.19}$$

$$P_r = f(C_{e,b}) = K_{e,r} \cdot C_{e,r} \tag{2.20}$$

$$0 \le Q_r \le Q_d \cdot \varphi_g, r \in A_{GDR}, d = L_g(r) \tag{2.21}$$

$$0 \le P_r \le P_d \cdot \varphi_e, r \in A_{EDR}, d = L_e(r) \tag{2.22}$$

where Q_r and P_r are the reduced gas and electric load under the incentive price of $C_{g,r}$ and $C_{e,r}$, respectively. $K_{g,r}$ and $K_{e,r}$ are the corresponding load elasticity. A_{GDR} and A_{EDR} are the set of gas and electric load that participate in demand response programs; $L_g(r)$ and $L_e(r)$ are the corresponding gas and electric load index of the rth DR participant. φ_g and φ_e are the proportion of the gas and electricity load that signed the demand response contract with the utility, assumed to be 10%. In this paper, our focus is to analyze the effects of demand response on the coordinated operation of IES, the models of demand response are designed to be linear. Actually, more accurate models could be adopted but may also need to decompose to piecewise linear functions when the optimization model is solved. With the interactions of demand response, the nodal balance equations of electricity and gas networks are rewritten as

$$\begin{aligned} \boldsymbol{Q}_{inj} = {} & \boldsymbol{I}_{nw} \cdot \boldsymbol{Q}_w - \boldsymbol{I}_{ns} \cdot d\boldsymbol{Q}_s - \boldsymbol{I}_{nf} \cdot \boldsymbol{Q}_f - \boldsymbol{I}_{nd} \cdot \boldsymbol{Q}_d \\ & + \boldsymbol{I}_{nr} \cdot \boldsymbol{Q}_r - \boldsymbol{I}_{np} \boldsymbol{f} - \boldsymbol{I}_{nc} F(\boldsymbol{H}_c) = -\boldsymbol{\Delta Q} \end{aligned} \tag{2.23}$$

$$\boldsymbol{P}_{inj} = \boldsymbol{I}_{lw} \cdot \boldsymbol{P}_w + \boldsymbol{I}_{lg} \cdot \boldsymbol{P}_g - \boldsymbol{I}_{ld} \cdot \boldsymbol{P}_d + \boldsymbol{I}_{lr} \cdot \boldsymbol{P}_r - \boldsymbol{I}_{lc} \cdot \boldsymbol{P}_c - \boldsymbol{I}_{lb} \cdot \boldsymbol{P}_{DR} - \boldsymbol{\Delta P} \tag{2.24}$$

It is worth noting that the utility could implement both electricity and natural gas demand

response coordinately to achieve the overall economic operation of IES.

2.4 Optimization Model for IES Considering Demand Response

2.4.1 Deterministic Optimization Model for IES Coordinated Operation

The total operating costs of the IES include two parts: the costs of electricity network consisting of the generation costs of non-gas power generators, the penalty for unserved power load and costs for electricity demand response; and the costs of the natural gas network consisting of costs of gas production, cost of compressors, and penalty for unserved gas load and cost for gas load demand response. It should be noted that the gas-fired generators are considered as a type of natural-gas load in the gas network. The generation cost of gas-fired generators mainly comes from the fuel cost, which is counted in the production and operation costs of gas network. The objective function of the optimal operation strategy in IES is given by

$$\min_{\boldsymbol{X}} \; J(\boldsymbol{X}) = \sum_{t}\Bigg(\sum_{g} f_g(P_{g,t}) + \lambda_g \sum_{c} Q_c(H_{c,t}) + \sum_{d} \lambda_g Q_{d,t} + \sum_{i} \lambda_{ui}\Delta P_{i,t} + \sum_{n} \lambda_{ug}\Delta Q_{n,t} + \sum_{r} C_{g,r} Q_r + \sum_{r} C_{\mathrm{e},r} P_r \Bigg) \tag{2.25}$$

where $\boldsymbol{X}$ is the control variable set: $\boldsymbol{X}=\{\boldsymbol{P_g}, \boldsymbol{\pi}, \boldsymbol{H}, \boldsymbol{C_{g,r}}, \boldsymbol{C_{e,r}}\}$, including power output of each thermal unit, pressure of each node, horsepower of each compressor, and price of demand response.

Subject to

Gas network constraints (2.1), (2.2), (2.5)-(2.10), (2.18), (2.20), (2.22)

Electricity network constraints (2.13)-(2.17), (2.19), (2.21), (2.24)

where $f_g(P_{g,t})$ is the cost function of all thermal generators. $\Delta P_{i,t}$ is the amount of unserved electricity load; $Q_{d,t}$ is the residential gas demand; $\Delta Q_{n,t}$ is the unserved amount of gas load. λ_{ul} and λ_{ug} are the penalty of unserved electricity and gas load, 1,000 $/MWh, and 200$/kcf, λ_g is the

price for producing each kcf gas, 6.23 $/kcf. The last term is the total cost for paying the demand response program.

2.4.2 Interval optimization model for IES coordinated operation

2.4.2.1 Interval based nonlinear optimization

As one of the effective alternatives to address uncertainties, interval analysis was firstly proposed by Moore [87]. The only available information is lower and upper bounds for inexact parameters. Then interval analysis was extended to interval mathematical programming by Huang [88]. The interval mathematics based optimization is able to address the uncertainties by interval numbers without requirements about accurate probability distribution information. It optimizes the output bounds regarding given input intervals with acceptable computational time. It has already been applied in the boundary estimation of power flow calculation with parameter uncertainty [82]. In this work, interval optimization is introduced to solve the optimal operation problem in gas-electricity IES.

The general mathematic formulation of a nonlinear optimization based on interval analysis is expressed by

$$\begin{aligned} &\min_{\boldsymbol{X}} f(\boldsymbol{X},\boldsymbol{U}) \\ s.t.\quad & g_i(\boldsymbol{X},\boldsymbol{U}) \geq b_i^I = [b_i^-, b_i^+],\ i \in L,\ \boldsymbol{X} \in \Omega^n \\ & \boldsymbol{U} \in \boldsymbol{U}^I = [\boldsymbol{U}^-, \boldsymbol{U}^+],\ U_i \in U_i^I = [U_i^-, U_i^+],\ i \in Q \end{aligned} \tag{2.26}$$

where X is an n-dimensional vector of the decision variables, U is the q-dimensional uncertain vector represented by interval numbers, b_i^I is the interval of the *i*th constraint.

To evaluate the optimal values, an order relation of interval numbers is introduced to compare two intervals [89], in which an index of interval possibility degree is used to indicate the possibility of interval A ≤ B. Then the uncertain constraints can be converted to deterministic

constraints

$$P(g_i^I(\boldsymbol{X}) \le b_i^I) \ge \lambda_i \tag{2.27}$$

where $\lambda_i \in [0,1]$, which is a predefined possibility, and $g_i^I(\boldsymbol{X}) = [g_i^-(\boldsymbol{X}), g_i^+(\boldsymbol{X})]$. Different from interval based linear optimization, this model has to be solved by two optimization process.

$$g_i^-(\boldsymbol{X}) = \min_{\boldsymbol{U}} g_i(\boldsymbol{X}, \boldsymbol{U}),\ \ g_i^+(\boldsymbol{X}) = \max_{\boldsymbol{U}} g_i(\boldsymbol{X}, \boldsymbol{U}) \tag{2.28}$$

Thus, all the uncertainty constraints have been transformed to deterministic constraints.

Next step, the objective function is also needed to be transformed to a deterministic objective function. For the uncertain objective function $f(\boldsymbol{X}, \boldsymbol{U})$, let $f^I(\boldsymbol{X}) = [f^-(\boldsymbol{X}), f^+(\boldsymbol{X})]$ be represented by the mean and width of the interval as $\left\langle f^m(\boldsymbol{X}), f^w(\boldsymbol{X}) \right\rangle$, where

$$\begin{aligned} f^m(\boldsymbol{X}) &= \frac{f^-(\boldsymbol{X}) + f^+(\boldsymbol{X})}{2} \\ f^w(\boldsymbol{X}) &= \frac{f^+(\boldsymbol{X}) - f^-(\boldsymbol{X})}{2} \end{aligned} \tag{2.29}$$

The mean value indicates the expected optimal value and the width denotes the uncertainty level of the optimal solution. In the context of uncertainty, we are trying to find a solution with minimum mean as well as the width. Then the uncertain objective function can be transformed to a deterministic multi-objective function that minimize both the mean and width of the interval objective value,

$$\min_{\boldsymbol{X}} (f^m(\boldsymbol{X}), f^w(\boldsymbol{X})) \tag{2.30}$$

Similarly, two optimization processes are applied to obtain $f^-(\boldsymbol{X})$ and $f^+(\boldsymbol{X})$

$$f^-(\boldsymbol{X}) = \min_{\boldsymbol{U}} f(\boldsymbol{X}, \boldsymbol{U}),\ \ f^+(\boldsymbol{X}) = \max_{\boldsymbol{U}} f(\boldsymbol{X}, \boldsymbol{U}) \tag{2.31}$$

For this deterministic objective function and constraints, a weighting factor β could be applied to solve this multi-objective optimization model, expressed as

$$\min_{\boldsymbol{X}} f(\boldsymbol{X}) = (1-\beta) f^{m}(\boldsymbol{X}) + \beta f^{w}(\boldsymbol{X})$$
$$s.t. \quad (2.27), \quad \boldsymbol{X} \in \Omega^{n} \tag{2.32}$$

The above model can be solved by a two-stage optimization. The upper stage is to search the optimal decision variables. According to the decision variables from the upper stage, the intervals of objective functions and constraints are calculated at the lower stage.

2.4.2.2 Interval optimization model for IES coordinated operation

With the consideration of wind power uncertainty, the interval mathematics is applied to the above deterministic optimization model. The wind power uncertainty is represented by interval numbers, defined by the upper and lower bounds of wind power forecasts.

$$W = \{P_{w,t} | P_{w,t}^{-} \le P_{w,t} \le P_{w,t}^{+}, \forall t \in T\} \tag{2.33}$$

Eq. (2.32) represents the interval numbers of wind power for each time interval during the study period T. The interval numbers are the upper and lower wind power uncertainty bounds that are obtained by wind power forecasting. The wind power forecasting techniques are referred to [90]–[92], which propose statistics methods for determining the interval numbers of wind power prediction. In this paper, we assume that the wind power uncertainty bounds are already obtained based on existing wind power forecasting techniques.

In interval optimization, with regard to the interval input of wind power, the objective value $J(\boldsymbol{X}, \boldsymbol{P}_{wind})$, i.e. the operating cost of the systems is obtained in the form of intervals, denoted as $\Psi = \left[J(\boldsymbol{X})^{-}, J(\boldsymbol{X})^{+} \right]$,

$$J(\boldsymbol{X})^{-} = \min_{\boldsymbol{P}_w \in W} J(\boldsymbol{X}, \boldsymbol{P}_w), \quad J(\boldsymbol{X})^{+} = \max_{\boldsymbol{P}_w \in W} J(\boldsymbol{X}, \boldsymbol{P}_w) \tag{2.34}$$

The objective function of IES optimal operation in (2.24) and the constraints in terms of $\boldsymbol{P}_w$ are represented in the interval form, thus we have the interval based optimization model of IES

optimal operation.

$$\min_{\boldsymbol{X}} \; J(\boldsymbol{X},\ \boldsymbol{P}_{\boldsymbol{wind}}) = \sum_{t}\Bigg(\sum_{g} f_g(P_{g,t}) + \lambda_g \sum_{c} Q_c(H_{c,t}) + \sum_{d} \lambda_g Q_{d,t} + \sum_{i} \lambda_{ui}\Delta P_{i,t} + \sum_{n} \lambda_{ug}\Delta Q_{n,t} + \sum_{r} C_{g,r} Q_r + \sum_{r} C_{\mathrm{e},r} P_r \Bigg) \tag{2.35}$$

$$\boldsymbol{P}_{\boldsymbol{w}} \in W \;\; \Delta P_i = [P_w^-, P_w^+] + P_{g,i} - P_{d,i} - P_{c,i} + P_{r,i} + \Delta P_i \tag{2.36}$$

The constraints in the deterministic model (2.25) will be modified in terms of interval numbers to include the uncertainty wind power interval then this interval based IES coordinated operation can be solved.

It should be noted that, in this work, the ramping limits of thermal and gas-fired generators (2.14)-(2.15) and capacity limits of gas storage (2.10) are involved in the multi-period constraints. The dimension of the optimization problem increases substantially due to the existing coupling between the different sub-periods of time. The optimization model is implemented in MATLAB with YALMIP and BONMIN solver on a PC with Intel Core i7 3.00 GHz CPU and 8 GB RAM.

2.5 Case Study and Results

The effectiveness of the proposed method was evaluated on two systems: a six-bus electricity network with seven-node natural gas network and the IEEE 118-bus with 14-node gas network.

2.5.1 Six-bus Electricity Network with Seven-node Natural Gas Network

A small IES consisting of a six-bus electricity network and a coupled seven-node gas network is depicted in Figure 2.1. In the electricity network, three gas-fired generators are located at node 1, 2 and 6 respectively; three electricity loads are at node 3, 4 and 5; a 70 MW wind turbine (WT) is installed on node 3. In the gas network, two gas wells are at node 6 and 7 respectively,

two residential gas loads are at node 1 and 3; and a compressor is installed on the pipeline between node 2 and 4. A gas storage is located at gas node 1. The two networks are coupled at three gas-fired generators, corresponding to gas load 1, 3, and 5. The detailed parameter data can be found in [93]. The wind power forecast data and its 20% uncertain bounds are shown in Figure 2.2. The multipliers of total electricity and gas load are shown in Figure 2.3. The scheduling horizon is 24 hours. The penalty for electricity load shedding is 1,000 $/MW and 200 $/kcf for gas load shedding.

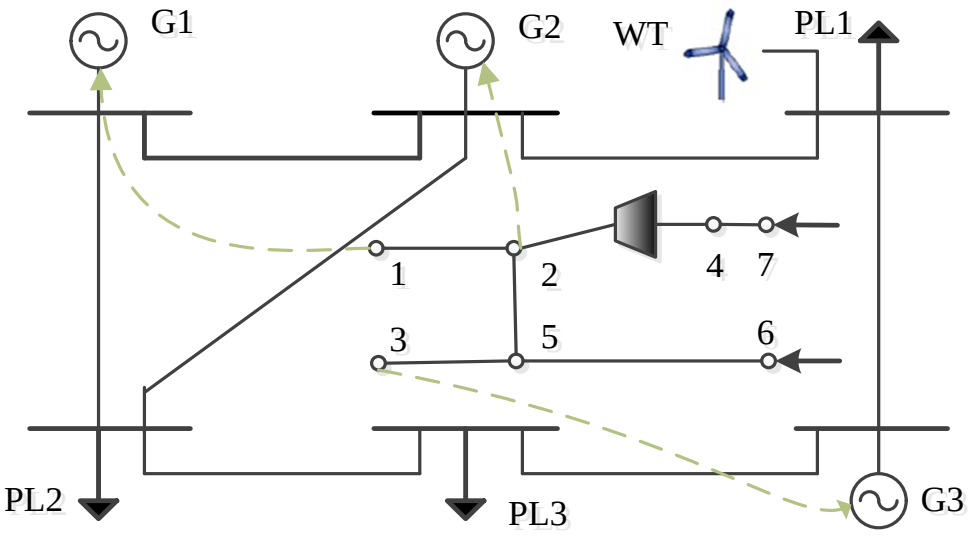

Figure 2.1 Six-bus electricity network coupled with a seven-node gas network

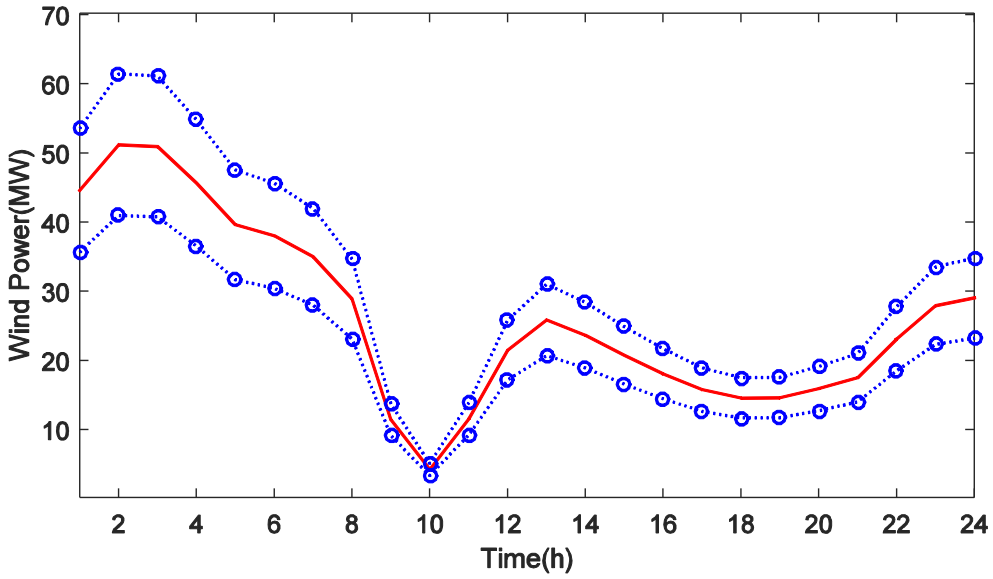

Figure 2.2 Wind power forecast data with 20% uncertain interval

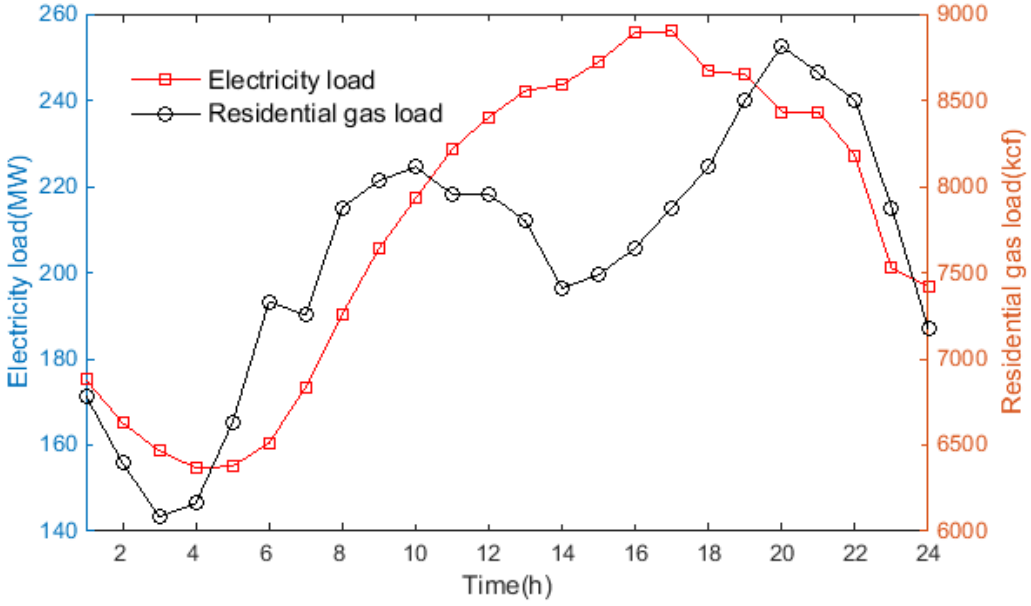

Figure 2.3 Base electricity load and residential gas load

2.5.1.1 Deterministic IES Model

First, the base case with wind forecast and base load data (named Case 0) is solved using the deterministic IES model. The results of power generation scheduling are shown in Figure 2.4, and the pressure at each node of the gas network is shown in Table 2.1. The gas production of gas wells is shown in Figure 2.5. Figure 2.6 shows the gas volume in the gas storage during the scheduling horizon. The storage level at the end of the day will be equal to that at the start of the day. No electricity load or natural gas load is shed. The output of unit 2 and 3 is very low since they are too expensive. By checking other results such as power flow and gas flow results, all the values are within corresponding security constraints of system operation.

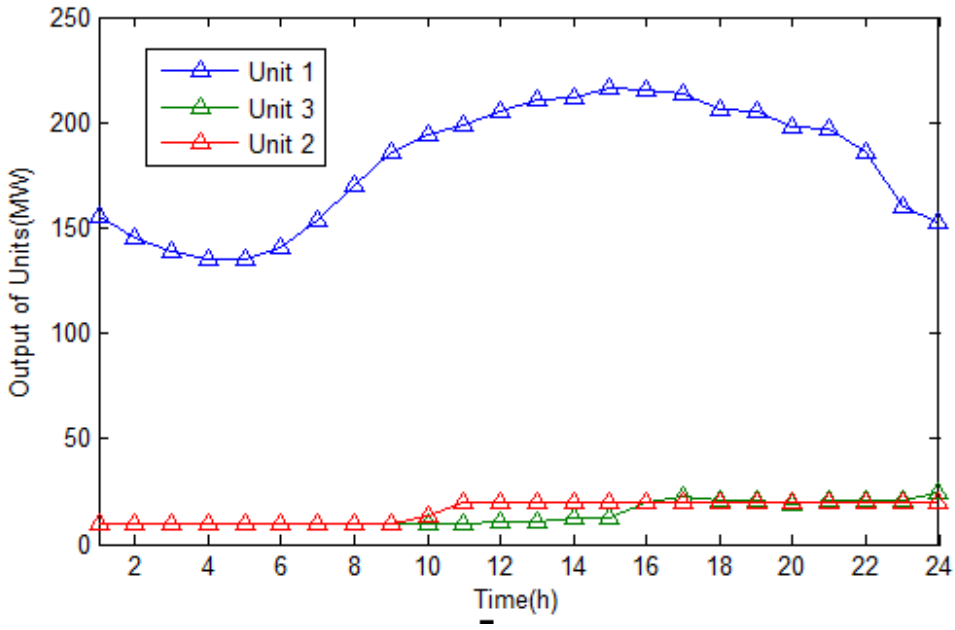

Figure 2.4 Optimal output of each unit in Case 0

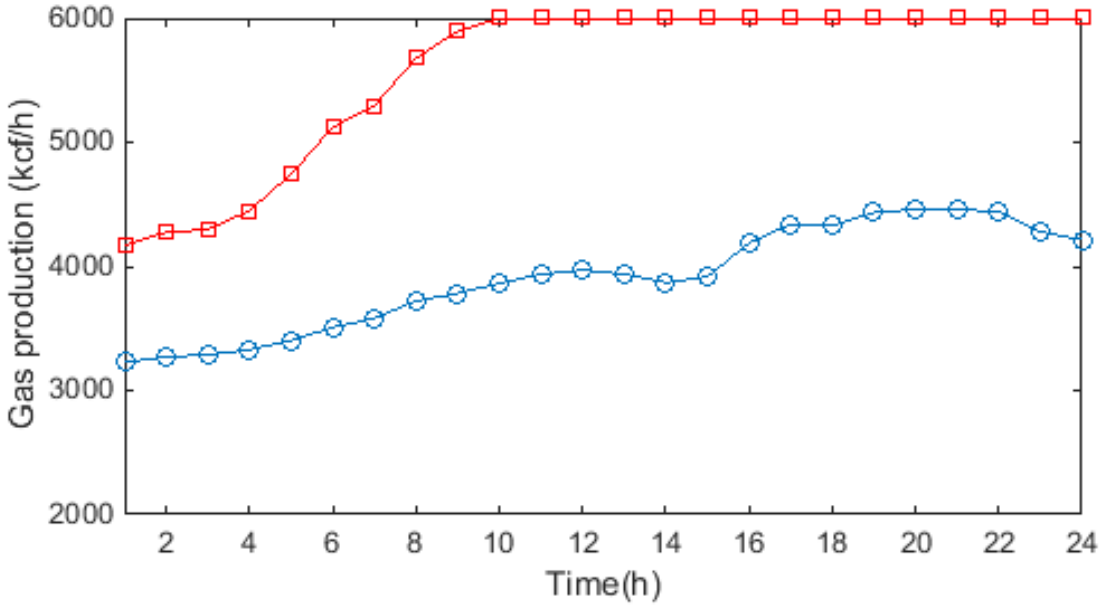

Figure 2.5 Gas production of gas wells in Case 0

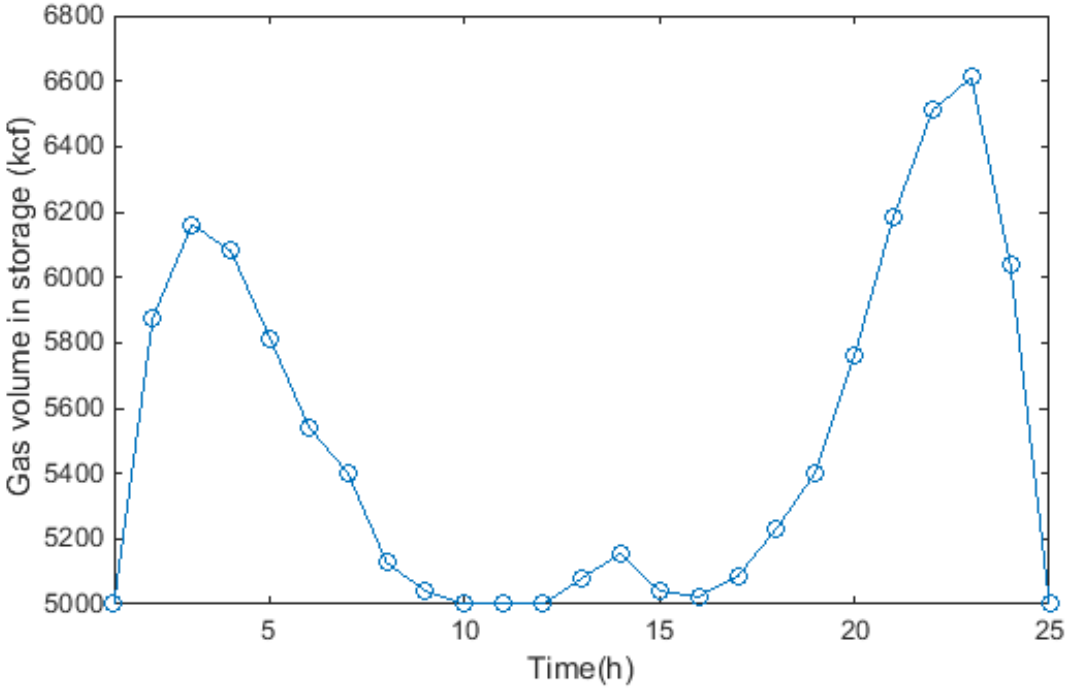

Figure 2.6 Gas volume in gas storage in Case 0

Table 2.1 Pressure at each node of gas network in Case 0 for 1-24 h

π/psia	1	2	3	4	5	6	7	8
Node1	116.23	113.62	112.51	110.98	109	107	105	102.7
Node2	151.05	152.35	153.09	154.33	156	159	162	166.2
Node3	156.16	160.07	162.23	164.74	168	172	177	182.8
Node4	79.39	80.82	81.52	82.87	85.3	89	91	96.08
Node5	161.2	164.45	166.15	168.7	173	177	182	188.6
Node6	182.25	186.27	187.96	191.81	198	207	213	222.7
Node7	102.22	103.88	104.65	106.21	109	113	116	121.5
π/psia	9	10	11	12	13	14	15	16
Node1	101	100	100	100	100	100	100	100
Node2	169	170	170	170	170	170	170	170
Node3	187	188.6	188	188	189	190.4	190	189
Node4	99	100	100	100	100	100	100	100
Node5	193	194.6	194	194	194	195.4	195	195
Node6	229	230.9	229	229	229	230.1	230	229
Node7	124	126.3	127	128	127	126.4	127	130
π/psia	17	18	19	20	21	22	23	24
Node1	100	100	100	100	100	100	100	100
Node2	170	170	170	170	170	170	170	170
Node3	188	187.01	185	184	184	185	188	192
Node4	100	100	100	100	100	100	100	100
Node5	194	193.03	192	191	191	192	194	196
Node6	229	228.14	227	226	227	227	229	231
Node7	132	132.11	134	134	134	134	132	131

To conduct a comparative study, several cases are designed to evaluate the interdependency between electricity and gas network. In Case 1, 2, and 3, the residential gas loads are increased by 20%, 30%, and 50% respectively. The power output of Unit 1 in the above cased are shown in Figure 2.7. And the comparison results of total cost, unserved electricity and gas loads during the scheduling horizon are shown in Table 2.2.

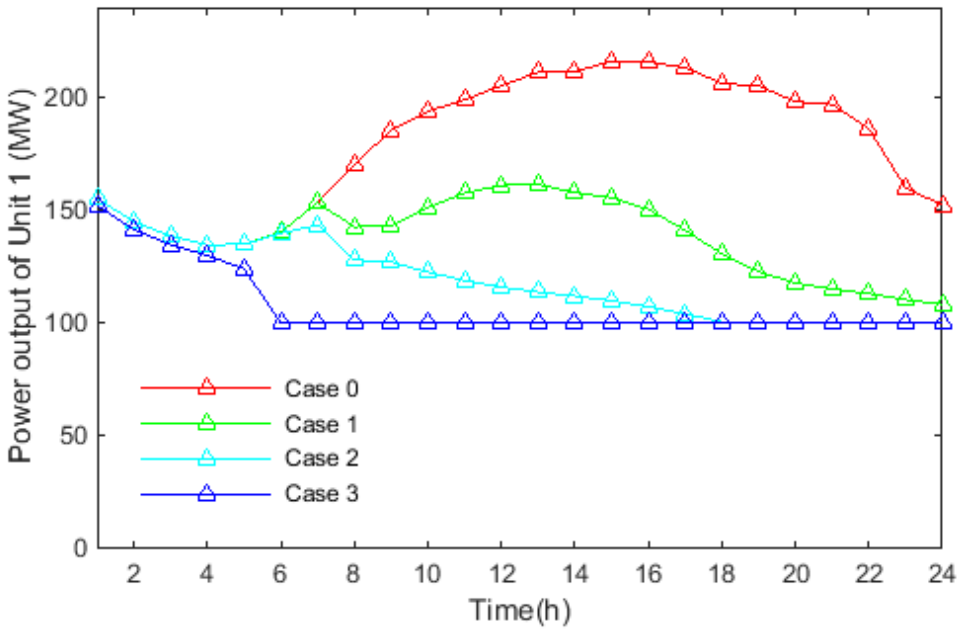

Figure 2.7 Power output of Unit 1 in Case 0-3

Table 2.2 Comparison results of the cases

	Total cost ($)	Total unserved electricity load(MW)	Total unserved gas load(kcf)
Case 0	1435328.02	0	0
Case 1	2197233.20	588.79	0
Case 2	2889961.51	1163.9	461.61
Case 3	5770446.32	1575.9	12578.0

Comparing Case 0 and Case 1, it can be seen that when the gas load increases, at 7th hour, the pressure different between node 1 and node 2 reach the limit. There will be not enough gas

supply for the gas-fired generations, leading to large amount of electricity load shedding. When the gas load increases further, the gas load shedding also occurs. The operating cost increases dramatically with the unserved load amount due to the large penalty for energy imbalance.

2.5.1.2 Deterministic IES Model with Demand Response

The incentive demand response program described in 2.3 is applied to the deterministic IES model. Based on Case 1, three cases with electricity demand response, gas demand response, and gas-electricity demand response are studied, which are denoted as Case 1-DR1, Case 1-DR2, and Case 1-DR3 respectively.

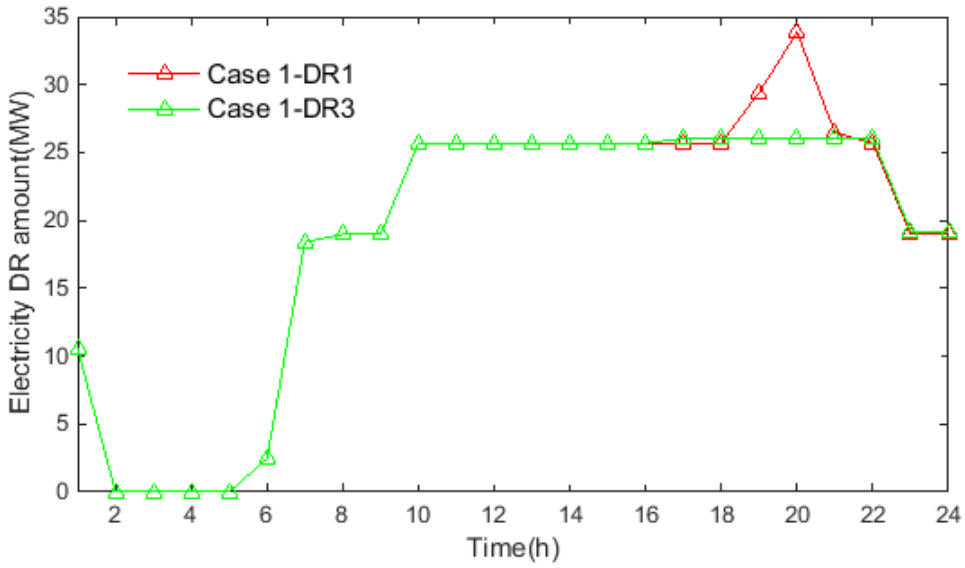

Figure 2.8 Power output of Unit 1 under different DR Cases

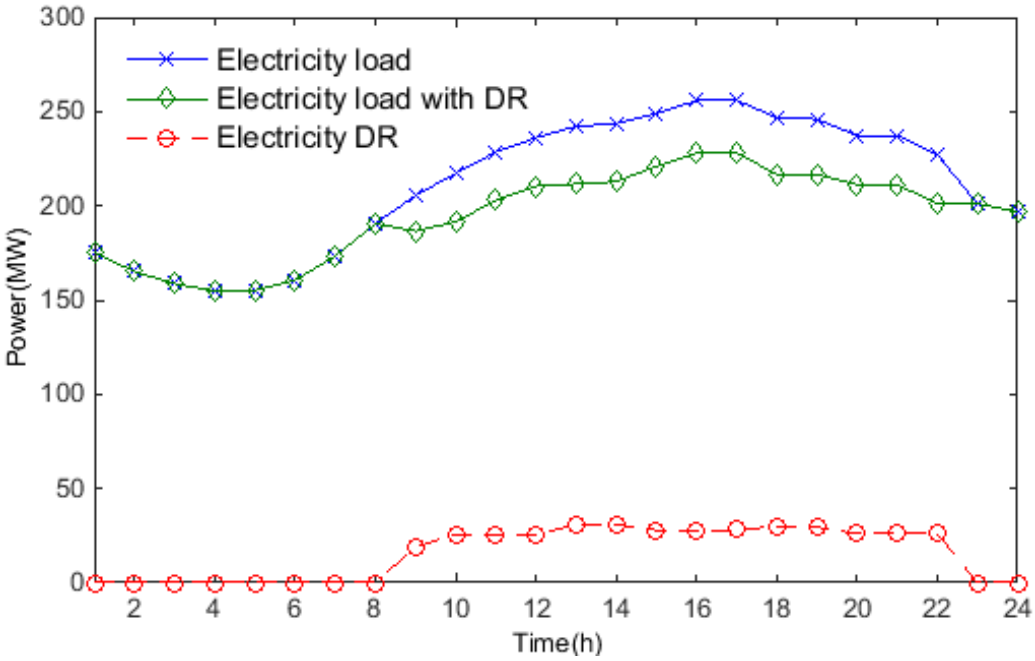

Figure 2.9 Power output of Unit 1 under different DR cases

Table 2.3 Electricity DR prices at each load node in Case 1-DR1

Price($/MW)	1	2	3	4	5	6	7	8	9	10	11	12
Load 1	23.47	0	0	0	0	5.48	41.91	42.15	42.15	54.58	54.59	55.58
Load 2	23.47	0	0	0	0	5.48	41.91	42.15	42.15	60.54	60.54	61.54
Load 3	23.47	0	0	0	0	5.48	41.91	42.15	42.15	59.41	59.41	59.41

Price($/MW)	13	14	15	16	17	18	19	20	21	22	23	24
Load 1	54.58	54.58	55.58	54.58	54.58	54.58	62.54	71.91	56.22	55.28	42.15	42.15
Load 2	60.54	60.54	60.54	60.54	60.54	60.54	69.36	79.75	62.35	62.35	42.15	42.15
Load 3	59.41	59.41	59.41	59.41	59.41	59.41	68.07	78.27	61.19	60.18	42.15	42.15

The results of the above three cases are compared with those of Case 1, shown in Table 2.4.

Table 2.4 Comparison results of the DR cases

	Total cost ($)	Electricity DR cost ($)	Gas DR cost ($)	Operating cost ($)
Case 1	2,197,233.20	-	-	2,197,233.20
Case 1-DR1	1,866,126.23	24,968	-	1,841,158.23
Case 1-DR2	1,588,197.77	-	9,459.2	1,578,739.57
Case 1-DR3	1,562,941.00	23,607	9,400.3	1,529,933.70

From the comparison in Table 2.4, it can be observed that the coordinated gas-electricity DR program achieves better system economy than single electricity DR or natural gas DR. The utilities will gain more profit if they implement a coordinated DR program in the IES.

2.5.1.3 Sensitivity analysis of incentive demand response

A sensitivity analysis of incentive DR with respect to the price elasticity of demand is performed to demonstrate the impact of DR model on system operation. In this study, based on Case 1, the assumption that electricity DR is implemented on PL1 and the gas DR is implemented on gas load node 1 is used for this sensitivity analysis.

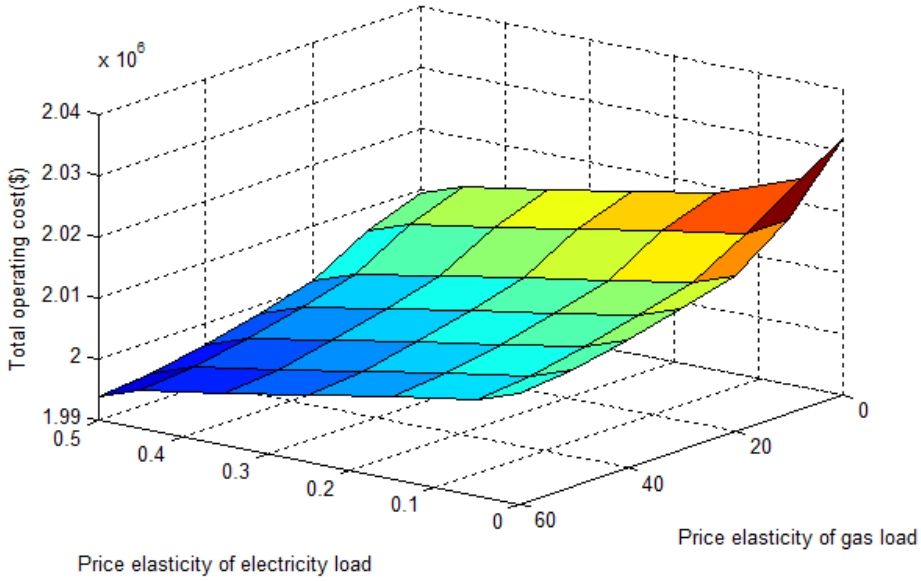

Figure 2.10 Sensitivity analysis of price elasticity of demand response

The total operation costs with respect to the price elasticity variations of the above nodes are shown in Figure 2.10. Denote the price elasticity of electricity load and gas load as K_e and K_g, respectively. It can be observed that when K_e = 0 and K_g = 0, that is, no DR is implemented, the operating cost is very high. With the increase of the elasticity, the total operating cost will decrease. From the viewpoint of a utility, they expect to see more consumers participate in the incentive DR programs. In this way, the price elasticity will be higher and the operating cost will be reduced. However, in real application, the elasticity is closely related to the willingness of the consumers to participate in the incentive DR programs. It should be noted that the scales of price e elasticity of electrical load and gas load are different because electrical load and gas load use different base units MW and kcf, respectively.

2.5.1.4 Interval optimization based IES model with demand response

According to the formulations and algorithms in 2.4.2, the interval optimization is applied to the IES model with DR. 3 different levels of wine power uncertainty are considered based on Case1. 10%, 20% and 30% wind power intervals are considered in Case I1, Case I2, and Case I3 respectively with coordinated gas-electricity DR program. Through solving the optimization model, the intervals of operating cost in the above three cases are summarized in Table 2.5.

Table 2.5 Intervals of the operating costs of IES

Uncertainty level (%)	Maximum costs ($)	Minimum costs ($)
Case 1 (±0%)	1,562,941.00	1,562,941.00
Case I1 (±10%)	1,579,311.65	1,548,089.09
Case I2 (±20%)	1,598,311.05	1,540,999.18
Case I3 (±30%)	1,620,279.62	1,541,541.58

Form Table 2.5, it can be observed that with higher uncertainty level of wind power, the width of the operating cost interval is larger. The interval results will provide the decision with the information that the operating cost will fall in which interval under a certain level of wind power uncertainty. The interval power output scheduling of Unit 1 under 20% wind power uncertainty is shown in Figure 2.11.

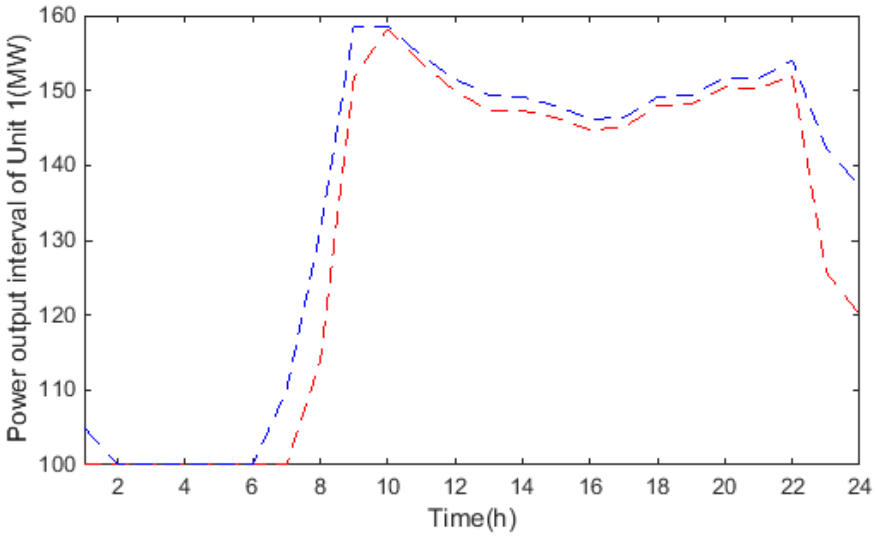

Figure 2.11 Power output of Unit 1 under 20% wind power uncertainty

2.5.2 IEEE 118-Bus System with 14-node Gas Network

In this section, a large gas and electricity IES consisting of a modified IEEE 118-bus system and 14-node gas network [94] is used to demonstrate the performance of the proposed method. In the modified 118-bus system, a total capacity of 1460 MW wind power is distributed on node 12, 17, 56, and 88, electricity DR program is implemented on node 3, 7, 16, 29, 40, 55, 80, 88, 95, and 112; gas demand response is implemented on 3, 5, 10, 11 and 14. The system structure is shown in Figure 2.12.

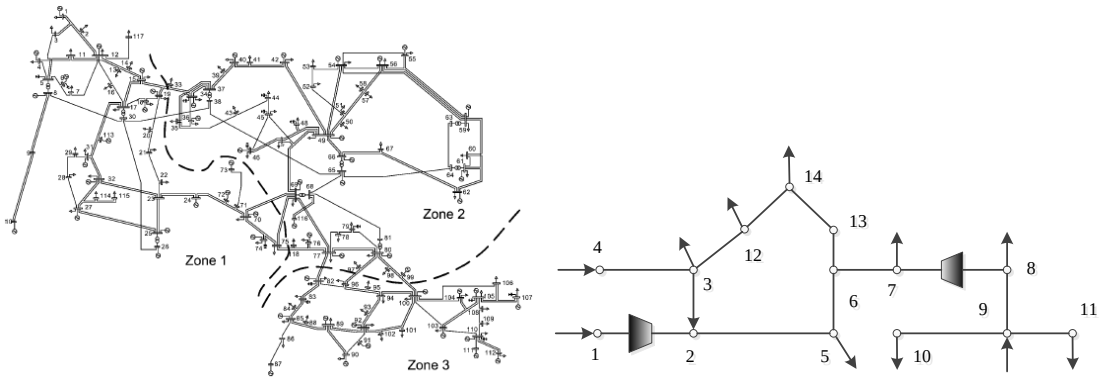

Figure 2.12 System configurations of the IEEE 118-bus with 14-node gas network IES

Using the interval based optimization method in this large IES, the optimal operating cost intervals at each hour under 20% wind power uncertainty are shown in Figure 2.13.

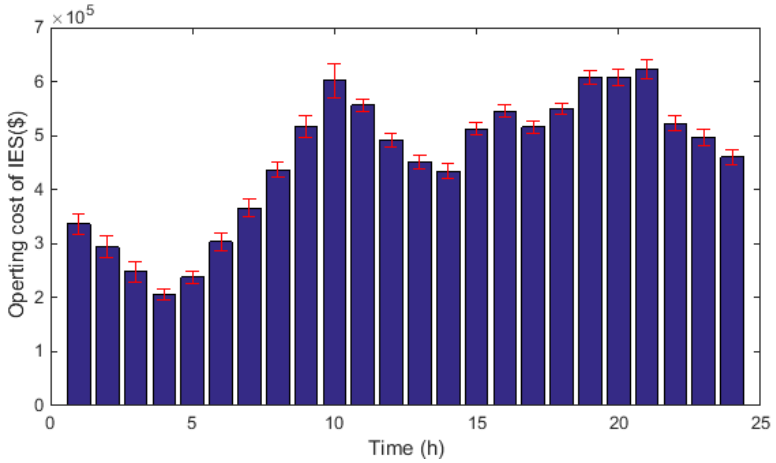

Figure 2.13 Operating cost intervals of IES system under 20% wind power uncertainty

The simulation is carried out using the BONMIN nonlinear optimization solver in YALMIP [95], the computational time of the algorithm on this system is 38.056 seconds, which perfectly satisfies the requirements of practical implementation.

2.6 Conclusions

In this chapter, an interval optimization based operating strategy of gas-electricity IES is proposed to optimally coordinate the operations of the coupled two energy sectors considering demand response and wind power uncertainty. The contributions of this work are summarized as follows:

1) The electricity and gas networks are modeled in details in purpose of coordinated operations within the security constraints of both systems.
2) An incentive demand response program is incorporated into the model that provides utilities with an intelligent compensation prices for electricity and gas demand response. The utility companies could coordinate the peak electricity and gas load through the optimized IES demand response.
3) Interval optimization is applied on the optimization model of IES coordinated operation to address wind power uncertainty.
4) The proposed method is verified by two case studies. The demand response program is proven to be effective in improving the operation efficiency in the IES. The interval optimization provides profit intervals with regarding to the wind power uncertainty levels for the decision makers.

The interval based optimization framework of gas-electricity IES and the demand response program is easy to implement for utilities or ISOs that supply both gas and electricity to customers. The proposed method has a promising value in engineering applications. The uncertainty of demand response can also be represented as interval numbers in the framework, which will be addressed in our future work.

CHAPTER 3

STOCHASTIC OPTIMAL SCHEDULING FOR INTEGRATED ENERGY SYSTEMS CONSIDERING GAS-ELECTRICITY *N*-1 CONTINGENCIES AND WIND POWER UNCERTAINTY

3.1 Introduction

In today's energy system, the interdependency between natural gas and electricity networks has increased dramatically. The natural gas network and wind power could affect the security and economics of power system operation. An optimal operation strategy is necessary for the gas-electricity integrated energy systems (IES) considering security constraints of both natural gas network and power system.

Extensive work has been done to analyze the effect of the interdependence between gas networks and power system operation and to optimally coordinate the energy flow in gas-electricity IES. A unified gas and power flow is proposed in [69] for a steady-state analysis of electricity and natural gas coupled systems. In [93], the security constrained unit commitment (SCUC) problem is modeled including natural gas transmission constraints. A multi-period generalized network flow model of the U.S. integrated energy system is built in considering the coordination of various energy resources. An integrated optimization model is proposed in [10] to incorporate the impact of the interdependency of electricity and natural gas networks on power system dispatch. Operating strategies for the coordinated operation of electricity and gas networks in Great Britain are investigated in [71] considering the uncertainty in wind power forecasts. The short-term scheduling of integrated gas networks and hydrothermal power systems was solved in

[96]. In [97], the coordination of interdependent natural gas and electricity infrastructures is optimized for firming wind power variability in day-ahead scheduling. Further, demand response is incorporated into the day-ahead scheduling of coordinated natural gas and electricity networks in [98]-[99].

However, few existing works addressed the contingencies in a gas-electricity IES. With the increasing interdependency of gas-fired generation, the impact of contingencies on the security of IES operation has developed to an extent that we cannot ignore. For instance, an interruption or pressure loss in a natural gas pipeline may lead to the loss of a generator or limit the amount of fuel delivered to gas-fired generators [72]. Thus, the economic and secure operation of the power system will be affected by the gas network contingencies. Several events have evidenced security issues in IES. In Texas, in 2011, some pipelines were frozen by the extreme weather, leading to several hours of power outages. In Colombia, in 2012, the rupture of a pipeline reduced the gas supply for gas-fired generators resulting in a power interruption [100]. The 2006 reliability report by NERC [101] pointed out that gas transmission security is important for power system reliability. In 2013, FERC also requested to include unexpected fuel transportation contingencies in power systems [102].

In existing literatures, [71] and [103] analyzed the impact of gas pipeline contingencies on power systems in the case studies but did not model the contingencies into the optimal dispatch problem. Reference [73] is the only work that proposed an optimal operation model considering *N*-1 contingencies for IES. In [73], a security-constrained optimal power and natural gas flow model is proposed, and a contingency-analysis is developed for gas network using linear sensitivity factors. However, this is a single-period energy flow formulation, and it does not take into account

the uncertainty in wind power. The uncertainty plays an important role in todays' power systems due to the increasing penetration of volatile renewable energy.

With the motivation discussed above, this work proposes a stochastic multi-period optimal operating strategy for gas-electricity IES considering both gas and electricity *N*-1 contingencies, as well as wind power uncertainty. The non-linear constraints of gas pipelines and compressors are linearized by the first-order Taylor expansion to improve their computational efficiency. The wind power uncertainty in IES is addressed by stochastic programming. Through solving the proposed optimization model, the expected operating cost is minimized considering a set of probabilistic wind power scenarios, and the multi-period power and gas flow are optimally determined. The effectiveness of the proposed method is verified by a coupled IEEE 6-bus electricity network and 7-node gas network. Further, the performance of the proposed method is evaluated by a coupled IEEE 118-bus system and 14-node gas network. The impacts of electricity network *N*-1 contingencies, gas network *N*-1 contingencies, and wind power uncertainty on IES operation are investigated.

3.2 Nomenclature

NG Set of natural gas-fired generators

CG Set of coal-fired generators

GW Set of gas wells

ED Set of electric demands

GD Set of gas demands

GC Set of gas compressors

GS Set of gas storages

GP Set of gas pipelines

ET Set of power transmission lines

GN Set of nodes in the gas network

EN Set of nodes in the electricity network

T Scheduling horizon

$\boldsymbol{S}$ Set of wind power scenarios

B Electric network DC power flow B matrix

$Q_{w,t}$ Gas production of well w at time t

$Q_{w,max}$, $Q_{w,min}$ Maximum / Minimum gas production of well w

$f_{p,t}$ Gas flow through pipeline p at time t

$f_{c,t}$ Gas flow through compressor c at time t

$\pi_{i,t}$ Pressure of node i at time t

$\pi_{i,max}$, $\pi_{i,min}$ Maximum/minimum pressure limit at node i

k_{c1}, k_{c2} Coefficients of compressor c

$H_{c,t}$ Horsepower of compressor c at time t

$R_{c,max}$, $R_{c,min}$ Maximum/minimum compression ratio of compressor c

$Q_{c,t}$ Gas consumption of compressor c at time t

α_c, β_c, γ_c Gas consumption coefficients for compressor c

$Q_{gs,t}$ Stored natural gas in storage gs at time t

$dQ_{gs,t}$ Gas in-flow/out-flow from storage gs at time t

$Q_{gs,max}$, $Q_{gs,min}$ Maximum/minimum gas capacity of storage gs

IR_{gs}, OR_{gs} Gas in-flow/out-flow rate limit of storage gs

$Q_{ng,t}$ Gas consumption of gas-fired unit ng at time t

k_{0g}, k_{1g}, k_{2g} Gas consumption coefficients of gas-fired unit g

$f_g(\ )$ Cost function of coal-fired generator g

λ_g Unit production cost of natural gas, \$/kcf

λ_{ue}, λ_{ug} Penalty for electric/gas load shedding

P_w Power output of wind farm w

$P_{g,t}$ Power output of generator g at time t

$P_{g,max}$, $P_{g,min}$ Maximum/minimum output of generator g

θ_j Voltage angle of bus j

$P_{flow,l,t}$ Power flow through line l at time t

$P_{l,max}$ Power flow limit of line l

RU_g, RD_g Ramp up/down limit of generator g

$SR_{g,t}$ Reserve capacity from generator g at time t

$SR_{t,min}$ Minimum required reserve at time t

ΔP, ΔQ Unserved electric load and natural gas load

s index of wind power scenario

ξ_s probability of scenario s

$\boldsymbol{I_{lw}, I_{lg}, I_{lf}, I_{ld}}$ Incidence matrix of wind turbines, thermal units, power transmission lines, and electric loads.

$\boldsymbol{I_{ns}, I_{nw}, I_{ng}, I_{nd}, I_{np}, I_{nc}}$ Incidence matrix of gas storages, gas wells, gas-fired units, gas loads, pipelines, and compressors.

Other variables with a superscript of s identify the variables in wind power scenario s.

3.3 Nominal IES Operation Considering N-1 Contingencies In Gas and Electricity Networks

The gas-electricity IES is composed of two energy sectors, the gas network and the electricity network. Due to the tight coupling between these two networks, it is desired to model them as an integrated energy system. In this section, a deterministic optimal scheduling model for IES is built based on the modeling of the gas and electricity networks. Then, to ensure that the IES is able to sustain *N*-1 contingencies in gas and electricity networks, *N*-1 contingencies in both networks are modeled and incorporated into the optimal scheduling model. Further, considering wind power uncertainty, the proposed model evolves into a stochastic optimal scheduling model considering both gas and electricity *N*-1 contingencies in IES in the presence of wind power uncertainty.

3.3.1 Deterministic Optimal Scheduling Model for IES

In this subsection, we introduce the gas-electricity coordination problem and present a deterministic optimal scheduling model for IES based on modeling gas and electricity networks.

The natural gas network consists of gas wells, gas pipelines, compressors, gas storages and gas loads. Natural gas is produced at gas wells and transmitted through pipelines propelled by compressors. Then, it is delivered to the gas load sites. The gas storage provides a buffer to coordinate the usage of gas during multiple periods. The steady state mathematical models of gas networks are built. More details about the gas network model are referred to [104], [105]. The electricity network adopts a DC power flow model, which is applicable for high voltage-level transmission systems. Gas-fired generators link the gas network and electricity network together to form an integrated energy system. The operations of gas networks and electricity networks should be coordinated to achieve the optimal system economy. In the deterministic optimal

scheduling model for IES, the objective of IES operation is to minimize the total operation cost during the scheduling horizon, including minimization of the production cost of natural gas, generation cost of coal-fired power plants, and penalties for electricity and gas load shedding. The constraints of the gas network and the electricity network are imposed. The optimization model of the deterministic optimal scheduling of IES is formulated as follows.

$$\min_{\boldsymbol{X}} \ J(\boldsymbol{X}) = \sum_{t\in T}\Bigg(\sum_{g\in CG} f_g(P_{g,t}) + \sum_{w\in GW} \lambda_g Q_{w,t} + \sum_{e\in ED} \lambda_{ue}\Delta P_{e,t} + \sum_{q\in GD} \lambda_{ug}\Delta Q_{q,t} \Bigg) \tag{3.1}$$

s.t.

1) Gas network constraints

$$Q_{w,\min} \le Q_{w,t} \le Q_{w,\max}, \quad \forall w \in GW, \quad \forall t \tag{3.2}$$

$$\begin{aligned} &f_{p,t} = \operatorname{sgn}(\pi_{m,t},\pi_{n,t}) C_{mn}\sqrt{\left|\pi_{m,t}^2 - \pi_{n,t}^2\right|}, \ \forall p \in GP, \ \forall t \\ &\operatorname{sgn}(\pi_{m,t},\pi_{n,t}) = \begin{cases} 1 & \pi_{m,t} \ge \pi_{n,t} \\ -1 & \pi_{m,t} < \pi_{n,t} \end{cases}, \ mn \in GN(p) \end{aligned} \tag{3.3}$$

$$\pi_{i,\min} \le \pi_{i,t} \le \pi_{i,\max}, \quad \forall i \in GN, \quad \forall t \tag{3.4}$$

$$f_{c,t} = \frac{\operatorname{sgn}(\pi_{m,t},\pi_{n,t}) \cdot H_{c,t}}{k_{c2} - k_{c1}[\dfrac{\max(\pi_{m,t},\pi_{n,t})}{\min(\pi_{m,t},\pi_{n,t})}]^{\alpha}}, \forall c \in GC, mn \in GN(c), \forall t \tag{3.5}$$

$$H_{c,\min} \le H_{c,t} \le H_{c,\max}, \quad \forall c \in GC, \quad \forall t \tag{3.6}$$

$$R_{c,\min} \le \frac{\max(\pi_{m,t},\pi_{n,t})}{\min(\pi_{m,t},\pi_{n,t})} \le R_{c,\max}, \forall c \in GC, mn \in GN(c), \forall t \tag{3.7}$$

$$Q_{c,t} = f_c(H_{c,t}) = \gamma_c + \beta_c H_{c,t} + \alpha_c H_{c,t}^2, \quad \forall c \in GC, \quad \forall t \tag{3.8}$$

$$Q_{gs,\min} \le Q_{gs,t} \le Q_{gs,\max}, \quad \forall gs \in GS, \quad \forall t \tag{3.9}$$

$$-IR_{gs} \le dQ_{gs,t} = \left(Q_{gs,t} - Q_{gs,t-1}\right) \le OR_{gs}, \quad \forall gs \in GS, \quad \forall t \tag{3.10}$$

$$\begin{aligned} \boldsymbol{I_{nw}} \cdot \boldsymbol{Q_w} - \boldsymbol{I_{ns}} \cdot d\boldsymbol{Q_{gs}} - \boldsymbol{I_{ng}} \cdot \boldsymbol{Q_{ng}} - \boldsymbol{I_{nd}} \cdot \boldsymbol{Q_d} \\ - \boldsymbol{I_{np}} \boldsymbol{f} - \boldsymbol{I_{nc}} \boldsymbol{Q_c} = \text{-}\boldsymbol{I_{nd}} \cdot \boldsymbol{\Delta Q_q} \end{aligned} \tag{3.11}$$

In the above model, constraint (3.2) indicates the limits of the available production of gas well in a day-ahead market when they are subjected to physical capability and long-term or mid-term contracts. Eq. (3.3) depicts the relationship between gas flow through a pipeline and the pressures at the two ends of the pipeline. $mn \in GN(P)$ indicates that nodes m and n are the two ends of pipeline p. $sgn(\pi_m, \pi_n)$ indicates the direction of the gas flow. When it is 1, the gas flows from node m to n. C_{mn} is the Weymouth factor related to the physical characteristics of each pipeline, such as the temperature, pipeline diameters, friction factor, etc. Eq. (3.4) imposes the bounds on the pressure of each node. The gas compressors are modeled as (3.5)-(3.8), where $mn \in GN(c)$ indicates that nodes m and n are the two ends of compressor c: (3.5) represents the gas flow from node m to node n through the compressor c; (3.6) indicates the limits of the horse power that the compressor can provide; the compression ratio between the outlet node and inlet node is subject to (3.7); and the gas consumption of compressors is modeled as (3.8). The gas storage is modeled as (3.9)-(3.10), where (3.9) represents the volume capacity of gas storage operation and (3.10) imposes the inflow and outflow rate limits on gas storage. Finally, the nodal balance equation for each node in gas network is presented in (3.11).

2) Electricity network constraints

$$B_l(\theta_{j,t} - \theta_{k,t}) - P_{flow,l,t} = 0, \quad \forall l \in ET, \ k \in EN(j), \ \forall t \tag{3.12}$$

$$-P_{l,\max} \le P_{flow,l,t} \le P_{l,max}, \ \forall l \in ET, \ \forall t \tag{3.13}$$

$$\theta_j^{\min} \le \theta_{j,t} \le \theta_j^{\max}, \quad \forall j \in EN, \ \forall t \tag{3.14}$$

$$P_{g,\min} \le P_{g,t} \le P_{g,\max}, \quad \forall g \in NG \bigcup CG, \ \forall t \tag{3.15}$$

$$P_{g,t} - P_{g,t-1} \le RU_g, \quad \forall g \in NG \bigcup CG, \ \forall t \tag{3.16}$$

$$P_{g,t-1} - P_{g,t} \le RD_g, \quad \forall g \in NG \bigcup CG, \ \forall t \tag{3.17}$$

$$\sum_g SR_{g,t} \ge SR_{t,\min}, \quad \forall g \in NG \bigcup CG, \ \forall t \tag{3.18}$$

$$\boldsymbol{I_{lw}} \cdot \boldsymbol{P_w} + \boldsymbol{I_{lg}} \cdot \boldsymbol{P_g} - \boldsymbol{I_{lf}} \cdot \boldsymbol{P_{flow}} - \boldsymbol{I_{ld}} \cdot \boldsymbol{P_d} = -\boldsymbol{I_{ld}} \cdot \Delta \boldsymbol{P_e} \tag{3.19}$$

A DC power flow model is adopted for all electricity networks. The generation limit of thermal units is shown in (3.15), and the ramping up/down limits are represented by (3.16) and (3.17), respectively. (3.18) indicates the spinning reserve requirement. The power flow on each transmission line is subject to power transmission capacity as shown in (3.13). The DC power flow equations are represented by (3.12) and (3.14). *EN*(*j*) is the set of nodes connected to node *j*. In (3.14), the chosen max and min bus angle values are ±0.6 radians [106]. The nodal power balance is shown in (3.19).

3) Linkage between gas and electricity networks

$$Q_{ng,t} = k_{2,g} P_{g,t}^2 + k_{1,g} P_{g,t} + k_{0,g} \quad \forall g \in NG, \forall ng \in GD \tag{3.20}$$

Gas-fired units are the components that link the two energy networks together. They consume natural gas as a type of gas load in gas networks, and are involved in gas nodal balance constraint (3.11). Meanwhile, they generate electric power for electricity networks and, thus, are involved in power nodal balance (3.19).

3.3.2 Modeling N-1 Contingencies

The ability of gas delivery will be limited due to the gas pipeline trip, which will significantly limit the generation capability of gas-fired units. Thus, in this work, both *N*-1

contingencies in gas network and electricity network are considered in the economic dispatch of IES. The optimal scheduling scheme of the proposed model should be able to sustain any single contingency in gas and electricity networks. The worst scenario is that *N*-1 contingencies occur in gas and electricity networks at the same time. This would impact both the deliverability of the gas network to satisfy gas loads and gas-fired units as well as the capability of power transmission. The modeling of *N*-1 contingencies in gas and electricity networks will be introduced as follows.

3.3.2.1 N-1 contingency in gas network

To incorporate the *N*-1 contingency into the optimization model, a state matrix $N1_g$ is introduced to represent the states of pipelines, where "1" indicates the normal state and "0" indicates the contingency occurrence of a pipeline. $N1_g$ is a $N_p \times (N_p+1)$ matrix, where N_p is the number of gas pipelines. Each row indicates an operation state. There are N_p+1 scenarios in total considering the normal operation state and all *N*-1 contingency states. The state matrix $N1_g$ is given by

$$N1_g = \left[\begin{array}{c|cccc} 1 & 0 & 1 & \cdots & 1 \\ 1 & 1 & 0 & \cdots & 1 \\ \vdots & \vdots & & \ddots & \\ 1 & 1 & 1 & \cdots & 0 \end{array}\right]_{N_p \times (N_p+1)} \tag{3.21}$$

To include every possible *N*-1 contingency in gas network, the pipeline constraints (3.3)-(3.4) should be rewritten as

$$f_{p,t} - \mathrm{sgn}(\pi_{m,t}, \pi_{n,t}) C_{mn} \sqrt{\left|\pi_{m,t}^2 - \pi_{n,t}^2\right|} + (1 + N1_{gpc}) \cdot M_{gp} \geq 0 \tag{3.22}$$

$$f_{p,t} - \mathrm{sgn}(\pi_{m,t}, \pi_{n,t}) C_{mn} \sqrt{\left|\pi_{m,t}^2 - \pi_{n,t}^2\right|} - (1 - N1_{gpc}) \cdot M_{gp} \leq 0 \tag{3.23}$$

$$-M_{gp} N1_{gpc} \leq f_{p,t} \leq M_{gp} N1_{gpc} \tag{3.24}$$

where $N1_{gkc}$ is the element in the pth row and cth column in the state matrix, which is a binary element. It indicates the status of the pth pipeline in the cth contingency. M_{gp} is for the pth pipeline constraints, which is often called the "big M" value that is large enough to make the constraint nonbinding. It must be larger than or at least equal to $C_{mn}\sqrt{\left|\pi^2_{m,\max}-\pi^2_{n,\min}\right|}$. When $N1_{gpc}$ = 0, the constraints (3.22)-(3.24) are relaxed. Then the constraints for the pipeline can be satisfied all the time.

3.3.2.2 N-1 contingency in electricity network

Similarly, a state matrix is defined for an electricity network as $N1_e$ to include *N-1* contingencies of power transmission, where N_e is the number of power transmission lines.

$$N1_e=\left[\begin{array}{c|cccc} 1 & 0 & 1 & \cdots & 1 \\ 1 & 1 & 0 & \cdots & 1 \\ \vdots & \vdots & & \ddots & \\ 1 & 1 & 1 & \cdots & 0 \end{array}\right]_{N_e\times(N_e+1)} \tag{3.25}$$

The elements in the matrix represent the state of the transmission lines. "0" indicates loss of a transmission line and "1" indicates normal operation. The transmission constraints in (3.12) and (3.13) are rewritten as

$$B_l(\theta_{j,t}-\theta_{k,t})-P_{flow,l,t}+(1-N1_{elc})M_{el}\geq 0 \tag{3.26}$$

$$B_l(\theta_{j,t}-\theta_{k,t})-P_{flow,l,t}-(1-N1_{elc})M_{el}\leq 0 \tag{3.27}$$

$$-P_{l,\max}N1_{elc}\leq P_{flow,l,t}\leq P_{l,\max}N1_{elc} \tag{3.28}$$

where $N1_{elc}$ is the binary element in the lth row and cth column in the state matrix. The "big M" value M_{el} for the lth transmission line flow constraints in (3.26)-(3.27) should be no less than $\left|B_l(\theta_{\max}-\theta_{\min})\right|$.

3.3.3 Linearization of the Gas Network Model

It comes to our attention that the inclusion of a gas network makes the optimization model non-linear and non-convex due to the pipeline and compressor models, i.e., constraints (3.3), (3.5) and (3.22)-(3.24). The non-convexity characteristics make the solution difficult and time-consuming. As a result, usually, only local optimums can be found.

The Taylor-series expansion [107] is adopted in this paper to linearize the pipeline constraints. The first-order Taylor expansion of equation (3.3) at the given pressure values π_M and π_N is given in (3.29).

$$f_{p,t}\left(\pi_{m,t},\pi_{n,t}\right) \le f_{mn}\left(\pi_M,\pi_N\right)+\frac{\partial f_{p,t}}{\partial \pi_m}\left(\pi_{m,t}-\pi_M\right) + \frac{\partial f_{p,t}}{\partial \pi_{n,t}}\left(\pi_{n,t}-\pi_N\right), \quad mn \in GN(p), \forall t \tag{3.29}$$

Introduce a set of Z evenly distributed points to split the range of node pressures for inlet and outlet nodes respectively, which gives Z tuples denoted as ($\pi_{M,z}$, $\pi_{N,z}$) for pipeline mn, where z = 1, 2,…, Z. Hence, replace the nonlinear Weymouth equation (3.3) with a set of linearized inequality constraints as

$$f_{p,t} \le C_{mn}\frac{\pi_{M,z}}{\sqrt{\pi_{M,z}^2-\pi_{N,z}^2}}\pi_{m,t} - C_{mn}\frac{\pi_{N,z}}{\sqrt{\pi_{M,z}^2-\pi_{N,z}^2}}\pi_{n,t} \tag{3.30}$$

where for each pipeline p, only the Z inequality constraints that have the best approximation will be binding.

The quantity of natural gas flow in pressurized pipelines is also linearized using the first-order Taylor-series expansion at a fixed point (H_{c0}, π_{m0}, π_{n0}). Check the initial compression ratio $R_0=\pi_{m0}/\pi_{n0}$ and make sure it is within the limits of the compressor. The linearized formulation of (3.5) is then given by:

$$f_{c,t} = -\frac{H_{c0}}{k_2 - k_1 R_0^{\alpha_j}} + \frac{\partial f_{c,t}}{\partial H_{c.t}} \times \left(H_{c,t} - H_{c0}\right) + \frac{\partial f_{c,t}}{\partial \pi_{m,t}} \times \left(\pi_{m,t} - \pi_{m0}\right) + \frac{\partial f_{c,t}}{\partial \pi_{n,t}} \times \left(\pi_{n,t} - \pi_{n0}\right) \tag{3.31}$$

where the partial derivatives can be found in Appendix B of Ref. [93]. A 50,000-sample Monte Carlo simulation shows a maximum approximation error of 0.5% of the accurate value, which is considered to be highly satisfactory.

In addition, the quadratic cost functions in (3.8) and (3.20) can be easily linearized by piece-wise linearization with the introducing of binary variables. Hence, the proposed model can be reformulated into a MILP problem.

3.4 Stochastic Optimal Scheduling Model for IES Considering N-1 Contingencies and Wind Uncertainty

In this paper, scenario based stochastic programming is applied to address wind power uncertainty. The stochastic approach is used to model decision-making problems for finding the optimal solution considering all possible scenarios. The stochastic optimal scheduling for IES aims to minimize the expected operating cost with *N*-1 network constraints under a set of probabilistic wind power forecast scenarios.

3.4.1 Stochastic Programming

The key steps in stochastic programming are scenario generation and reduction. A set of possible scenarios is generated to model wind uncertainties based on the Monte Carlo simulation with known probability distribution function [108][109]. For each sampling period, the main principle is to take a sample from a probability distribution function such that for a given value *x*, we have an associated probability *p*(*x*).

A large number of scenarios are required for accurate modeling of any stochastic process; however, this can make the optimization model intractable. Considering computational requirements, an effective scenario reduction technique is adopted to obtain a small number of scenarios with a high probability of occurrence to approximate the initial probability distribution. The basic idea of scenario reduction is to eliminate scenarios with very low probability and bundle scenarios that have a high probability. Accordingly, scenario-reduction algorithms determine a subset of scenarios and calculate probabilities for new scenarios, such that the reduced probability measure is closest to the original probability measure in terms of a certain probability distance between the two measures [110].

The scenario-reduction algorithm reduces and bundles the scenarios using the Kantorovich distance (KD) matrix. KD is defined as the probability distance between two different scenario sets, which can be used to evaluate the closeness of different scenario sets. The KD between scenario ε_i and ε_j is

$$L_{KD}(\varepsilon_{i,}\,\varepsilon_j) = \left\|\varepsilon_i - \varepsilon_j\right\|_2 \quad i, j = 1, 2, ..., N \tag{3.32}$$

Fast forward selection (FFS) method [111] is used in this paper. The FFS is to select a subset $\boldsymbol{S}$ from the original finite scenario set Ω such that $\boldsymbol{S}$ is the subset of the prescribed size that has the shortest distance to the remaining scenarios. Considering the probability of each scenario, the weighted distance of the scenario to the others is

$$WL_{KD}(\varepsilon_{i,}\,\varepsilon_j) = \left\|\varepsilon_i - \varepsilon_j\right\|_2 \cdot p_i \quad j = 1, 2, ..., N \tag{3.33}$$

For each scenario ε_i, the probability distance of every candidate scenario is calculated. The closest scenario ε_j is obtained and marked according to the minimum weighted distance $min\{WL_{KD}(\varepsilon_i,\varepsilon_j)\}$. Then, this scenario is deleted from Ω and added to $\boldsymbol{S}$. The new probability of

preserved scenarios is equal to the sum of its former probability and the probability of deleted scenarios that are closest to it. The above process is repeated until the size of $\boldsymbol{S}$ reaches the predefined value.

The resulting several scenarios are representative for modeling wind power uncertainties.

3.4.2 Stochastic Optimization Model of IES Operation

Let ξ_s, $s \in \boldsymbol{S}$, denote the probability of S different wind power scenarios. The objective of stochastic optimal scheduling model for IES considering both gas and electricity N-1 contingencies and wind uncertainty is to minimize the expected total operating cost, described as (3.34).

$$\begin{aligned} &\min_{\boldsymbol{X}^s} \sum_{s\in S} \xi_s J(\boldsymbol{X}^s) \\ &= \min \sum_{s\in S} \xi_s \sum_{t\in T} \Bigg(\sum_{g\in CG} f_g(P_{g,t}^s) + \lambda_g \sum_{w\in GW} Q_w^s \\ &\qquad + \sum_{e\in ED} \lambda_{ue} \Delta P_{e,t}^s + \sum_{q\in GD} \lambda_{ug} \Delta Q_{q,t}^s \Bigg) \end{aligned} \tag{3.34}$$

s.t. Gas network constraints in (3.2), (3.22)-(3.24), (3.5)-(3.11)

Electricity network constraints in (3.26)-(3.28), (3.14)-(3.19)

All constraints are under scenario s, $\forall s \in \boldsymbol{S}$

For each wind forecast scenario, the constraints of both the gas and the electricity networks should be satisfied. This optimization model will seek the optimal scheduling of the gas-electricity IES in the presence of wind power uncertainty which is able to maintain N-1 security in both gas and electricity networks.

3.5 Case Studies

In this section, a six-bus electricity network with a seven-node natural gas network is used to illustrate and verify the proposed method. Then the IEEE 118-bus with 14-node gas network is

adopted to evaluate the performance of the proposed method in large systems. The simulation has been performed in MATLAB with YALMIP [95] and CPLEX solver, which has the capability to solve large-scale optimization problems. The simulations are carried out on a PC with Intel Core i7 3.00 GHz CPU and 8 GB RAM.

3.5.1 Six-bus Electricity Network with Seven-node Gas Network

An IES consisting of a 6-bus electricity network and a coupled 7-node gas network is depicted in Figure 3.1. The detailed network parameters are given in [93]. In the electricity network, three gas-fired generators are located at nodes 1, 2 and 6; three electricity loads are at nodes 3, 4 and 5; and a wind turbine (WT) is installed on node 3 with the wind power forecast curve shown in Figure 3.2. In the gas network, two gas wells are at nodes 6 and 7; a gas storage is installed at node 1; two residential gas loads are at nodes 1 and 3; and a compressor is installed on the pipeline between nodes 2 and 4. The total electricity load and residential gas load are shown in Figure 3.3. The scheduling horizon is 24 hours. The penalties for electric and gas load shedding are 1,000 $/MW and 200 $/kcf.

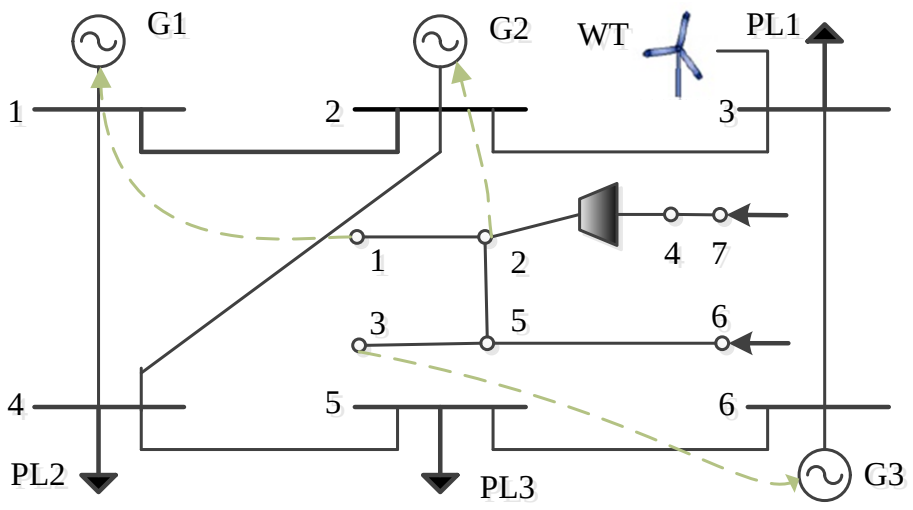

Figure 3.1 Six-bus electricity network coupled with a seven-node gas network

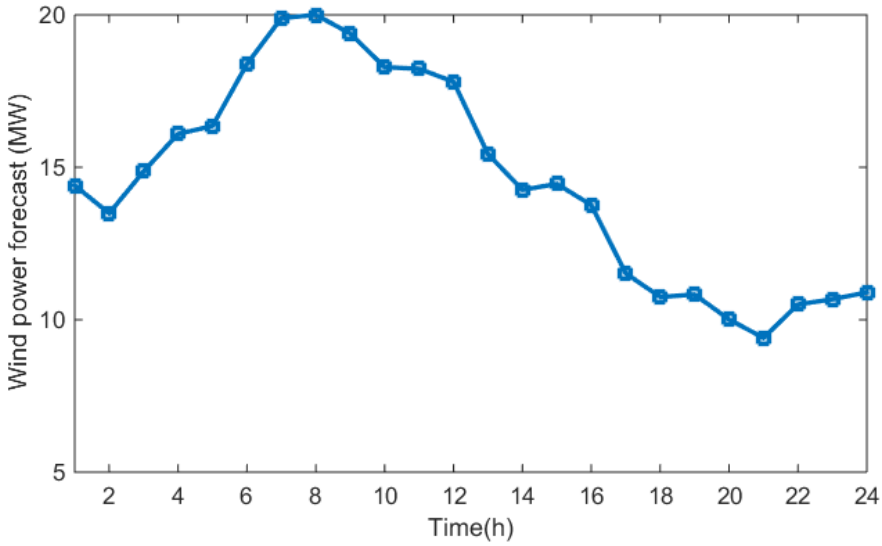

Figure 3.2 Wind power forecast

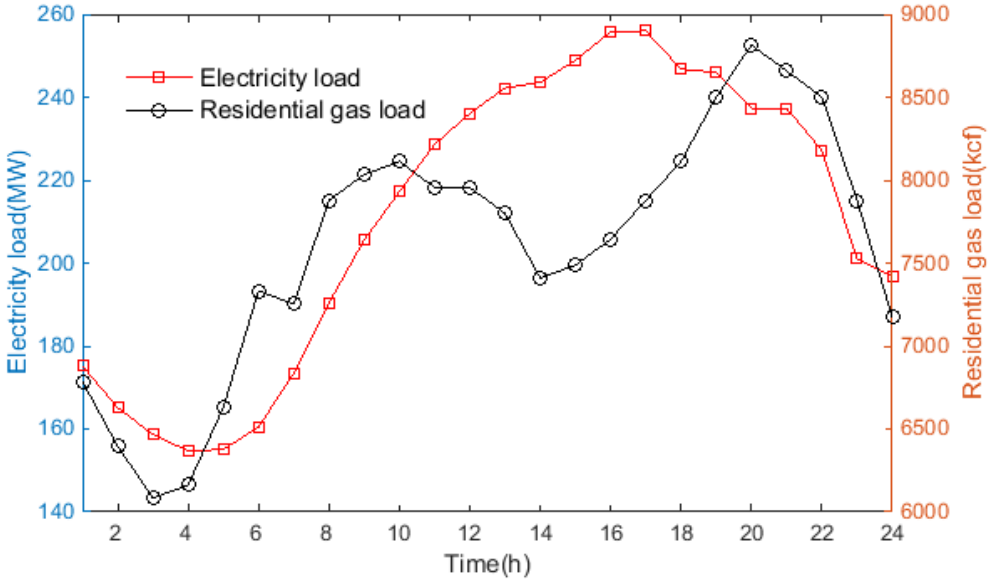

Figure 3.3 Total electricity load and residential gas load

In this subsection, four cases are designed to investigate the impact of power transmission contingencies and gas pipeline contingencies on day-ahead scheduling of IES:

- *Case 1* (base case): IES scheduling without contingencies;
- *Case 2*: IES scheduling with electricity *N*-1 contingencies;
- *Case 3*: IES scheduling with gas pipeline *N*-1 contingencies;
- *Case 4*: IES scheduling considering both electrical network and natural gas pipeline *N*-1 contingencies.

The above cases are discussed as follows.

In *Case 1*, to analyze the impact of wind power on the economic dispatch of IES, two scenarios with/without wind power are compared and the results are shown in Figure 3.4. It can be observed that with wind power integration, the power output of the generators decreases, especially for the expensive units G2 and G3. Since wind power has no fuel cost, the total operating cost of wind-integrated system is 1.39M$, which is low compared to 1.44M$ without wind. Hence, the IES

could accommodate a certain level of wind power penetration, and wind power can contribute to the economic operation of IES.

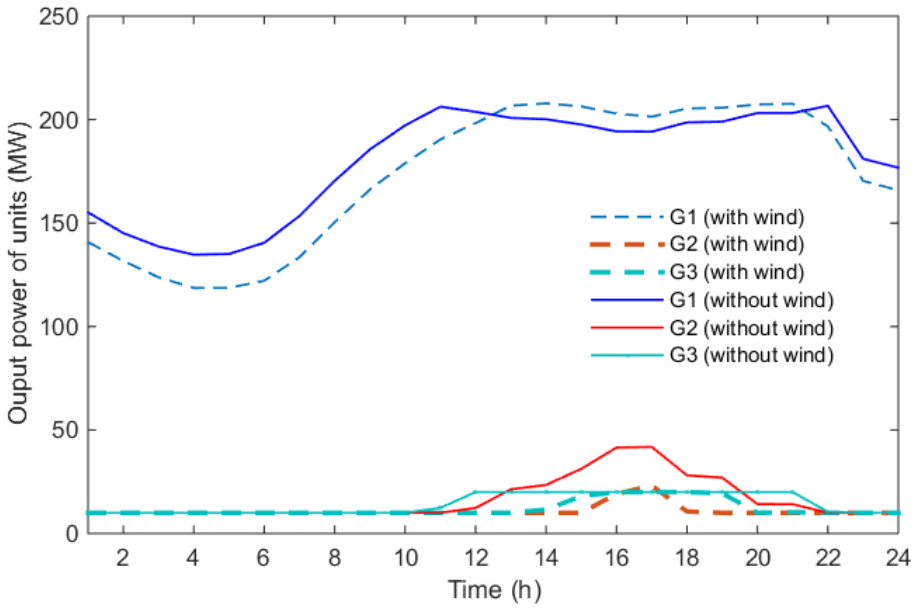

Figure 3.4 Comparison of unit dispatch with and without wind power

To investigate the impact of *N*-1 contingencies on economic dispatch of IES, the optimal scheduling results in *Cases* 2, 3, and 4 are compared with deterministic wind power shown in Fig. 2. Note that wind power uncertainty is further considered in *Case* 5, after the discussion of *Cases* 1-4.

Figure 3.5 shows the power scheduling of G1 in *Case* 1-4. Comparing *Case* 1 and *Case* 2, to ensure the system could sustain electric power network *N*-1 contingency, the output power of G1 is limited and more power is generated by the expensive units G2 and G3. When the contingency occurs, the output of units can be re-dispatched within its ramping ability. If *Case* 1 and *Case* 3 are compared to study the impact from gas contingencies, the gas flow in the gas network is redistributed such that the IES could address any gas network outage while satisfying residential

gas loads and gas-fired generators as much as possible. Since the residential gas loads have higher priority, the fuel deliverability of gas network for gas-fired generators is limited, and electric load shedding occurs at hours 19-21 in *Case* 3. In *Case* 4, both power transmission and gas transmission contingencies are considered, contributing to a more conservative solution.

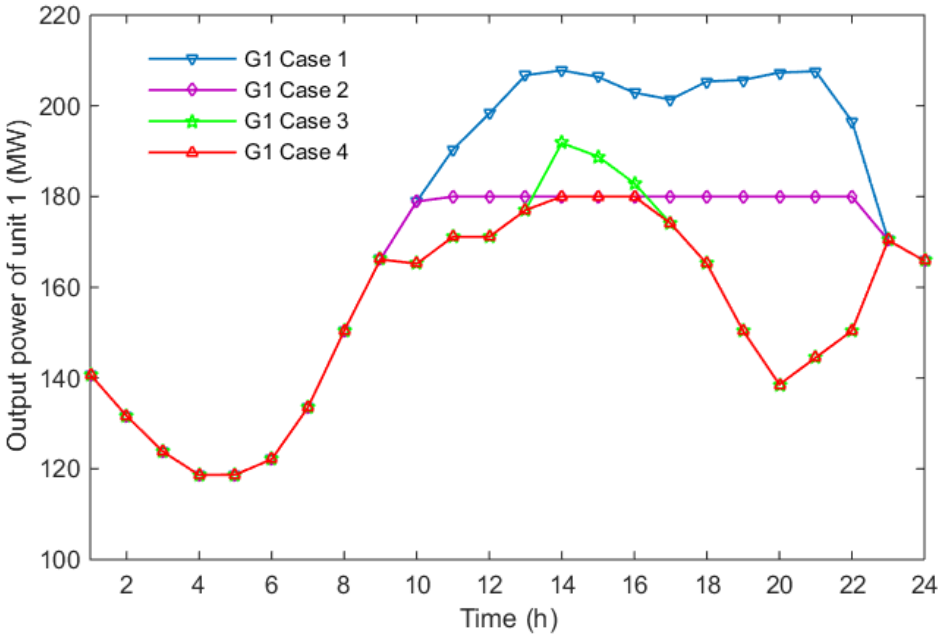

Figure 3.5 Comparison of unit dispatch in Case 1-4

Table 3.1 Comparison of the optimization results of *Case* 1-4

Cases	Case 1	Case 2	Case 3	Case 4
Daily production cost ($)	1,394,850	1,421,623	1,436,093	1,438,951
Load shedding cost ($)	0	0	23,529	23,529
Total operating cost ($)	1,394,850	1,421,623	1,459,622	1,462,480
Load shedding (MW)	0	0	23.53	23.53

The total operating costs for the 24-hour period and load shedding amounts in the four cases are summarized in Table 3.1. From Table 3.1, it can be observed that gas *N*-1 contingencies have a significant impact on the IES operation. Additional costs are incurred to improve the security of IES operation. With increasingly tight coupling between the two energy sectors, it may be necessary to consider both *N*-1 contingencies in IES operation to prevent possible severe consequences.

More details of the optimization results are shown and compared in Figure 3.6, Figure 3.7 and Figure 3.8. Figure 3.6 shows the power flow on Branch 1-4. Since the output power of G1 is adjusted for *N*-1 contingencies, the power supply from G1 to PL2 is reduced and more power is supplied by G2 through Branch 2-4. Hence, the power flow of Branch 1-4 decreases in *Cases* 2-4 in comparison with the base case.

The comparison of gas flow on Pipeline 2-5 (in gas network) is made in Figure 3.7. Since G2 and G3 consume more gas in *Case* 2, the gas flow from node 5 to node 2 decreases if compared with *Case* 1. It can be observed that the gas flows of *Case* 3 and *Case* 4 are basically the same, which means that they are both considered gas *N*-1 contingencies. The nodal pressures in gas networks play a key role in optimizing gas flow. The pressures of node 2 in the four cases are depicted in Figure 3.8. When gas transmission *N*-1 contingencies are considered, the pressures of node 2 in *Cases* 3 and 4 are lower than in *Cases* 1 and 2. This is to keep a certain amount of pressure margin to address any possible gas network contingency.

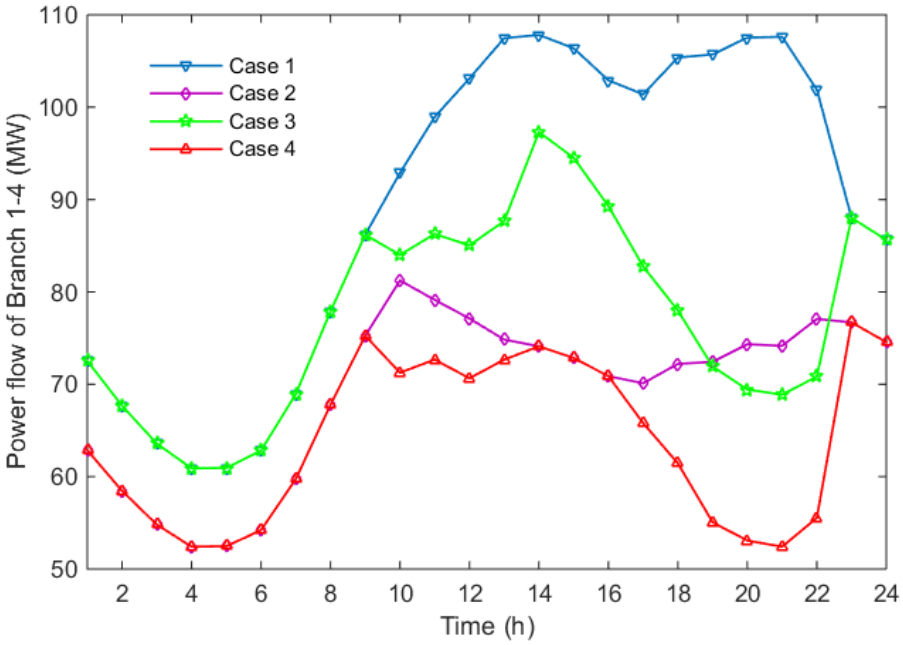

Figure 3.6 Power flow of Branch 1-4 in Case 1-4

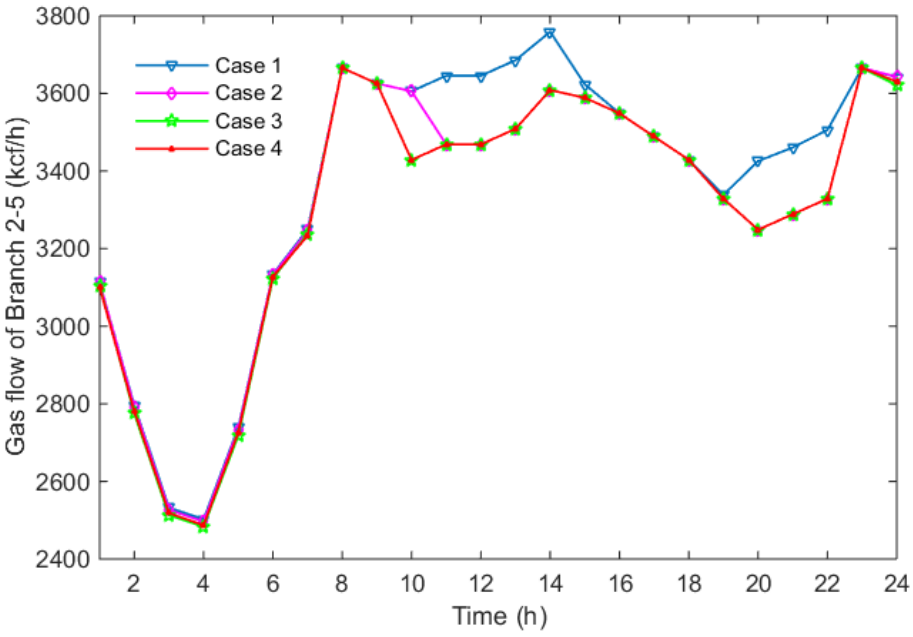

Figure 3.7 Gas flow of Pipeline 2-5 in Case 1-4

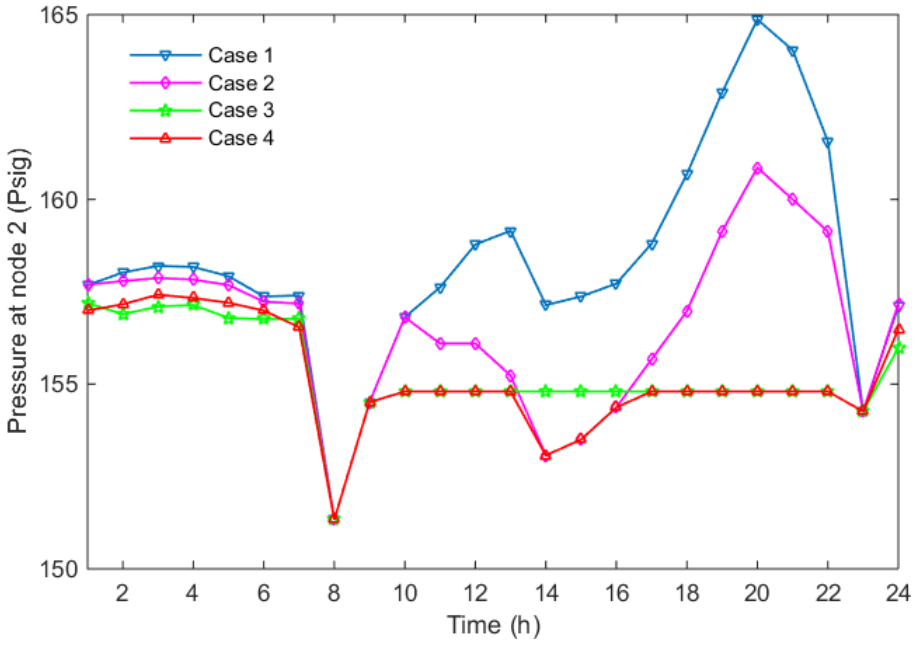

Figure 3.8 Pressures at node 2 in gas network in Case 1-4

Another case, *Case* 5, is designed to study stochastic IES optimal operation considering wind power uncertainty and *N*-1 contingencies. In this case, based on the forecasted wind power, we randomly generated 1000 scenarios and then reduced to 5 representative scenarios with probabilities through the application of the scenario reduction technique. The five wind power forecast scenarios and their corresponding probabilities are shown in Figure 3.9.

The optimization results of the IES considering both power transmission line and gas pipeline contingencies are shown in Table 3.2. The expected total operating cost of IES is $1,462,576 considering all probabilistic wind power forecast scenarios. With higher wind power penetration, the impact of wind power scenario on IES operation will be more obvious. For nominal IES operation model, the wind power can be fully utilized in this case. However, considering *N*-1 contingencies, the wind power uncertainty affects the amount of load shedding. It indicates that wind power plays a more significant role in *N*-1 secured IES. Therefore, the proposed stochastic

method is effective to address wind uncertainty and *N*-1 contingencies (gas and electricity) in the IES optimal dispatch.

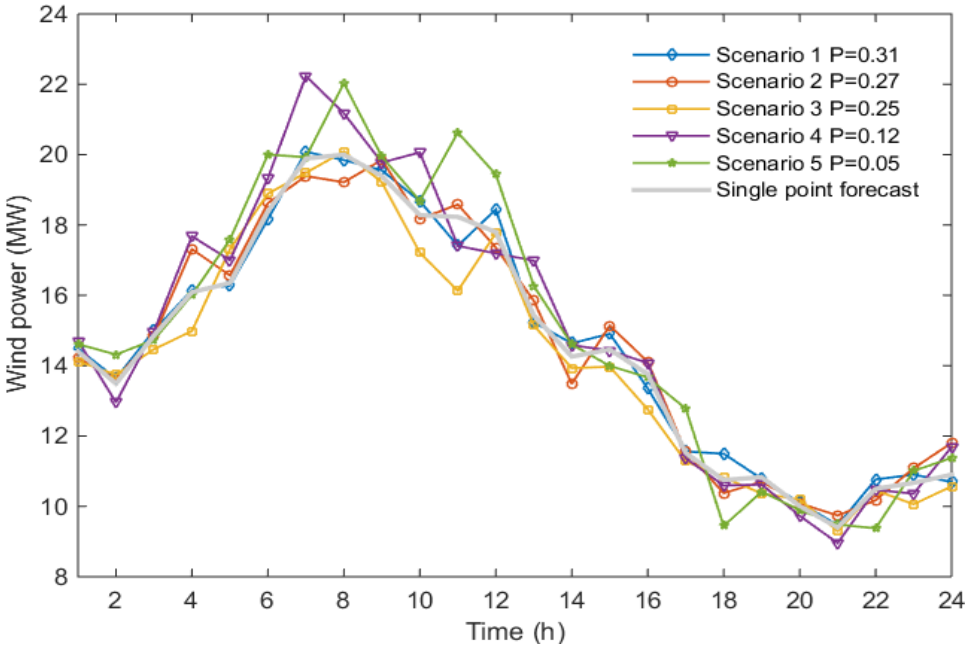

Figure 3.9 Wind power scenarios

Table 3.2 Optimization results of *Scenarios* 1-5 in Case 5

Scenarios	Scenario1	Scenario2	Scenario3	Scenario4	Scenario5
Production cost ($)	1,438,613	1,438,817	1,440,226	1,437,817	1,437,542
Load shedding cost ($)	23,417	23,242	23,912	24,460	23,974
Total operating cost ($)	1,462,031	1,462,060	1,464,139	1,462,332	1,461,516
Load shedding (MW)	23.42	23.24	23.91	24.46	23.97

3.5.2 IEEE 118-bus System with 14-node Gas Network

To evaluate the performance of the proposed method, a large gas and electricity IES consisting of a modified IEEE 118-bus system and 14-node gas network [93] is used in this study.

In the modified 118-bus system, a total capacity of 1460 MW wind power is distributed on nodes 12, 17, 56, and 88, the system structure is shown in Figure 3.10.

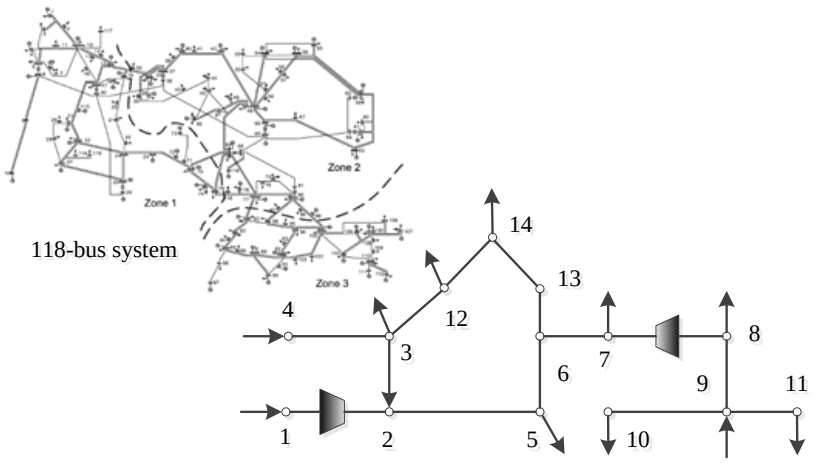

Figure 3.10 IEEE 118-bus system with 14-node gas network IES

Table 3.3 Optimization results of *Scenarios* 1-5 in IEEE 118 bus with 14-node IES

Scenarios	Scenario1	Scenario2	Scenario3	Scenario4	Scenario5
Probability	0.04	0.27	0.38	0.18	0.13
Total operating cost ($)	4,099,622	3,821,587	3,890,246	3,925,841	3,775,983

The proposed stochastic *N*-1 model for this IES is solved, and the optimization results for each scenario are shown in Table 3.3. The expected total operating cost is $3,871,636.

For the base case, the computational time is 1.37s for the linearized model using Taylor expansion in this paper. The linearization also facilitates the computation for solving stochastic *N*-1 IES operation model, which requires much more computational resources.

Similar to the previous case, 5 cases are simulated and the computational time for each case is summarized in Table 3.4.

Table 3.4 Computational time of Case 1-5

Cases	Case1	Case2	Case3	Case4	Case5
CPU Time(s)	1.37	1736	6.34	2028	13140

From Table 3.4, as expected, it can be observed that the computational time is significantly increased due to the *N*-1 constraints. The computational time is acceptable for day-ahead economic dispatch for IES. The computational time could be reduced by considering only several important or most credible contingencies based on the operators' experience. Also, the time can be further lowered by using a more powerful computer.

3.6 Conclusions

In this chapter, an optimal scheduling model for gas-electricity IES is proposed with the considerations of wind uncertainty and gas-electricity *N*-1 contingencies. Two case studies are conducted to demonstrate the effectiveness and performance of the proposed method. The contributions of this paper are summarized as follows.

1) Both power transmission and natural gas pipeline *N*-1 contingencies are modeled and incorporated into the optimization of IES operation. The impacts of electricity *N*-1 contingency only, gas network *N*-1 contingency only, and both contingencies on IES operation are investigated.
2) The non-convex gas network model is linearized by the first-order Taylor expansion, which significantly reduces the solution complexity.
3) The impact of wind power uncertainty on gas-electricity IES is addressed by stochastic programming.
4) The proposed model ensures that the IES is able to sustain any possible contingency in gas network or electricity network in the presence of wind power uncertainty.

5) The proposed model could coordinate various energy sources and optimize the energy flow in an integrated network with transmission constraints.

With increasing natural gas being utilized for electric power generation, both gas and electricity networks are closely coupled as a unified IES. The proposed method has practical significance for the secure and economic operation of IES, especially considering the high-penetration of wind power.

CHAPTER 4

ROBUST SCHEDULING FOR WIND INTEGRATED ENERGY SYSTEMS CONSIDERING GAS PIPELINE AND POWER TRANSMISSION *N*-1 CONTINGENCIES

4.1 Introduction

The significant amount of natural gas being utilized for power generation and high penetration of wind power has significant impact on modern power system operation. To address the wind power uncertainty, robust optimization has been applied to provide a robust scheduling that is immune to any possible scenario of the uncertainty set [76]. In [112], an affine multi-period robust OPF model is proposed for power network with renewables and storages. Now, there is a general consensus that the impact of gas network on the security of power network cannot be ignored. An interruption or pressure loss in natural gas pipeline may lead to a loss of generator or limit the amount of fuel delivered to gas-fired generators. In [93], a model for security-constrained unit commitment is presented to include gas network constraints. In 2013, FERC suggested to include unexpected fuel transportation contingencies in the power system operation [102]. Meanwhile, the research in power system security or contingency continues developing [113], [114]. However, there are few literatures that consider the impact of gas pipeline contingency and power system contingency simultaneously, not to mention renewable uncertainties. With this motivation, this work proposes a robust scheduling model considering both gas pipeline and power transmission line N-1 contingencies in the presence of wind uncertainty.

4.2 Modeling of Gas Pipeline and Power Transmission N-1 Contingencies in Gas-Electric Networks

The detailed gas network and power network models can be found in [93]. The gas network constraints have direct impacts to the dispatchability of gas-fired generators, thus affecting the power generation schedules. The constraints of gas pipelines and power transmission lines are modeled to include possible single contingency in gas-electricity systems.

A set of binary variables for state c and gas pipeline p, $N1_{gpc}$ is introduced for N_g pipelines in the gas network. $N1_{gpc}$=0 represents contingency occurring on the pipeline p. For c=0, $N1_{gc0}$=1 for N_g pipelines, indicating the normal operation state.

$$N1_{gpc} = \begin{Bmatrix} 0 & if\ c = p \\ 1 & otherwise \end{Bmatrix}, \quad \forall c > 0,\ p \tag{4.1}$$

$$\sum_{\forall p} N1_{gpc} = N_g - 1, \quad \forall c > 0 \tag{4.2}$$

$$\sum_{\forall c>0} N1_{gpc} = N_g - 1, \quad \forall p \tag{4.3}$$

Similarly, for electricity network [115], $N1_{elk}$ is introduced for the state k and power transmission line l, $l \in N_e$.

The gas network constraints with contingencies are modeled in (4.4)-(4.6):

$$f_{mn,t} - \mathrm{sgn}(\pi_{m,t}, \pi_{n,t}) C_{mn} \sqrt{\left|\pi_{m,t}^2 - \pi_{n,t}^2\right|} + (1 - N1_{gpc}) \cdot M_{gp} \geq 0 \tag{4.4}$$

$$f_{mn,t} - \mathrm{sgn}(\pi_{m,t}, \pi_{n,t}) C_{mn} \sqrt{\left|\pi_{m,t}^2 - \pi_{n,t}^2\right|} - (1 - N1_{gpc}) \cdot M_{gp} \leq 0 \tag{4.5}$$

$$-N1_{gpc} \cdot M_{gp} \leq f_{mn,t} \leq N1_{gpc} \cdot M_{gp} \tag{4.6}$$

where t is the time interval, f_{mn} is the gas flow from node m to node n of pipeline p, π is the nodal pressure, π_{min} and π_{max} are the upper and lower pressure limits, C_{mn} is a physical constant for

pipeline p, and M_{gp} is for the pipeline k constraint, which is called the "big M" value which is larger than or at least equal to $C_{mn}\sqrt{\left|\pi_{m,\max}^2-\pi_{n,\min}^2\right|}$ to ensure the constraint nonbinding. When $N1_{gkc}$=0, the constraints (4.4)-(4.5) are relaxed and the pipeline constraints can be satisfied all the time and (4.6) forced the gas flow to zero.

The electricity network constraints with contingencies are modeled in (4.7)-(4.9).

$$B_l(\theta_{i,t}-\theta_{j,t})-P_{flow,l,t}+(1-N1_{elk})M_{el}\geq 0,\ \forall i\in\mathcal{B}, j\in\mathcal{B}(i) \tag{4.7}$$

$$B_l(\theta_{i,t}-\theta_{j,t})-P_{flow,l,t}-(1-N1_{elk})M_{el}\leq 0 \tag{4.8}$$

$$-P_{l,\max}N1_{elk}\leq P_{flow,l,t}\leq P_{l,\max}N1_{elk} \tag{4.9}$$

where B is the susceptance matrix, $P_{flow,l}$ is the power flow on line l, $P_{l,\max}$ is the transmission limit, θ is the voltage angle, M_{el} is a big value that is larger than $\left|B_l(\theta_{\max}-\theta_{\min})\right|$, and $\mathcal{B}$ is the set of buses. $\mathcal{B}(i)$ is the set of buses connected to bus i. The first-order Taylor expansion is adopted for linearizing the gas pipeline and compressor constraints such that the gas-electricity network constraints are linearized to facilitate the implementation of robust optimization.

4.3 Robust Scheduling Model

Denote the set of wind farm buses as $\mathcal{W}$, the predicted wind power as P_W, and the uncertain wind power as P_W. The uncertainty set of wind power is defined by $\Gamma=\{P_{W,i}: P_{W,i}-P_{W,i}\zeta_i\leq P_W \leq P_{W,i}+P_{W,i}\zeta_i,\ \forall i\in\mathcal{W}\}$, where ζ_i is the uncertainty level.

Considering the N-1 contingencies of gas pipelines and power transmission lines, the robust scheduling model for wind integrated energy systems is formulated as

$$\min_{\boldsymbol{x},\boldsymbol{y}} \max_{\boldsymbol{w}} \sum_{t=1}^{T}\sum_{i\in G}\sum_{k}^{N_k}\left(c_{ik}P_{Gi,k,t}+c_{i0}\right)\Delta t+\sum_{t=1}^{T}\sum_{i\in GW}\sigma_g Q_{i,t}\Delta t + \sum_{t=1}^{T}\sum_{i\in PD}\sigma_{ps}\Delta P_{i,t}\Delta t+\sum_{t=1}^{T}\sum_{i\in GD}\sigma_{gs}\Delta Q_{i,t}\Delta t \tag{4.10}$$

$$\text{s.t. } e(\boldsymbol{x},\boldsymbol{w})\le 0 \quad \forall \boldsymbol{w}\in \boldsymbol{\Gamma},\ \forall i,\ \forall t \tag{4.11}$$

$$g(\boldsymbol{x},\boldsymbol{y})\le 0 \quad \forall i\in NG,\ \forall t \tag{4.12}$$

where $\boldsymbol{x}$ is the power scheduling decisions, $\boldsymbol{y}$ is the gas network scheduling decisions, and $\boldsymbol{w}$ is the uncertain wind power. The objective function is to minimize the total operation cost, including power generation cost, gas production cost, electric load and gas load shedding cost over the scheduling horizon T under the worse-case wind power scenario. The quadratic generation cost function regarding the thermal output P_{Gi} is linearized by N_k piecewise linear segments with slop c_{ik} and a fixed cost c_{i0}. G is the set of all thermal generators, $G=CG\cup NG$, where CG and NG are the sets of coal-fired and gas-fired generators, respectively. GW, PD, and GD are the sets of gas wells, electric loads, and gas loads. Q, ΔP, and ΔQ are the gas production, electric load shedding, and gas load shedding, respectively. σ_g, σ_{ps}, and σ_{gs} are the gas price, power load shedding penalty, and gas load shedding penalty, respectively. Eq. (4.11) represents the electricity network constraints with power transmission N-1 contingencies, and (4.12) are the gas network constraints considering pipeline N-1.

The automatic generation control (AGC) for adjusting power output of units is utilized for accommodating wind power uncertainty. The participation factor β_i is used to allocate the power adjustment of unit i, $\sum_{i\in G}\beta_i=1,\ \beta_i\ge 0,\ \forall i$. According to [112], by eliminating the uncertain variables, the adjustable robust counterpart of this model is derived as a quadratic programming problem, which can be solved by available optimization software.

4.4 Case Studies

A modified IEEE 6-bus electricity system coupled with a 7-node natural gas network is used for case study. The details of the system can be found in [78]. A wind farm is connected to node 2. The wind power penetration r=20%. The proposed model is implemented in MATLAB and solved using CPLEX on a PC with Intel Core i7 3.00 GHz CPU and 8 GB RAM. Four case studies are designed and discussed as follows:

Case 1: robust scheduling with no contingencies; *Case 2*: robust scheduling considering only power transmission line *N*-1 contingencies; *Case 3*: robust scheduling considering only gas pipeline *N*-1 contingencies; *Case 4*: robust scheduling considering both *N*-1 contingencies.

Table 4.1shows the results for all cases with r=20% and ζ varying from 0 to 60%, and Case 1 under r=20% and ζ=0 is the basis for comparison with other scenarios. Table 2 shows the results for all cases with ζ =20 and r varying from 0 to 60%, and Case 1 under ζ=20% and r=0 is the basis for comparison with other scenarios. It can be observed that if compared with Case 1, Case 2 (considering power transmission *N*-1 contingencies only) or Case 3 (gas pipeline contingencies only) leads to an increase in total generation cost. By considering both of the contingencies, the proposed model generates the most conservative solution (Case 4) at the highest generation cost. It can be easily observed that the robust scheduling raises the cost in order to address wind power uncertainty. This is reasonable and anticipated. Similarly, from Table 4.2, we can observe that with more constraints, a high-cost solution is needed. Also, the total cost reduces when more renewables are integrated.

Table 4.1 Percentage increase in expected cost under different uncertainty levels with 20% wind power penetration

ζ	Case 1	Case 2	Case 3	Case 4
0%	0	0.0496	0.1144	0.1199
20%	0.0076	0.0571	0.1219	0.1274
40%	0.0171	0.0663	0.1311	0.1367
60%	0.0280	0.0768	0.1416	0.1471

Table 4.2 Percentage increase in expected cost with different wind penetrations under 20% uncertainty level

r	Case 1	Case 2	Case 3	Case 4
0%	0	0.0900	0.2676	0.2726
20%	-0.0928	-0.0482	0.0101	0.0151
40%	-0.1363	-0.1243	-0.0940	-0.0929
60%	-0.1654	-0.1645	-0.1456	-0.1455

Further, the proposed model is applied to a modified IEEE 118-bus system with 14-node gas network. A 20% penetration of wind power is distributed at nodes 12, 17, 56, and 88. The uncertainty level is set to 20%. Here, 5 single power transmission contingency scenarios and all possible gas pipeline contingencies are considered. The computational time of the four cases are summarized in Table 4.3.

Table 4.3 Computational time of robust model

	Case 1	Case 2	Case 3	Case 4
CPU time(s)	5.8	80.2	6.9	110.3

Not surprisingly, the *N*-1 contingencies brings more computational burden. With more contingencies, the computational time increases substantially because each transmission contingency scenario needs a full N-1 transmission model while the gas network *N*-1 does not slow down the computation much due to the limited number of pipelines. The computational time can be acceptable for day-ahead power scheduling, esp., if only a few root-cause *N*-1 contingencies are modeled and a few critical lines are monitored.

CHAPTER 5

ROBUST EXPANSION CO-PLANNING FOR INTEGRATED GAS AND ELECTRICITY ENERGY SYSTEMS CONSIDERING WIND POWER AND LOAD UNCERTAINTIES

5.1 Introduction

During the past decade, power systems have undergone significant revolutions with the trend moving towards low-carbon and economic energy system. The outstanding features include the rapid development of natural gas-fired generators and renewable generation. Under the Clean Power Plan [116], the development of natural gas and renewables is accelerated, altering the way power grids operate. Driven by large gas reserve, high efficiency, operation flexibility, and low emissions, natural gas-fired generators gained increasing popularity for electricity generation. In New England ISO (ISO-NE), more than 50% of electricity is now generated from natural gas, compared to only 15% in 2000 [70]. The interdependency between gas and electricity networks is dramatically increased. The construction of new gas-fired generators should consider not only the capability of electricity network to send out electric power but also the fuel supply constraints of gas network for power generation [117]. In addition, the operation and planning of the gas-electricity integrated energy systems (IES) is facing more challenges that come from the uncertainties of increasing penetration of renewable generation and multiple energy loads, i.e., electric load and gas load. For future energy system planning, it necessitates a coordinated expansion planning model for gas and electricity IES that fully consider the interactions between the two energy sectors and system uncertainties [72][73].

There is some existing literature that addresses the coordinated operation and planning of gas and electricity IES. The short-term coordinated scheduling of gas and electricity IES have been studied in [7], [118]–[124]. For the co-planning of IES, in [2], an expansion planning model for combined gas and electricity networks is proposed to minimize gas and electricity operational costs and network expansion costs simultaneously. In [125], a reliability-based optimal planning model is proposed for an electricity and natural gas interconnection of energy hubs with multiple energy infrastructures. A long-term multi-area, multi-stage model integrated expansion planning of electricity and natural gas systems is presented in [4]. In [117], a linear programming approach is proposed for expansion co-planning in gas and electricity markets. In [126], a multi-objective optimization model for combined gas and electricity network expansion planning is proposed and solved by NSGA-II, which is a heuristic method and cannot guarantee global optimal solution. In [3], a security-constrained co-optimization planning model of electricity and natural gas transportation infrastructures is proposed.

Extensive researches have incorporated the uncertainties into power system planning. In [127], a tri-level reliability-constrained robust power system expansion planning framework is presented modeling the uncertainties of wind power and electricity demand. A robust optimization approach is presented in [128] for transmission network expansion planning under uncertainties of renewables generation and wind power. In [129], [130], stochastic programming is applied for power system planning under uncertainties. However, few works comprehensively consider the uncertain factors in the co-planning of gas-electricity IES. For the target year, the growth of both electric and gas loads may not be accurately predicted and the wind generation profiles are not forecasted perfectly. The system adequacy of the energy systems cannot be guaranteed without considering those uncertainties.

Therefore, this work proposes a two-stage robust expansion co-planning model for gas-electricity IES considering the uncertainties of wind power, gas load and electric loads. In the proposed model, the first stage minimizes the total investment cost and the second stage minimizes the total operation cost. The non-linear constraints of gas pipelines and compressors are linearized by the first-order Taylor expansion such that a mixed-integer linear programming (MILP) model is formulated, which can be solved efficiently. Further, to incorporate the uncertain factors, a two-stage robust optimization model is built. The locations and capacity of new gas-fired generators, power transmission lines and gas pipelines are optimally determined such that the future energy system is able to address the uncertainties of multi-energy loads growth and wind power. The effectiveness of the proposed method is verified by a coupled IEEE 6-bus electricity network and 7-node gas network.

5.2 Nomenclature

EG Set of existing power generators

ENG Set of existing natural gas-fired generators

PN Set of electricity network nodes

GN Set of natural gas network nodes

GW Set of gas wells

PD Set of electric demands

GD Set of gas demands

GC Set of gas compressors

GP Set of existing gas pipelines

NPGN Set of non-power gas nodes in gas network

EL Set of existing power transmission lines

CG Set of candidate gas-fired generators

CL Set of candidate power transmission lines

CP Set of candidate gas pipelines

$\mathcal{W}$ Set of wind power nodes

T Planning time horizon

$\boldsymbol{I_{lw}, I_{lg}, I_{lf}, I_{ld}}$ Incidence matrix of wind turbines, thermal units, power transmission lines, and electric loads.

$\boldsymbol{I_{nw}, I_{ng}, I_{nd}, I_{np}, I_{nc}}$ Incidence matrix of gas wells, gas-fired units, gas loads, pipelines, and compressors.

B Electric network DC power flow B matrix

$Q_{w,max}, Q_{w,min}$ Maximum / Minimum gas production of well w

C_p Pipeline p flow constant

$\pi_{m,max}, \pi_{m,min}$ Maximum/minimum pressure limit at node m

k_{c1}, k_{c2} Coefficients of compressor c

$R_{c,max}, R_{c,min}$ Maximum/minimum compression ratio of compressor c

$\alpha_c, \beta_c, \gamma_c$ Gas consumption coefficients for compressor c

Q_{ng} Gas consumption of gas-fired unit ng

$f_g( )$ Cost function of coal-fired generator g

λ_g Unit production price for natural gas, \$/kcf

$\lambda_{ue}, \lambda_{ug}$ Penalty for electric/gas load shedding

$P_{g,max}, P_{g,min}$ Maximum/minimum output of generator g

$\theta_{min}, \theta_{max}$ Minimum and Maximum angle limit

$P_{l,max}$ Power flow limit of line l

P_w Output of wind power

θ_{ref} Phase angle of reference bus at time t

μ_g Energy conversion efficiency of unit g

ζ_i, ξ_i, τ_i Uncertainty level of wind power, electric load and gas load at node i

$EENS_T$ Target value of expected energy not supplied

$x_g^G, x_l^{elec}, x_p^{gas}$ Status of unit g, power transmission line l, and gas pipeline p (1 constructed, 0 otherwise)

$Q_{w,t}$ Gas production of well w at time t

$\Delta P, \Delta Q$ Unserved electric load and natural gas load

Q_c Natural gas consumption of compressor c

H_c Horsepower of compressor c

$f_{p,t}$ Gas flow through pipeline p at time t

$f_{c,t}$ Gas flow through compressor c at time t

$\pi_{m,t}$ Pressure of node m at time t

$P_{g,t}$ Power output of generator g at time t

$P_{flow,l,t}$ Power flow through line l at time t

θ_i Voltage angle of bus i

5.3 Linearized Gas Network Model

The natural gas network consists of gas well, gas pipeline, compressor, gas storage and gas loads. Natural gas is produced at gas wells and transmitted through pipelines propelled by compressors then delivered to the gas load sites. In this paper, two types of gas loads are considered: gas consumptions for gas-fired generators and residential/industrial/commercial gas

loads. In this section, the models of the gas network are presented. In addition, the non-convex gas pipeline and compressor models are linearized using the first-order Taylor expansion to make the optimization model in Section 5.4 computational efficient and trackable.

5.3.1 Gas Wells

The gas suppliers are modeled as positive gas injections at the gas well nodes. In each period, upper and lower limits are imposed on the available production of gas suppliers limited by the physical characteristics and long-term, mid-term gas contracts. In this proposed planning model, both natural gas storage and gas well facilities are modeled as natural gas suppliers [3].

$$Q_{w,\min} \le Q_{w,t} \le Q_{w,\max}, \quad \forall w \in GW, \forall t \tag{5.1}$$

5.3.2 Gas Pipeline

The gas flow through the pipeline is driven by the pressure difference between the two ends of a pipeline. Meanwhile, the physical factors, such as the length, diameter, operating temperature, altitude drop, and the friction of pipelines, also affect the gas flow. The gas flow from node *m* to node *n*, f_p (kcf/hr) is expressed as

$$f_{p,t} = \text{sgn}(\pi_{m,t}, \pi_{n,t}) C_p \sqrt{\left|\pi_{m,t}^2 - \pi_{n,t}^2\right|}, \ \forall p \in GP, \forall t$$
$$\text{sgn}(\pi_{m,t}, \pi_{n,t}) = \begin{cases} 1 & \pi_{m,t} \ge \pi_{n,t} \\ -1 & \pi_{m,t} < \pi_{n,t} \end{cases} \tag{5.2}$$

where $\text{sgn}(\pi_m, \pi_n)$ indicates the direction of the gas flow, when it is 1, the gas flows from node *m* to *n*.

5.3.3 Gas Compressor

To compensate for the pressure loss, the gas compressors utilize horse power to provide pressure for the gas flow.

The gas flow from node *m* to node *n* through the compressor *c*, f_c is expressed as

$$f_{c,t} = \mathrm{sgn}(\pi_{m,t}, \pi_{n,t}) \frac{H_{c,t}}{k_{c2} - k_{c1}[\frac{\max(\pi_{m,t}, \pi_{n,t})}{\min(\pi_{m,t}, \pi_{n,t})}]^{\alpha}}, c \in GC, \forall t \quad (5.3)$$

The horse power of gas compressor *c* is subject to its physical limits.

$$H_{c,\min} \le H_{c,t} \le H_{c,\max} \quad (5.4)$$

The ratio between the pressures of the outlet node and inlet node is limited by (5.5).

$$R_{c,\min} \le \frac{\max(\pi_{m,t}, \pi_{n,t})}{\min(\pi_{m,t}, \pi_{n,t})} \le R_{c,\max} \quad (5.5)$$

The gas consumption of compressors is expressed as

$$Q_{c,t} = f_c(H_{c,t}) = \gamma_c + \beta_c H_{c,t} + \alpha_c H_{c,t}^2 \quad (5.6)$$

5.3.4 Gas Flow Nodal Balance

For each node in the gas network, the total natural gas positive injections and negative injections are balanced at each period.

$$\boldsymbol{I_{nw} \cdot Q_w - I_{ng} \cdot Q_{ng} - I_{nd} \cdot Q_d - I_{np} f - I_{nc} Q_c = -\Delta Q} \quad (5.7)$$

5.3.5 Linearization of Gas Network Model

The Taylor-series expansion is adopted in this paper to linearize the non-convex equations (5.2) and (5.3). The first-order Taylor expansion of equation (5.2) at the given pressure values π_M and π_N is given in (5.8).

$$f_p(\pi_m,\pi_n) \le f_p(\pi_M,\pi_N) + \frac{\partial f_p}{\partial \pi_m}(\pi_m - \pi_M) + \frac{\partial f_p}{\partial \pi_n}(\pi_n - \pi_N), \quad p \in GP \tag{5.8}$$

Introduce a set of Z evenly distributed points to split the range of node pressures for inlet and outlet nodes respectively, which gives Z tuples denoted as ($\pi_{M,z}$, $\pi_{N,z}$) for pipeline p, where z = 1, 2,…, Z. Hence, replace the nonlinear Weymouth equation (5.2) with a set of linearized inequality constraints as

$$f_{p,t} \le C_p \frac{\pi_{M,z}}{\sqrt{\pi_{M,z}^2 - \pi_{N,z}^2}} \pi_{m,t} - C_p \frac{\pi_{N,z}}{\sqrt{\pi_{M,z}^2 - \pi_{N,z}^2}} \pi_{n,t}, \ \forall p \in GP \tag{5.9}$$

where for each pipeline p (from node m to node n), only one of the Z inequality constraints that best approximate the original constraint (5.2) will be binding [99].

The natural gas flow through the gas pipeline with compressors can also be linearized using first-order Taylor-series expansion at a fixed point (H_{c0}, π_{m0}, π_{n0}). The linearized formulation of (5.3) is given by

$$f_{c,t} = -\frac{H_{c0}}{k_2 - k_1 R_0^{\alpha_j}} + \frac{\partial f_c}{\partial H_c} \times (H_{c,t} - H_{c0}) + \frac{\partial f_c}{\partial \pi_m} \times (\pi_{m,t} - \pi_{m0}) + \frac{\partial f_c}{\partial \pi_n} \times (\pi_{n,t} - \pi_{n0}), \ c \in GC \tag{5.10}$$

The initial compression ratio $R_0=\pi_{m0}/\pi_{n0}$ should be checked and make sure it is within the compression ratio limits. In addition, constraint (5.6) can be easily linearized by piece-wise linearization method. Therefore, the gas network model can be linearized to facilitate solving the proposed two-stage robust expansion co-planning model.

5.4 Mixed Integer Linear Programming for Expansion Co-planning of IES

The framework for IES expansion co-planning can be divided into two layers where the upper level is to optimize the investment decisions and the lower level is the optimal operation layer. The objective of the planning problem is to minimize the total investment cost and the operation cost over the planning horizon. The investment cost results from installing new equipment, i.e., gas-fired generators, power transmission lines, and gas pipelines. The operation cost consists of the gas production cost, generation cost of non-gas fired generators, as well as penalty for unserved electric and gas loads. The gas network uses the linearized model presented in Section II and the electricity network adopts the direct current (DC) power flow model. The two energy sectors are linked by the gas-fired generators, which can be viewed as power sources in the electricity network and meanwhile gas load in the gas network. The expansion co-planning model for gas-electricity IES can be formulated as follows.

$$\begin{aligned}\min\ J(\boldsymbol{X},\boldsymbol{Y}) = & \underbrace{\sum_{g\in CG} C_g^G \cdot x_g^G + \sum_{l\in CL} C_l^{elec} \cdot x_l^{elec} + \sum_{p\in CP} C_p^{gas} \cdot x_p^{gas}}_{\text{Investment cost}} \quad \text{Planning layer} \\ & \left.\begin{aligned} & + \underbrace{\sum_{t\in T}\left(\sum_{g\in EG\setminus ENG} f_g(P_{g,t}) + \sum_{w\in GW} \lambda_w \cdot Q_{w,t}\right)}_{\text{Production cost}} \\ & + \underbrace{\sum_{t\in T}\sum_{i\in PN} \lambda_{ue} \cdot \Delta P_{i,t} + \sum_{t\in T}\sum_{m\in NPGN} \lambda_{ug} \cdot \Delta Q_{m,t}}_{\text{Penalty for unserved loads}} \end{aligned}\right\} \text{Operation layer}\end{aligned} \tag{5.11}$$

s.t.

1) Investment variables

$$\begin{aligned} & x_g^G \in \{0,1\},\ x_l^{elec} \in \{0,1\},\ x_p^{gas} \in \{0,1\} \\ & \forall g \in CG,\ \forall l \in CL,\ \forall p \in CP \end{aligned} \tag{5.12}$$

2) Gas network constraints:

(5.1), (5.4)-(5.10)

$$f_{p,t} - C_p \left(\frac{\pi_{M,z}}{\sqrt{\pi_{M,z}^2 - \pi_{N,z}^2}} \pi_{m,t} - \frac{\pi_{N,z}}{\sqrt{\pi_{M,z}^2 - \pi_{N,z}^2}} \pi_{n,t} \right) \le M_g \cdot (1 - x_p^{gas}) \tag{5.13}$$

$$-M_g \cdot x_p^{gas} \le f_{p,t} \le M_g \cdot x_p^{gas} \tag{5.14}$$

$$0 \le \Delta Q_{i,t} \le Q_{d,t}, \quad \forall i \in NPGN, \forall t \tag{5.15}$$

$$\pi_{m,\min} \le \pi_{m,t} \le \pi_{m,\max}, \quad \forall m \in GN, \forall t \tag{5.16}$$

Power network constraints:

$$\boldsymbol{I_{lw}} \cdot \boldsymbol{P_w} + \boldsymbol{I_{lg}} \cdot \boldsymbol{P_g} - \boldsymbol{I_{lf}} \cdot \boldsymbol{P_{flow}} - \boldsymbol{I_{ld}} \cdot \boldsymbol{P_d} = -\Delta \boldsymbol{P} \tag{5.17}$$

$$P_{g,\min} \le P_{g,t} \le P_{g,\max}, \quad \forall g \in EG, \forall t \tag{5.18}$$

$$P_{g,\min} \cdot x_g^G \le P_{g,t} \le P_{g,\max} \cdot x_g^G, \quad \forall g \in CG, \forall t \tag{5.19}$$

$$0 \le \Delta P_{i,t} \le P_{d,t}, \quad \forall i \in PN, \forall t \tag{5.20}$$

$$B_l(\theta_{i,t} - \theta_{j,t}) - P_{flow,l,t} = 0, \quad l \in EL, \forall t \tag{5.21}$$

$$B_l(\theta_{i,t} - \theta_{j,t}) - P_{flow,l,t} \le M_e \cdot (1 - x_l^{elec}), \quad \forall l \in CL, \forall t \tag{5.22}$$

$$B_l(\theta_{i,t} - \theta_{j,t}) - P_{flow,l,t} \ge -M_e \cdot (1 - x_l^{elec}), \quad \forall l \in CL, \forall t \tag{5.23}$$

$$-P_{l,\max} \le P_{flow,l,t} \le P_{l,max}, \quad l \in EL, \forall t \tag{5.24}$$

$$-P_{l,\max} \cdot x_l^{elec} \le P_{flow,l,t} \le P_{l,max} \cdot x_l^{elec}, \quad \forall l \in CL, \forall t \tag{5.25}$$

$$\theta_{\min} \le \theta_{i,t} \le \theta_{\max}, \quad \forall i \in PN, \forall t \tag{5.26}$$

$$\theta_{ref,t} = 0, \quad \forall t \tag{5.27}$$

$$EENS \le EENS_T \tag{5.28}$$

In the above model, the investment decision variables of gas-fired generators, power transmission lines, and gas pipelines are defined as binary variables in (5.12), where 1 indicates

new construction and 0 otherwise. (5.1) and (5.4)-(5.10) represent the existing network model. (5.13) and (5.14) model the operation constraints of candidate gas pipelines. The unserved gas load amount is subject to constraint (5.15) and all the nodal pressure should respect its upper and lower limit in (5.16). In (5.13) and (5.14), Mg is the big-M value that ensures the constraints no-binding when this candidate pipeline is not selected. When $x_p^{gas} = 1$, the candidate pipeline will be built and the gas flow through this pipeline will subject to pipeline flow equation (5.8). When $x_p^{gas} = 0$, the candidate pipeline will not be built and (5.14) forces the pipeline flow to 0.

(5.17)-(5.28) represent the power network constraints. (5.17) is the power nodal balance that includes all existing and candidate generators and power transmission lines. (5.18) and (5.19) is the generation limits for existing and candidate generators respectively. (5.21) is the line flow equation of the existing power transmission lines. (5.22)-(5.23) are the operation constraints of candidate power transmission lines, where the Me is the big-M value for power transmission such that the two constraints will be relaxed if this candidate power transmission line is not selected. (5.24) and (5.25) are the line flow constraints for existing and candidate transmission lines. (5.26) is the voltage angle limit, where the chosen max and min bus angle values are ±0.6 radians. The phase angle of the reference bus is set to 0 in (5.27). The total expected energy not supplied (EENS) for the target year should meet the requirement in (5.28).

3) Linkage between gas and electricity networks

$$P_{g,t} = \mu_g Q_{ng,t} \quad \forall g \in ENG, \forall t \tag{5.29}$$

$$P_{g,t} \cdot x_g^G = \mu_g Q_{ng,t} \cdot x_g^G \quad \forall g \in CG, \forall t \tag{5.30}$$

The relationship between power generation and natural gas consumption is modeled through an energy conversion efficiency as show in (5.29) and (5.30). A typical heat rate of natural

gas is adopted. Gas-fired units are the components that link the two energy networks together. They consume natural gas as a type of gas load in the gas network and are involved in gas nodal balance constraint (5.7). Meanwhile, they generate electric power for the electricity network and thus are involved in power nodal balance (5.17). It is noted that the operation cost of gas-fired generating units is not included in the objective function since it has been reflected by the production cost in the natural gas network.

5.5 Two-stage Robust Optimization Model for Expansion Co-planning of IES

The forecasting of wind power generation, electric load demand and gas load demand will directly impact the investment decision of the target planning year in the expansion co-planning of IES [95]. A two-stage robust optimization model is formulated in this paper to address the uncertainties of wind power as well as electric/gas loads. The uncertainty set is defined as

$$\mathbf{\Gamma}=\begin{Bmatrix} P_{w,i}: P_{w,i}-P_{w,i}\zeta_i \le P_{w,i} \le P_{w,i}+P_{w,i}\zeta_i,\ i\in\mathcal{W} \\ P_{d,i}: P_{d,i}-P_{d,i}\xi_i \le P_{d,i} \le P_{d,i}+P_{d,i}\xi_i,\quad i\in PD \\ Q_{d,i}: Q_{d,i}-Q_{d,i}\tau_i \le Q_{d,i} \le Q_{d,i}+Q_{d,i}\tau_i, i\in NPGN \end{Bmatrix} \tag{5.31}$$

Firstly, the model in Section III is rewritten in a compact form incorporating the uncertainties of wind power and load demands.

$$\min_{\mathbf{X,Y}} \quad \mathbf{C}^{\mathbf{T}}\cdot\mathbf{X}+\mathbf{B}^{\mathbf{T}}\cdot\mathbf{Y} \tag{5.32}$$

$$s.t. \quad \mathbf{AY}\ge\mathbf{D} \tag{5.33}$$

$$\mathbf{KY}\ge\mathbf{u} \tag{5.34}$$

$$\mathbf{GX}-\mathbf{EY}\ge\mathbf{H} \tag{5.35}$$

$$\mathbf{X}\in\{0,1\},\ \mathbf{u}\in\mathbf{\Gamma} \tag{5.36}$$

where **u** represents the uncertain variables, i.e. $\mathbf{P_w}$, $\mathbf{P_d}$, and $\mathbf{Q_d}$. **X** is the set of investment binary variables and **Y** is the set of operational continuous variables. The terms $\mathbf{C^T}\cdot\mathbf{X}$ and $\mathbf{B^T}\cdot\mathbf{Y}$ represent

the investment cost and operation cost, respectively. (5.34) denotes the constraints that contain the uncertain variables. (5.35) represents the constraints that include both investment variables and operation variables. And (5.33) summarize all other constraints of optimal gas-electricity energy flow.

Further, the model (5.32)-(5.36) can be recast as a "min-max-min" two-stage robust optimization model as follows. Aiming to minimize the total investment and operation cost, the first stage determines the optimal investment decision that is prior to the realization uncertain variables. The second stage optimally coordinates the operation of the gas network and electricity network under the worst-case realization of uncertain wind power, gas and electricity load demands.

$$\min_{\mathbf{X}}\left(\mathbf{C}^{\mathbf{T}}\cdot\mathbf{X}+\max_{\mathbf{u}\in\Gamma}\min_{\mathbf{Y}\in\boldsymbol{\Phi}}\mathbf{B}^{\mathbf{T}}\cdot\mathbf{Y}\right) \tag{5.37}$$

$$s.t.\quad \mathbf{AY}\geq\mathbf{D},\ \ \mathbf{X}\in\{0,1\} \tag{5.38}$$

$$\boldsymbol{\Phi}=\left\{\mathbf{KY}\geq\mathbf{u},\mathbf{GX}-\mathbf{EY}\geq\mathbf{H}\right\} \tag{5.39}$$

The optimal solution of this model will provide a least-cost investment decision, including the sites and capacity of gas-fired units, installment of gas pipelines and power transmission lines that is robust against the uncertainties in the co-expansion planning of IES.

5.6 Solution Methodology

The column and constraint generation (C&CG) algorithm [96] is applied to solve the proposed two-stage robust optimization model of co-expansion planning of IES. The C&CG is a cutting plane procedure with a master-subproblem iterative process. It has been proven to be more efficient than the widely-used Bender Decomposition method [97]. The implementation of C&CG in solving the proposed two-stage robust optimization model will be introduced in this section.

Firstly, the model in (5.37)-(5.39) is decomposed into a master problem (MP) and a sub-problem (SP).

5.6.1 Sub-problem

The operation subproblem is the max-min part in (5.37), which generates the worst-case scenario for the master problem. The optimal objective value is used to set an upper bound for (5.37). For a given optimal solution of the investment master problem $\mathbf{X}^*$, i.e. investment decision variables, the subproblem is expressed as follows.

$$\begin{aligned}(\mathbf{SP}) \qquad \Psi(\mathbf{X}^*) = \max_{\mathbf{u}\in\boldsymbol{\Gamma}} \min_{\mathbf{Y}\in\boldsymbol{\Phi}(\mathbf{X}^*)} \{ & \mathbf{B}^{\mathrm{T}}\mathbf{Y} : \mathbf{A}\mathbf{Y} \geq \mathbf{D}, \\ & \mathbf{K}\mathbf{Y} \geq \mathbf{u}, \mathbf{G}\mathbf{X}^* - \mathbf{E}\mathbf{Y} \geq \mathbf{H}\}\end{aligned} \tag{5.40}$$

To solve this bi-level problem, the inner "min" primal problem, which is a linear model, can be converted to the "max" dual problem according to the strong duality theory. In this way, it becomes a "max-max" problem. Hence, the subproblem can be transformed to a single level "max" problem, formulated as follows.

$$\begin{aligned}(\mathbf{SP}) \qquad \Psi(\mathbf{X}^*) = \max_{\boldsymbol{\pi},\boldsymbol{\lambda},\mathbf{z},\mathbf{u}} \{ & \mathbf{D}^{\mathrm{T}}\boldsymbol{\pi} + \mathbf{u}^{\mathrm{T}}\boldsymbol{\lambda} + (\mathbf{H} - \mathbf{G}\mathbf{X}^*)^{\mathrm{T}}\mathbf{z} : \\ & \mathbf{A}^{\mathrm{T}}\boldsymbol{\pi} + \mathbf{K}^{\mathrm{T}}\boldsymbol{\lambda} + \mathbf{E}^{\mathrm{T}}\mathbf{z} \leq \mathbf{D} \\ & \boldsymbol{\pi}, \boldsymbol{\lambda}, \mathbf{z} \geq \mathbf{0} \quad \mathbf{u} \in \boldsymbol{\Gamma}\}\end{aligned} \tag{5.41}$$

where $\boldsymbol{\pi}$, $\boldsymbol{\lambda}$, and $\mathbf{z}$ are the dual variables corresponding to each constraint in (5.40). In (5.41), both $\mathbf{u}$ and $\boldsymbol{\lambda}$ are variables, which make the term $\mathbf{u}^{\mathrm{T}}\boldsymbol{\lambda}$, thus the whole model bi-linear. However, the optimal solution of this subproblem will be on either the upper or lower bound of the uncertainty set $\boldsymbol{\Gamma}$. Thus, by using the big-M method, this bilinear term can be eliminated. The uncertainty variables can be expressed as

$$\mathbf{u} = \mathbf{u}^{-} + (\mathbf{u}^{+} - \mathbf{u}^{-}) \cdot \boldsymbol{\varepsilon} \tag{5.42}$$

where $\mathbf{u}^-$ and $\mathbf{u}^+$ are the lower and upper bound of the uncertain variables. $\boldsymbol{\varepsilon}$ is binary variable. If $\boldsymbol{\varepsilon}$=1, the uncertain variable reaches the upper bound. Then the bilinear term $\mathbf{u}^{\mathbf{T}}\boldsymbol{\lambda}$ can be represented as

$$\mathbf{u}^{\mathbf{T}}\boldsymbol{\lambda} = \left(\mathbf{u}^- + \left(\mathbf{u}^+ - \mathbf{u}^-\right)\boldsymbol{\varepsilon}\right)^{\mathbf{T}}\boldsymbol{\lambda} = \left(\mathbf{u}^-\right)^{\mathbf{T}}\boldsymbol{\lambda} + \boldsymbol{\varepsilon}^{\mathbf{T}}\left(\mathbf{u}^+ - \mathbf{u}^-\right)^{\mathbf{T}}\boldsymbol{\lambda} \tag{5.43}$$

By introducing a new continuous variable $\mathbf{T}$ and big-M constraints, the bilinear term can be linearized as

$$\mathbf{u}^{\mathbf{T}}\boldsymbol{\lambda} = \left(\mathbf{u}^-\right)^{\mathbf{T}}\boldsymbol{\lambda} + \left(\mathbf{u}^+ - \mathbf{u}^-\right)^{\mathbf{T}}\mathbf{T} \tag{5.44}$$

$$\boldsymbol{\lambda} - M(1-\boldsymbol{\varepsilon}) \le \mathbf{T} \le \boldsymbol{\lambda} + M(1-\boldsymbol{\varepsilon}) \tag{5.45}$$

$$-M\boldsymbol{\varepsilon} \le \mathbf{T} \le M\boldsymbol{\varepsilon} \tag{5.46}$$

Then the model in (5.41) can be reformulated as a mix integer linear programming (MILP) problem as

$$\begin{aligned}
&(\mathbf{SP})\ \ \Psi(\mathbf{X}^*) = \\
&\quad \max_{\boldsymbol{\pi},\boldsymbol{\lambda},\mathbf{z},\boldsymbol{\varepsilon},\mathbf{T}} \Big\{ \mathbf{D}^{\mathbf{T}}\boldsymbol{\pi} + (\mathbf{H} - \mathbf{G}\mathbf{X}^*)^{\mathbf{T}}\mathbf{z} + \left(\mathbf{u}^-\right)^{\mathbf{T}}\boldsymbol{\lambda} + \left(\mathbf{u}^+ - \mathbf{u}^-\right)^{\mathbf{T}}\mathbf{T} : \\
&\qquad\qquad \mathbf{A}^{\mathbf{T}}\boldsymbol{\pi} + \mathbf{K}^{\mathbf{T}}\boldsymbol{\lambda} + \mathbf{E}^{\mathbf{T}}\mathbf{z} \le \mathbf{D} \\
&\qquad\qquad \boldsymbol{\lambda} - M(1-\boldsymbol{\varepsilon}) \le \mathbf{T} \le \boldsymbol{\lambda} + M(1-\boldsymbol{\varepsilon}) \\
&\qquad\qquad -M\boldsymbol{\varepsilon} \le \mathbf{T} \le M\boldsymbol{\varepsilon} \\
&\qquad\qquad \boldsymbol{\varepsilon} \in \{0,1\} \quad \boldsymbol{\pi}, \boldsymbol{\lambda}, \mathbf{z} \ge \mathbf{0} \ \Big\}
\end{aligned} \tag{5.47}$$

5.6.2 Master Problem

The investment master problem is to find the optimal investment decision, which can be formulated as

$$(\mathbf{MP}) \qquad \min_{\mathbf{X},\eta,\mathbf{Y_k}} \ \mathbf{C}^{\mathbf{T}} \cdot \mathbf{X} + \eta \tag{5.48}$$

$$s.t. \qquad \eta \ge \mathbf{B}\mathbf{Y_k}, \ \mathbf{X} \in \{0,1\} \tag{5.49}$$

$$\mathbf{K}\mathbf{Y}_{\mathbf{k}} \geq \mathbf{u}_{\mathbf{k}} \tag{5.50}$$

$$\mathbf{G}\mathbf{X} - \mathbf{E}\mathbf{Y}_{\mathbf{k}} \geq \mathbf{H} \tag{5.51}$$

where $\mathbf{u_k}$ represents the worst-case scenario and $\mathbf{Y_k}$ is the optimal solution identified by the subproblem in the *k*th iteration.

5.6.3 Column and Constraint Generation Algorithm

The procedure of the C&CG algorithm is descried in the following steps to illustrate the solving process of the proposed two stage robust model.

Initialization: set LB=-∞, UB=+∞, k=0; Set a convergence tolerance κ;

WHILE UB−LB>κ :

Solve the MILP master problem in (5.48)-(5.51) to obtain an optimal solution $\mathbf{X}^*$ and η^* and update the LB=max{LB, $\mathbf{C}^{\mathbf{T}}\mathbf{X}^*+\eta^*$};

For the given $\mathbf{X}^*$, solve the MILP subproblem in (5.47), if the subproblem is feasible, the optimal objective $\Psi(\mathbf{X}^*)$, the optimal solution $\mathbf{Y_k}$, and the corresponding worst-case scenario ($\boldsymbol{\varepsilon}^*$, $\mathbf{u}^*$); otherwise, $\Psi(\mathbf{X}^*)$ is set to +∞. Then update the UB= min{UB, $\mathbf{C}^{\mathbf{T}}\mathbf{X}+\Psi(\mathbf{X}^*)$};

IF $\Psi(\mathbf{X}^*)<+\infty$ **THEN**

Create variables $\mathbf{Y_{k+1}}$ and add the following constraints to the master problem.

$$\eta \geq \mathbf{B}\mathbf{Y}_{\mathbf{k}+1} \tag{5.52}$$

$$\mathbf{K}\mathbf{Y}_{\mathbf{k}+1} \geq \mathbf{u}_{\mathbf{k}+1} \tag{5.53}$$

$$\mathbf{G}\mathbf{X} - \mathbf{E}\mathbf{Y}_{\mathbf{k}+1} \geq \mathbf{H} \tag{5.54}$$

ELSE

Create variables $\mathbf{Y_{k+1}}$ and add constraints (5.53) and (5.54) to the master problem;

END IF

1. k=k+1;

END WHILE

The constraints generated in Step 4 are optimality cuts and those in Step 5 are feasibility cuts. When the convergence criteria is reached, the iteration process stops and the optimal solution is achieved. This method could converge in a small number of iterations.

5.7 Case Studies

In this section, the proposed robust co-planning model is validated on a six-bus electricity network with a seven-node natural gas network. The proposed mode is implemented in MATLAB with YALMIP and solved by GUROBI 6.5 [131], which has the capability to solve large-scale optimization problems. The simulations are carried out on a PC with Intel Core i7 3.00 GHz CPU and 8 GB RAM.

A small IES consisting of a six-bus electricity network and a coupled seven-node gas network (denoted as the P6G7IES system) is depicted in Figure 5.1. The detailed network parameters are given in [7]. In the electricity network, three gas-fired generators are located at node 1, 2 and 6 respectively; three electricity loads are at node 3, 4 and 5; a 50-MW wind turbine (WT) is installed on node 3. In the gas network, two gas wells are at node 6 and 7 respectively, two residential gas loads are at node 1 and 3; and a compressor is installed on the pipeline between node 2 and 4. The penalty for electricity load shedding is 1,000 $/MW and 200 $/kcf for gas load shedding.

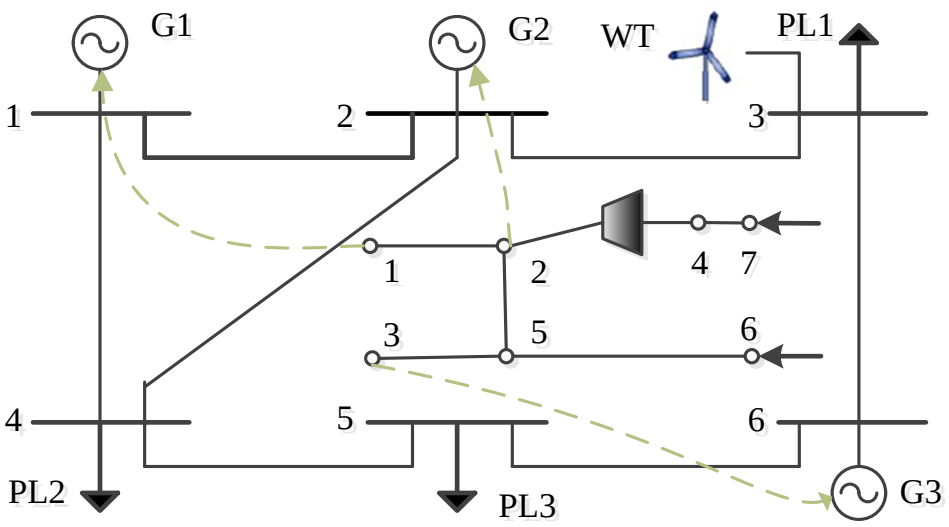

Figure 5.1 System topology of the P6G7IES system

The load blocks in the base year is shown in Table 5.1. For the target year, the electric load and gas load are expected to be increased by 50% and 30% respectively. The wind power output is divided into ten blocks within its capacity with preset probabilities, which are obtained through statistics analysis of typical yearly wind power profile. Combining 4 electric load blocks, 4 gas load blocks, and 10 wind power blocks, there are 160 scenarios generated in total with different probabilities during the target year. The EENS is set to 0.02% of the total electric demand in the electricity system. In the C&CG algorithm, the convergence tolerance is set to 1% and the MILP optimality gap is set to 0.01% by default.

Table 5.1 Load blocks in base year

Subperiod	1	2	3	4
Duration (%)	1	29	50	20
Electric Load (MW)	255.2	234.8	201.16	153.4
Gas load (kcf/hour)	6048	5565.6	4838.4	4356.0

The candidate power transmission line data is listed in Table 5.2. For the IES network, two candidate pipelines and transmission lines are considered on each corridor and two candidate 100 MW gas-fired generating units are considered on each bus. Thus, there are 12 candidate gas-fired units, 10 gas pipelines and 22 power transmission lines in total in this IES. The parameters of each gas pipeline are the same with the existing pipeline on that corridor. The investment cost for each pipeline is set to $1000,000 and the cost for per 100 MW gas fired unit is $ 500, 000. All the investment costs are annualized.

The uncertainties of electric load, gas load, and wind power are all set to 20% in this case study.

Table 5.2 Candidate power transmission line data

Line	From	To	X(p.u.)	Capacity (MW)	Investment Cost ($/MW)
T1	1	2	0.17	200	5000
T2	1	4	0.258	100	12000
T3	2	4	0.197	100	10000
T4	5	6	0.14	100	5000
T5	2	3	0.037	100	12000
T6	4	5	0.037	100	10000
T7	3	6	0.018	100	5000
T8	1	5	0.2	100	12000
T9	1	6	0.48	100	10000
T10	2	5	0.31	100	12000
T11	2	6	0.31	100	10000

Five cases are studied.

Case 1 (base case): IES co-planning without considering uncertainties;

Case 2: IES co-planning considering 20% wind power uncertainty.

Case 3: IES co-planning considering 20% electric load uncertainty;

Case 4: IES co-planning considering 20% gas load uncertainty.

Case 5: IES co-planning considering all uncertainties from wind power, electric load, and gas load.

By applying the robust expansion co-planning model and C&CG algorithm, the planning schemes of the above five cases are optimally determined and shown in Table 5.3.

Table 5.3 Optimal planning schemes of Case 1-5 in the P6G7IES system

Case	Unit	Transmission Line	Gas Pipeline	Total Cost (M$)
Case 1	Bus 6	(1-5)	(1-2)	319
Case 2	Bus 6	(1-5)	(1-2)	321
Case 3	Bus 1 Bus 6	(1-4)	2×(1-2) (5-6) (4-7)	354
Case 4	Bus 6	(1-5)	2×(1-2) (3-5) (4-7)	383
Case 5	Bus 1, 6	(1-4)	2×(1-2) (3-5) (4-7) (5-6)	508

Comparing Case 1 and Case 2, it can be observed that the impact of wind power uncertainty is not big enough to change the investment decisions. But the operation cost of Case 2 is higher than Case 1 due to additional operation cost induced by the wind power uncertainty. In Case 3, because of the electric load uncertainty, an additional gas-fired geneartor is installed on Bus 1 compared to Case 1. To ensure the fuel supply for the gas-fired generators, four new gas pipelines are invested to enhance the gas network to fullfil the capability requirement of delivering natural gas. This reflects the interdependency between the gas network and power system. If the gas load uncertainty is further included, more infrustrures are added in Case 5 to ensure the energy adequcy

for both electricity network and gas network. Concenquently, the total cost is increased significantly due to higher operation cost and investement cost.

The compuational time of the above five cases is shown in Table 5.4. Case 1 is actually a deterministic model without considering any uncertainties. So the solving process is very fast compared to the other cases. For the robust co-planning models, the C&CG algorithm in Section V is applied and the optimization process is finished in two iterations. If more uncertain factors are considered, more binary varaibles will be introduced in the robust optimiazion model and thus the computational time will be raised. Therefore, the computational time of Case 5 is the highest.

Table 5.4 Computational time of Case 1-5

Case	Computational Time (seconds)
Case 1	10.97
Case 2	106.93
Case 3	269.34
Case 4	274.15
Case 5	369.56

From what discussed above, it can be observed that if all the uncertain factors are considered, the most conservative solution will be obtained, which causes higher cost as well as compuational resources. However, this would be the most robust scheme that is immune against all the uncertainties and ensures the energy supply capability for all the energy demands in the system.

5.8 Conclusions

This work presents a two-stage robust expansion co-planning model for gas-electricity IES considering the uncertainties of wind power, electric load, and gas load. The proposed model co-optimizes the planning decisions of both gas network and electricity network fully considering their

interactions and uncertain factors. The impacts of various uncertain factors are studied. The case studies demonstrate the interdependency between gas network and electricity network and it is necessary to co-plan the two energy systems together. It also shows that the robust model needs more computational resource and higher investment cost to address the uncertainties.

The main contributions of this are summarized as follows.

(1) Jointly consider the gas network and electricity network to formulate an expansion co-planning model. The gas network model is linearized and the planning model is formulated as a MILP problem, which can be solved efficiently.

(2) Address the uncertainties in future integrated system planning, such as multi-energy loads and wind power, by further proposing a two-stage robust expansion co-planning model.

The proposed planning model comprehensively considers the system adequacy of power generation and transmission resource as well as fuel supply network, system economy and system uncertainties in future IES planning, which has practical significance for the increasingly tight-coupled multiple energy systems.

CHAPTER 6

CONCLUSION

6.1 Main Contributions and Conclusion

This work consists of four main parts: 1) interval optimization based operation strategy considering wind power uncertainty; 2) stochastic optimization based day-ahead scheduling considering N-1 contingency and wind uncertainty; 3) robust scheduling for wind integrated energy systems considering both gas pipeline and power transmission N-1 contingencies; 4) a two-stage robust expansion co-planning model for gas-electricity IES considering uncertainties of wind power, electric load and gas load.

In Chapter 2, an interval optimization based operation strategy considering wind power uncertainty is proposed for gas-electricity IES. Both electricity and gas networks are modeled in detail and their security constraints are considered in the coordinated operation of IES. An incentive demand response program is incorporated into the model that provides both electricity and gas demand response options to customers. The utility companies could coordinate the peak electricity and gas load through the optimized IES demand response. Interval optimization is applied to the optimization model of IES coordinated operation to address wind power uncertainty.

In Chapter 3, a stochastic optimization based day-ahead scheduling model is proposed considering N-1 contingency and wind uncertainty. To fully consider the security issues in an integrated energy system, N-1 contingencies of both power transmission and natural gas pipeline are modeled and incorporated into the optimization of IES operation. The impacts of electricity *N*-1 contingency only, gas network *N*-1 contingency only, and both contingencies on IES operation are investigated. The non-convex gas network model is linearized by the first-order Taylor

expansion, which significantly reduces the solution complexity. Wind power uncertainty in the IES is addressed by stochastic programming. The proposed model ensures that the IES is able to sustain any possible single contingency in gas or power transportation networks in the presence of wind power uncertainty. The proposed model could coordinate various energy sources and optimize the energy flow in an integrated network with transmission constraints.

In Chapter 4, a robust scheduling model is proposed for wind integrated energy systems considering both power transmission and gas pipeline N-1 contingencies. The optimization model of the coordinated gas-electricity scheduling problem is reformulated to facilitate the application of robust optimization. Both gas pipeline and power transmission line N-1 contingencies are modeled and incorporated into the optimization model. The impact of various wind power penetrations and uncertainty levels on the optimization results is investigated.

In Chapter 5, a robust expansion co-planning model is proposed for IES considering wind power and multi-energy load uncertainties. An optimization model is proposed for coordinating the expansion planning of gas-electricity integrated energy systems fully considering the interactions between gas network and power system. A two-stage robust planning model is built for IES with considerations of wind power, electric load and gas load uncertainties. The optimal investment decisions are robust against any scenario in the uncertainty set.

6.2 Future Research Work

In the future work, the following aspects may be worthwhile to investigate:

1. Energy storage is playing an increasingly important role in system operation. In the future work, the impact of both electrical energy storage and gas storage could be studied in the operation of gas-electricity integrated energy systems.

2. The proposed co-optimization framework can also be expanded to multiple energy interconnections, such as district heating networks, smart transportation system and water-energy nexus.

LIST OF REFERENCES

[1] EIA, “Annual Energy Outlook 2016,” *U.S. Energy Inf. Adm.*, p. ES-5, 2016.

[2] M. Chaudry, N. Jenkins, M. Qadrdan, and J. Wu, “Combined gas and electricity network expansion planning,” *Appl. Energy*, vol. 113, pp. 1171–1187, 2014.

[3] X. Zhang, M. Shahidehpour, A. S. Alabdulwahab, and A. Abusorrah, “Security-Constrained Co-Optimization Planning of Electricity and Natural Gas Transportation Infrastructures,” *IEEE Trans. Power Syst.*, vol. 30, no. 6, pp. 2984–2993, 2015.

[4] C. Unsihuay-Vila, J. W. Marangon-Lima, a. C. Z. De Souza, I. J. Perez-Arriaga, and P. P. Balestrassi, “A model to long-term, multiarea, multistage, and integrated expansion planning of electricity and natural gas systems,” *IEEE Trans. Power Syst.*, vol. 25, no. 2, pp. 1154–1168, 2010.

[5] S. A. S. An, Q. L. Q. Li, and T. W. Gedra, “Natural gas and electricity optimal power flow,” in *2003 IEEE PES Transmission and Distribution Conference and Exposition IEEE*, 2003, vol. 1, no. 1, pp. 138–143.

[6] C. Unsihuay, J. W. M. Lima, and a. C. Z. De Souza, “Modeling the Integrated Natural Gas and Electricity Optimal Power Flow,” *2007 IEEE Power Eng. Soc. Gen. Meet.*, pp. 1–7, 2007.

[7] C. Liu, M. Shahidehpour, Y. Fu, and Z. Li, “Security-constrained unit commitment with natural gas transmission constraints,” *IEEE Trans. Power Syst.*, vol. 24, no. 3, pp. 1523–1536, 2009.

[8] M. Geidl and G. Andersson, “Optimal power flow of multiple energy carriers,” *IEEE Trans.*

Power Syst., vol. 22, no. 1, pp. 145–155, 2007.

[9] M. Chaudry, N. Jenkins, and G. Strbac, "Multi-time period combined gas and electricity network optimisation," *Electr. Power Syst. Res.*, vol. 78, no. 7, pp. 1265–1279, 2008.

[10] A. Quelhas, E. Gil, J. D. McCalley, and S. M. Ryan, "A Multiperiod Generalized Network Flow Model of the US Integrated Energy System: Part I-Model Description," *IEEE Trans. Power Syst.*, vol. 22, no. 2, pp. 829–836, 2007.

[11] A. Quelhas, E. Gil, J. D. McCalley, and S. M. Ryan, "A Multiperiod Generalized Network Flow Model of the U.S. Integrated Energy System: Part II – Simulation Results," *IEEE Trans. Power Syst.*, vol. 22, no. 2, pp. 829–836, 2007.

[12] P. Jirutitijaroen, S. Kim, O. Kittithreerapronchai, and J. Prina, "An optimization model for natural gas supply portfolios of a power generation company," *Appl. Energy*, vol. 107, pp. 1–9, 2013.

[13] R. Rubio, D. Ojeda-Esteybar, O. Ano, and A. Vargas, "Integrated natural gas and electricity market: A survey of the state of the art in operation planning and market issues," in *2008 IEEE/PES Transmission and Distribution Conference and Exposition: Latin America*, 2008, pp. 1–8.

[14] G. Strbac, "Demand side management: Benefits and challenges," *Energy Policy*, vol. 36, no. 12, pp. 4419–4426, 2008.

[15] C. Sahin, Z. Li, M. Shahidehpour, and I. Erkmen, "Impact of natural gas system on risk-constrained midterm hydrothermal scheduling," *IEEE Trans. Power Syst.*, vol. 26, no. 2,

pp. 520–531, 2011.

[16] X. Zhang, M. Shahidehpour, A. Alabdulwahab, and A. Abusorrah, “Hourly Electricity Demand Response in the Stochastic Day-Ahead Scheduling of Coordinated Electricity and Natural Gas Networks,” *IEEE Trans. Power Syst.*, vol. 31, no. 1, pp. 592–601, 2016.

[17] J. Guo, Y. Zhang, and M. A. Young, “Design and Implementation of a Real-Time Off-Grid Operation Detection Tool from a Wide-Area Measurements Perspective,” *IEEE Trans. Smart Grid*, vol. 6, no. 4, pp. 2080–2087, 2015.

[18] D. Zhou, J. Guo, Y. Zhang, and J. Chai, “Distributed data analytics platform for wide-area synchrophasor measurement systems,” *IEEE Trans. Smart Grid*, vol. 7, no. 5, pp. 2397–2405, 2016.

[19] J. Chai, J. Zhao, W. Yao, J. Guo, and Y. Liu, “Application of wide area power system measurement for digital authentication,” in *Proceedings of the IEEE Power Engineering Society Transmission and Distribution Conference*, 2016, pp. 1–5.

[20] J. Chai, Y. Liu, Y. Liu, N. Bhatt, and A. D. Rosso, “Measurement-based System Reduction Using Autoregressive Model,” in *Proc. IEEE Power Eng. Soc. Transm. Distrib. Conf.*, 2016, pp. 1–5.

[21] F. Hu, K. Sun, A. Del Rosso, E. Farantatos, and N. Bhatt, “Measurement-Based Real-Time Voltage Stability Monitoring for Load Areas,” *IEEE Trans. Power Syst.*, vol. 31, no. 4, pp. 2787–2798, 2016.

[22] K. Sun, F. Hu, and N. Bhatt, “A new approach for real-time voltage stability monitoring

using PMUs," *2014 IEEE Innov. Smart Grid Technol. - Asia (ISGT ASIA)*, pp. 232–237, 2014.

[23] F. Hu, K. Sun, A. Del Rosso, E. Farantatos, and N. Bhatt, "An adaptive three-bus power system equivalent for estimating voltage stability margin from synchronized phasor measurements," *2014 IEEE PES Gen. Meet. | Conf. Expo.*, pp. 1–5, 2014.

[24] F. Hu *et al.*, "Measurement-based Voltage Stability Assessment and Control on CURENT Hardware Test Bed System," in *IEEE Power Eng. Soc. Gen. Meet.*, 2016, pp. 1–5.

[25] T. Jiang, L. Bai, H. Jia, H. Yuan, and F. Li, "Identification of voltage stability critical injection region in bulk power systems based on the relative gain of voltage coupling," *IET Gener. Transm. Distrib.*, vol. 10, no. 7, pp. 1495–1503, 2016.

[26] L. Bai, T. Jiang, X. Li, F. Li, Y. Xu, and H. Jia, "Regions via Electrical Network Response and Dynamic Relative Gain," in *IEEE Power Eng. Soc. Gen. Meet.*, 2016, no. 1, pp. 1–5.

[27] T. Jiang, L. Bai, X. Li, H. Jia, F. Li, and Y. Xu, "Volt-VAR Interaction Evaluation in Bulk Power Systems," in *IEEE Power Eng. Soc. Gen. Meet.*, 2016, pp. 1–5.

[28] Y. Xu and F. Li, "Adaptive PI control of STATCOM for voltage regulation," *IEEE Trans. Power Deliv.*, vol. 29, no. 3, pp. 1002–1011, 2014.

[29] Y. Xu, F. Li, Z. Jin, and C. Huang, "Flatness-based adaptive control (FBAC) for STATCOM," *Electr. Power Syst. Res.*, vol. 122, pp. 76–85, 2015.

[30] T. Jiang, L. Bai, G. Li, H. Jia, Q. Hu, and H. Yuan, "Estimating inter-area dominant

oscillation mode in bulk power grid using multi-channel continuous wavelet transform," *J. Mod. Power Syst. Clean Energy*, vol. 4, no. 3, pp. 394–405, 2016.

[31] L. E. Bernal, F. Hu, and K. Sun, "Identification and Wide-area Visualization of the Centers of Oscillation for a Large-scale Power System," in *IEEE Power Eng. Soc. Gen. Meet.*, 2014, pp. 1–5.

[32] T. Jiang, L. Bai, F. Li, H. Jia, Q. Hu, and X. Jin, "Synchrophasor measurement-based correlation approach for dominant mode identification in bulk power systems," *IET Gener. Transm. Distrib.*, vol. 10, no. 11, pp. 2710–2719, 2016.

[33] X. Li, F. Li, H. Yuan, H. Cui, and Q. Hu, "GPU-based Fast Decoupled Power Flow with Preconditioned Iterative Solver and Inexact Newton Method," *IEEE Trans. Power Syst.*, 2016.

[34] X. Li and F. Li, "GPU-based power flow analysis with Chebyshev preconditioner and conjugate gradient method," *Electr. Power Syst. Res.*, vol. 116, pp. 87–93, 2014.

[35] F. Li and X. Li, "Estimation of the largest eigenvalue in Chebyshev preconditioner for parallel conjugate gradient method-based power flow computation," *IET Gener. Transm. Distrib.*, vol. 10, no. 1, pp. 123–130, 2016.

[36] Y. Xu, F. Li, Z. Jin, and M. Hassani Variani, "Dynamic Gain-Tuning Control (DGTC) Approach for AGC with Effects of Wind Power," *IEEE Trans. Power Syst.*, vol. 31, no. 5, pp. 3339–3948, 2016.

[37] C. Huang, F. Li, and Z. Jin, "Maximum Power Point Tracking Strategy for Large-Scale

Wind Generation Systems Considering Wind Turbine Dynamics," *IEEE Trans. Ind. Electron.*, vol. 62, no. 4, pp. 2530–2539, 2015.

[38] C. Huang, F. Li, T. Ding, Z. Jin, and X. Ma, "Second-order cone programming-based optimal control strategy for wind energy conversion systems over complete operating regions," *IEEE Trans. Sustain. Energy*, vol. 6, no. 1, pp. 263–271, 2015.

[39] Z. Jin and C. Huang, "DFIG Voltage Control Based on Dynamically Adjusted Control Gains," *J. Power Energy Eng.*, vol. 2, no. 8, pp. 45–58, 2014.

[40] H. Hu, Q. Shi, Z. He, J. He, and S. Gao, "Potential harmonic resonance impacts of PV inverter filters on distribution systems," *IEEE Trans. Sustain. Energy*, vol. 6, no. 1, pp. 151–161, 2015.

[41] Q. Shi, H. Hu, W. Xu, and J. Yong, "Low-order harmonic characteristics of photovoltaic inverters," *Int. Trans. Electr. Energy Syst.*, vol. 26, no. 2, pp. 347–364, 2016.

[42] R. Torquato, Q. Shi, W. Xu, and W. Freitas, "A Monte Carlo simulation platform for studying low voltage residential networks," *IEEE Trans. Smart Grid*, vol. 5, no. 6, pp. 2766–2776, 2014.

[43] C. Jiang, Q. Shi, Y. Tian, X. Li, S. Lin, and Y. Liu, "Sensitivity study on the stray voltage of low voltage residential networks," *2016 IEEE 8th Int. Power Electron. Motion Control Conf. IPEMC-ECCE Asia 2016*, pp. 2571–2576, 2016.

[44] X. Kou, "Particle Swarm Optimization Based Reactive Power Dispatch for Power Networks with Distributed Generation," Denver University, 2015.

[45] X. Fang, F. Li, Y. Wei, R. Azim, and Y. Xu, "Reactive power planning under high penetration of wind energy using Benders decomposition," *IET Gener. Transm. Distrib.*, vol. 9, no. 14, pp. 1835–1844, 2015.

[46] X. Fang, Q. Hu, F. Li, B. Wang, and Y. Li, "Coupon-Based Demand Response Considering Wind Power Uncertainty: A Strategic Bidding Model for Load Serving Entities," *IEEE Trans. Power Syst.*, vol. 31, no. 2, pp. 1025–1037, 2016.

[47] H. Cui, F. Li, X. Fang, and R. Long, "Distribution network reconfiguration with aggregated electric vehicle charging strategy," in *IEEE Power and Energy Society General Meeting*, 2015, pp. 1–5.

[48] Y. Xu, Q. Hu, and F. Li, "Probabilistic model of payment cost minimization considering wind power and its uncertainty," *IEEE Trans. Sustain. Energy*, vol. 4, no. 3, pp. 716–724, 2013.

[49] Q. Hu, F. Li, X. Fang, and L. Bai, "A Framework of Residential Demand Aggregation with Financial Incentives," *IEEE Trans. Smart Grid*, 2016.

[50] X. Fang, F. Li, Q. Hu, and Y. Wei, "Strategic CBDR bidding considering FTR and wind power," *IET Gener. Transm. Distrib.*, vol. 10, no. 10, pp. 2464–2474, 2016.

[51] X. Fang *et al.*, "Risk Constrained Scheduling of Energy Storage for Load Serving Entities Considering Load and LMP Uncertainties," *IFAC-PapersOnLine*, vol. 49, no. 27, pp. 318–323, 2016.

[52] X. Fang, F. Li, Y. Wei, and H. Cui, "Strategic scheduling of energy storage for load serving

entities in locational marginal pricing market," *IET Gener. Transm. Distrib.*, vol. 10, no. 5, pp. 1258–1267, 2016.

[53] J. Xiao, L. Bai, F. Li, H. Liang, and C. Wang, "Sizing of energy storage and diesel generators in an isolated microgrid Using Discrete Fourier Transform (DFT)," *IEEE Trans. Sustain. Energy*, vol. 5, no. 3, pp. 907–916, 2014.

[54] J. Xiao, L. Bai, Z. Lu, and K. Wang, "Method, implementation and application of energy storage system designing," *Int. Trans. Electr. Energy Syst.*, vol. 24, no. 3, pp. 378–394, 2014.

[55] L. Bai, F. Li, Q. Hu, H. Cui, and X. Fang, "Application of Battery-Supercapacitor Energy Storage System for Smoothing Wind Power Output: An Optimal Coordinated Control Strategy," *IEEE PES Gen. Meet.*, pp. 1–5, 2016.

[56] Y. Zhang, R. A. Dougal, and H. Zheng, "Tieline reconnection of microgrids using controllable variable reactors," *IEEE Trans. Ind. Appl.*, vol. 50, no. 4, pp. 2798–2806, 2014.

[57] A. Anwar, H. Zheng, R. A. Dougal, and Y. Zhang, "Fault-aware-soft-restart method for shipboard MVAC power system using inverter coupled energy storage system," *2013 IEEE Electr. Sh. Technol. Symp. ESTS 2013*, pp. 166–172, 2013.

[58] Y. Zhang, H. Zheng, H. A. Mohammadpour, and R. A. Dougal, "Real-time synchronization control for standalone distribution networks in islanded power systems," *45th North Am. Power Symp. NAPS 2013*, 2013.

[59] X. Kong, L. Bai, Q. Hu, F. Li, and C. Wang, "Day-ahead optimal scheduling method for

grid-connected microgrid based on energy storage control strategy," *J. Mod. Power Syst. Clean Energy*, vol. 4, no. 4, pp. 648–658, 2016.

[60] L. Bai, Q. Hu, F. Li, T. Ding, and H. Sun, "Robust mean-variance optimization model for grid-connected microgrids," *IEEE Power Energy Soc. Gen. Meet.*, pp. 1–5, 2015.

[61] H. Jiang, J. J. Zhang, W. Gao, and Z. Wu, "Fault Detection , Identification , and Location in Smart Grid Based on Data-Driven Computational Methods," vol. 5, no. 6, pp. 2947–2956, 2014.

[62] H. Jiang, Y. Zhang, J. J. Zhang, D. W. Gao, and E. Muljadi, "Synchrophasor-Based Auxiliary Controller to Enhance the Voltage Stability of a Distribution System with High Renewable Energy Penetration," *IEEE Trans. Smart Grid*, vol. 6, no. 4, pp. 2107–2115, 2015.

[63] H. Jiang, X. Dai, D. W. Gao, J. J. Zhang, Y. Zhang, and E. Muljadi, "Spatial-Temporal Synchrophasor Data Characterization and Analytics in Smart Grid Fault Detection, Identification, and Impact Causal Analysis," *IEEE Trans. Smart Grid*, vol. 7, no. 5, pp. 2525–2536, 2016.

[64] J. Xiao, L. Bai, Z. Zhang, and H. Liang, "Determination of the optimal installation site and capacity of battery energy storage system in distribution network integrated with distributed generation," *IET Gener. Transm. Distrib.*, vol. 10, no. 3, pp. 601–607, 2016.

[65] C. Huang *et al.*, "Data quality issues for synchrophasor applications Part II: problem formulation and potential solutions," *J. Mod. Power Syst. Clean Energy*, vol. 4, no. 3, pp.

353–361, 2016.

[66] C. Huang *et al.*, “Data quality issues for synchrophasor applications Part I: a review,” *J. Mod. Power Syst. Clean Energy*, vol. 4, no. 3, pp. 342–352, 2016.

[67] C. Huang, F. Li, T. Ding, Y. Jiang, J. Guo, and Y. Liu, “A Bounded Model of the Communication Delay for System Integrity Protection Schemes,” *IEEE Trans. Power Deliv.*, vol. 31, no. 4, pp. 1921–1933, 2016.

[68] EIA, “Annual Energy Review 2010,” 2011.

[69] C. Martinez-Mares, C. Fuerte-Esquivel, “A Unified Gas and Power Flow Analysis in Natural Gas and Electricity Coupled Networks,” *IEEE Trans. Power Syst.*, vol. 27, no. 4, pp. 2156–2166, 2012.

[70] H. Hunt, D. Dolan, and J. Rudiak, “New England Gas-Electric Focus Group Final Report,” 2014.

[71] M. Qadrdan, J. Wu, N. Jenkins, and J. Ekanayake, “Operating strategies for a gb integrated gas and electricity network considering the uncertainty in wind power forecasts,” *IEEE Trans. Sustain. Energy*, vol. 5, no. 1, pp. 128–138, 2014.

[72] T. Li, M. Eremia, and M. Shahidehpour, “Interdependency of natural gas network and power system security,” *IEEE Trans. Power Syst.*, vol. 23, no. 4, pp. 1817–1824, 2008.

[73] C. M. Correa-Posada and P. Sánchez-Martin, “Security-constrained optimal power and natural-gas flow,” *IEEE Trans. Power Syst.*, vol. 29, no. 4, pp. 1780–1787, 2014.

[74] H. Quan, D. Srinivasan, A. M. Khambadkone, and A. Khosravi, "A computational framework for uncertainty integration in stochastic unit commitment with intermittent renewable energy sources," *Appl. Energy*, vol. 152, pp. 71–82, 2015.

[75] J. Wang and A. Botterud, "Wind power forecasting uncertainty and unit commitment," *Appl. Energy*, vol. 88, no. 11, pp. 4014–4023, 2011.

[76] R. Jiang, S. Member, J. Wang, Y. Guan, and A. Sets, "Robust Unit Commitment With Wind Power and Pumped Storage Hydro," *IEEE Trans. Power Syst.*, vol. 27, no. 2, pp. 800–810, 2012.

[77] A. Martinez-mares, "A Robust Optimization Approach for the Interdependency Analysis of Integrated Energy Systems Considering Wind Power Uncertainty," in *IEEE Power Eng. Soc. Gen. Meet.*, 2014, pp. 1–5.

[78] Y. An and B. Zeng, "Exploring the modeling capacity of two-stage robust optimization: Variants of robust unit commitment model," *IEEE Trans. Power Syst.*, vol. 30, no. 1, pp. 109–122, 2015.

[79] C. Liu, C. Lee, and M. Shahidehpour, "Look ahead robust scheduling of wind-thermal system with considering natural gas congestion," *IEEE Trans. Power Syst.*, vol. 30, no. 1, pp. 544–545, 2015.

[80] T. Ding, Z. Bie, L. Bai, and F. Li, "Adjustable robust optimal power flow with the price of robustness for large-scale power systems," *IET Gener. Transm. Distrib.*, vol. 10, pp. 164–174, 2016.

[81] Y. Liu, C. Jiang, J. Shen, and J. Hu, "Coordination of Hydro Units with Wind Power Generation Using Interval Optimization," *IEEE Trans. Sustain. Energy*, vol. 6, no. 2, pp. 443–453, 2015.

[82] H. Huang, F. Li, and Y. Mishra, "Modeling Dynamic Demand Response Using Monte Carlo Simulation and Interval Mathematics for Boundary Estimation," *IEEE Trans. Smart Grid*, vol. 6, no. 6, pp. 2704–2713, 2015.

[83] L. Montuori, M. Alcázar-Ortega, C. Álvarez-Bel, and A. Domijan, "Integration of renewable energy in microgrids coordinated with demand response resources: Economic evaluation of a biomass gasification plant by Homer Simulator," *Appl. Energy*, vol. 132, pp. 15–22, 2014.

[84] Y. Mu, J. Wu, N. Jenkins, H. Jia, and C. Wang, "A Spatial-Temporal model for grid impact analysis of plug-in electric vehicles," *Appl. Energy*, vol. 114, pp. 456–465, 2014.

[85] L. Wu, M. Shahidehpour, and Z. Li, "Comparison of scenario-based and interval optimization approaches to stochastic SCUC," *IEEE Trans. Power Syst.*, vol. 27, no. 2, pp. 913–921, 2012.

[86] Y. Wang, Q. Xia, and C. Kang, "Unit commitment with volatile node injections by using interval optimization," *IEEE Trans. Power Syst.*, vol. 26, no. 3, pp. 1705–1713, 2011.

[87] R. E. Moore, R. B. Kearfott, and M. J. Cloud, *Introduction to Interval Analysis*. Society for Industrial and Applied Mathematics, 2009.

[88] G. Huang, B. W. Baetz, and G. G. Patry, "A grey linear programming approach for

municipal solid waste management planning under uncertainty," *Civ. Eng. Syst.*, vol. 9, pp. 319–335, 1992.

[89] A. Sengupta and T. K. Pal, "On comparing interval numbers: A study on existing ideas," *Stud. Fuzziness Soft Comput.*, vol. 238, pp. 25–37, 2009.

[90] J. Dobschinski, a. Wessel, B. Lange, K. Rohrig, L. Bremen, and M. Saint-Drenan, "Estimation of wind power prediction intervals using stochastic methods and artificial intelligence model ensembles," *Proc. Ger. Wind Energy Conf. DEWEK, Bremen*, vol. 54, p. 258, 2008.

[91] P. Pinson, H. A. Nielsen, H. Madsen, and G. Kariniotakis, "Skill forecasting from ensemble predictions of wind power," *Appl. Energy*, vol. 86, no. 7–8, pp. 1326–1334, 2009.

[92] C. Wan, Z. Xu, P. Pinson, Z. Y. Dong, and K. P. Wong, "Probabilistic forecasting of wind power generation using extreme learning machine," *IEEE Trans. Power Syst.*, vol. 29, no. 3, pp. 1033–1044, 2014.

[93] C. Liu, M. Shahidehpour, Y. Fu, and Z. Li, "Security-Constrained Unit Commitment With Natural Gas Transmission Constrains," *IEEE Trans. Power Syst.*, vol. 24, no. 3, pp. 1523–1536, 2009.

[94] Q. Li, S. An, and T. Gedra, "Solving natural gas loadflow problems using electric loadflow techniques," *Proc. North Am. Power Symp.*, 2003.

[95] J. Lofberg, "YALMIP : a toolbox for modeling and optimization in MATLAB," *2004 IEEE Int. Conf. Comput. Aided Control Syst. Des.*, pp. 284–289, 2004.

[96] C. Unsihuay, J. W. Marangon-Lima, and A. C. Zambroni De Souza, "Short-term operation planning of integrated hydrothermal and natural gas systems," in *2007 IEEE Lausanne POWERTECH, Proceedings*, 2007, pp. 1410–1416.

[97] A. Alabdulwahab, A. Abusorrah, X. Zhang, and M. Shahidehpour, "Coordination of Interdependent Natural Gas and Electricity Infrastructures for Firming the Variability of Wind Energy in Stochastic Day-Ahead Scheduling," *IEEE Trans. Sustain. Energy*, vol. 6, no. 2, pp. 606–615, 2015.

[98] L. Bai, F. Li, H. Cui, T. Jiang, H. Sun, and J. Zhu, "Interval optimization based operating strategy for gas-electricity integrated energy systems considering demand response and wind uncertainty," *Appl. Energy*, vol. 167, pp. 270–279, 2016.

[99] H. Cui, F. Li, Q. Hu, L. Bai, and X. Fang, "Day-ahead coordinated operation of utility-scale electricity and natural gas networks considering demand response based virtual power plants," *Appl. Energy*, vol. 176, pp. 183–195, 2016.

[100] C. M. Correa-Posada and P. Sanchez-Martin, "Stochastic contingency analysis for the unit commitment with natural gas constraints," in *2013 IEEE Grenoble Conference PowerTech, POWERTECH 2013*, 2013.

[101] M. Urbina and Z. Li, "A combined model for analyzing the interdependency of electrical and gas systems," *2007 39th North Am. Power Symp. NAPS*, pp. 468–472, 2007.

[102] P. J. Hibbard and T. Schatzki, "The Interdependence of Electricity and Natural Gas: Current Factors and Future Prospects," *Electr. J.*, vol. 25, no. 4, pp. 6–17, 2012.

[103] M. Shahidehpour, Yong Fu, and T. Wiedman, "Impact of Natural Gas Infrastructure on Electric Power Systems," *Proc. IEEE*, vol. 93, no. 5, pp. 1042–1056, 2005.

[104] D. De Wolf and Y. Smeers, "The Gas Transmission Problem Solved by an Extension of the Simplex Algorithm," *Manage. Sci.*, vol. 46, no. October 2014, pp. 1454–1465, 2000.

[105] L. Ouyang and K. Aziz, "Steady-state gas flow in pipes," *J. Pet. Sci. Eng.*, vol. 14, no. 3–4, pp. 137–158, 1996.

[106] K. W. Hedman, M. C. Ferris, R. P. O'Neill, E. B. Fisher, and S. S. Oren, "Co-optimization of generation unit commitment and transmission switching with N-1 reliability," *IEEE Trans. Power Syst.*, vol. 25, no. 2, pp. 1052–1063, 2010.

[107] G. Hasle, K.-A. Lie, E. Quak, T. Hagen, M. Henriksen, and J. Hjelmervik, "Optimization Models for the Natural Gas Value Chain," in *Geometric Modelling, Numerical Simulation, and Optimization*, 2007, pp. 211–264.

[108] Q. Wang, Y. Guan, and J. Wang, "A chance-constrained two-stage stochastic program for unit commitment with uncertain wind power output," *IEEE Trans. Power Syst.*, vol. 27, no. 1, pp. 206–215, 2012.

[109] Y. Liu, S. Gao, H. Cui, and L. Yu, "Probabilistic load flow considering correlations of input variables following arbitrary distributions," *Electr. Power Syst. Res.*, vol. 140, pp. 354–362, 2016.

[110] Y. Liu and N. C. Nair, "A Two-Stage Stochastic Dynamic Economic Dispatch Model Considering Wind Uncertainty," *IEEE Trans. Sustain. Energy*, vol. 7, no. 2, pp. 819–829,

2016.

[111] H. Heitsch and W. Römisch, “Scenario reduction algorithms in stochastic programming,” *Comput. Optim. Appl.*, vol. 24, no. 2–3, pp. 187–206, 2003.

[112] R. A. Jabr, S. Karaki, and J. A. Korbane, “Robust Multi-Period OPF With Storage and Renewables,” *IEEE Trans. Power Syst.*, vol. 30, no. 5, pp. 2790–2799, 2014.

[113] Y. Jia, Z. Xu, L. L. Lai, and K. P. Wong, “Risk-Based Power System Security Analysis Considering Cascading Outages,” *IEEE Trans. Ind. Informatics*, vol. 12, no. 2, pp. 872–882, 2016.

[114] Y. Jia, K. Meng, and Z. Xu, “N-k Induced Cascading Contingency Screening,” *IEEE Trans. Power Syst.*, vol. 30, no. 5, pp. 2824–2825, 2015.

[115] K. W. Hedman, R. P. O’Neill, E. B. Fisher, and S. S. Oren, “Optimal transmission switching with contingency analysis,” *IEEE Trans. Power Syst.*, vol. 24, no. 3, pp. 1577–1586, 2009.

[116] W. W. Hogan, “Electricity Markets and the Clean Power Plan,” *Electr. J.*, vol. 28, no. 9, pp. 9–32, 2015.

[117] J. Qiu, H. Yang, Z. Y. Dong, S. Member, and A. Parameters, “A Linear Programming Approach to Expansion Co-Planning in Gas and Electricity Markets,” *IEEE Trans. Power Syst.*, vol. 31, no. 5, pp. 1–13, 2015.

[118] M. Shahidehpour, C. Shao, X. Wang, X. Wang, and B. Wang, “An MILP-based Optimal Power Flow in Multi-Carrier Energy Systems,” *IEEE Trans. Sustain. Energy*, vol. 3029, no.

c, pp. 1–1, 2016.

[119] C. He, L. Wu, T. Liu, and M. Shahidehpour, “Robust Co-Optimization Scheduling of Electricity and Natural Gas Systems via ADMM,” *IEEE Trans. Sustain. Energy*, 2016.

[120] C. Wang *et al.*, “Robust Defense Strategy for Gas-Electric Systems Against Malicious Attacks,” *IEEE Trans. Power Syst.*, 2016.

[121] A. Zlotnik, L. Roald, S. Backhaus, M. Chertkov, and G. Andersson, “Coordinated Scheduling for Interdependent Electric Power and Natural Gas Infrastructures,” *IEEE Trans. Power Syst.*, vol. PP, no. 99, pp. 1–1, 2016.

[122] G. Li *et al.*, “Optimal dispatch strategy for integrated energy systems with CCHP and wind power,” *Appl. Energy*, 2016.

[123] G. Li, R. Zhang, T. Jiang, H. Chen, L. Bai, and X. Li, “Security-constrained bi-level economic dispatch model for integrated natural gas and electricity systems considering wind power and power-to-gas process,” *Appl. Energy*, 2016.

[124] L. Bai, F. Li, T. Jiang, and H. Jia, “Robust Scheduling for Wind Integrated Energy Systems Considering Gas Pipeline and Power Transmission N-1 Contingencies,” *IEEE Trans. Power Syst.*, vol. PP, no. 99, pp. 1–2, 2016.

[125] X. Zhang, L. Che, M. Shahidehpour, A. S. Alabdulwahab, and A. Abusorrah, “Reliability-based optimal planning of electricity and natural gas interconnections for multiple energy hubs,” *IEEE Trans. Smart Grid*, vol. PP, no. 99, 2015.

[126] Y. Hu, Z. Bie, T. Ding, and Y. Lin, "An NSGA-II based multi-objective optimization for combined gas and electricity network expansion planning," *Appl. Energy*, vol. 167, pp. 280–293, 2016.

[127] S. Dehghan, N. Amjady, and A. J. Conejo, "Reliability-Constrained Robust Power System Expansion Planning," *IEEE Trans. Power Syst.*, vol. 31, no. 3, pp. 2383–2392, 2016.

[128] R. A. Jabr, "Robust transmission network expansion planning with uncertain renewable generation and loads," *IEEE Trans. Power Syst.*, vol. 28, no. 4, pp. 4558–4567, 2013.

[129] J. A. Lopez, K. Ponnambalam, and V. H. Quintana, "Generation and Transmission Expansion Under Risk Using Stochastic Programming," *IEEE Trans. Power Syst.*, vol. 22, no. 3, pp. 1369–1378, 2007.

[130] P. Jirutitijaroen and C. Singh, "Reliability constrained multi-area adequacy planning using stochastic programming with sample-average approximations," *IEEE Trans. Power Syst.*, vol. 23, no. 2, pp. 504–513, 2008.

[131] G. O. Inc., "Gurobi Optimizer reference manual," *www.Gurobi.Com*, vol. 6, p. 572, 2014.

APPENDIX

List of Abbreviations

IES	Integrated Energy System
SCUC	Security Constrained Unit Commitment
CPP	Clean Power Plan
CURENT	Center for Ultra-Wide-Area Resilient Electric Energy Transmission
DA	Day Ahead
NERC	North American Electric Reliability Corporation
FERC	Federal Energy Regulatory Commission
DR	Demand Response
ED	Economic Dispatch
MILP	Mixed Integer Linear Programming
ISO	Independent System Operator
ISO-NE	New-England Independent System Operator
UTK	University of Tennessee at Knoxville
KD	Kantorovich Distance
OPF	Optimal Power Flow
AGC	Automatic Generation Control
WT	Wind Turbine
PV	Photovoltaics
LMP	Locational Marginal Price
C&CG	Column and Constraint Generation
EENS	Expected Energy Not Supplied
EV	Electric Vehicle

FFS	Fast forward selection

Publications during Ph.D. Study

Related Journal Papers

[J1] **Linquan Bai**, Fangxing Li, "Robust scheduling for wind integrated energy systems considering gas pipeline and power transmission N-1 contingencies," IEEE Trans. Power System, in press, 2016.

[J2] **Linquan Bai**, Fangxing Li, Hantao Cui, et al, "Interval optimization based operating strategy for gas-electricity integrated energy systems considering demand response and wind uncertainty," Applied Energy, vol. 167, pp. 270–279, 2016.

[J3] **Linquan Bai**, Fangxing Li, Hantao Cui, "Stochastic Optimal Scheduling for Integrated Energy Systems Considering Gas-Electricity *N*-1 Contingencies and Wind Power Uncertainty," to be submitted.

[J4] **Linquan Bai**, Fangxing Li, "Robust expansion co-planning for gas-electricity integrated energy systems considering uncertainties of wind power and multi-energy loads," IEEE Trans. Power Systems, submitted.

[J5] Jun Xiao, **Linquan Bai**, Fangxing Li, Haishen Liang, and Chengshan Wang, "Sizing of Energy Storage and Diesel Generators in an Isolated Microgrid using Discrete Fourier Transform (DFT)," IEEE Trans. Sustain. Energy, vol. 5, no. 3, pp. 907-916, Jul. 2014.

[J6] Tao Jiang, **Linquan Bai**, Hongjie Jia, Haoyu Yuan, Fangxing Li, "Identification of Voltage Stability Critical Injection Region in Bulk Power Systems based on the Relative Gain of Voltage Coupling," IET Gener. Transm. Distrib., vol. 10, no. 7, pp. 1495-1503, 2016.

[J7] Tao Jiang, **Linquan Bai**, Fangxing Li, et al, "Synchrophasor measurement-based correlation approach for dominant mode identification in bulk power systems", IET Gener. Transm. Distrib., vol. 10, no. 11, pp. 2710-2719, 2016.

[J8] Xiangyu Kong, **Linquan Bai**, Qinran Hu, Fangxing Li, Chengshan Wang, "Day-ahead optimal scheduling method for grid-connected microgrid based on energy storage control strategy", Journal of Modern Power Systems and Clean Energy, vol. 4, no. 4, pp. 648-548, 2016.

[J9] Tao Ding, Zhaohong Bie, **Linquan Bai**, Fangxing Li, "An adjustable robust optimal power flow with the price of robustness for large-scale power systems," IET Gener. Transm. Distrib., vol. 10, no. 1, pp. 164-174, Jan. 2016.

[J10] Hantao Cui, Fangxing Li, Qinran Hu, **Linquan Bai**, Xin Fang, "Day-ahead coordinated operation of utility-scale electricity and natural gas networks considering demand response based virtual power plants," Applied Energy, 2016.

[J11] Houhe Chen, Rufeng Zhang, Guoqing Li, **Linquan Bai**, Fangxing Li, "Economic dispatch of wind integrated power systems with energy storage considering composite operating costs," IET Gener. Transm. Distrib., vol 10, no. 5, pp. 1294-1303, 2016.

[J12] Qinran Hu, Fangxing Li, Xin Fang, **Linquan Bai**, "An Optimal Framework of Incentive based Residential Demand Aggregation," IEEE Trans. Smart Grid, In Press, 2016.

Conference Papers

[C1] **Linquan Bai**, Tao Ding, Qinran Hu, Fangxing Li, and Hongbin Sun, "Robust Mean-Variance Optimization Model for Grid-Connected Microgrids," *IEEE PES General Meeting 2015,* 5 pages, Denver, Colorado, July 26-30, 2015.

[C2] Fengzhang Luo, Tianyu Zhang, Zhaofeng Mi, Fangxing Li, **Linquan Bai**, Guangyi Liu, Qiang Sun, and Xue Wang, "Study on Low-carbon Comprehensive Benefits of Grid-connected Photovoltaic Generation," *IEEE PES General Meeting 2015,* 5 pages, Denver, Colorado, July 26-30, 2015.

[C3] **Linquan Bai**, Fangxing Li, Qinran Hu, Hantao Cui, Xin Fang, "Application of Battery-Supercapacitor Energy Storage System for Smoothing Wind Power Output: An Optimal Coordinated Control Strategy," IEEE PES General Meeting 2016, Boston, MA, 2016.

[C4] **Linquan Bai**, Tao Jiang, Fangxing Li, et al, "Partitioning Voltage Stability Critical Injection Regions via Electrical Network Response and Dynamic Relative Gain," IEEE PES General Meeting 2016, Boston, MA, 2016.

[C5] Tao Jiang, **Linquan Bai**, Hongjie Jia, et al, "Volt-VAR Interaction Evaluation in Bulk Power Systems," IEEE PES General Meeting 2016, Boston, MA, 2016.

VITA

Linquan Bai joined The University of Tennessee at Knoxville in August 2013 to pursue the Ph.D. degree in Electrical Engineering. He received his B.S. degree and M.S. degree both from Tianjin University, Tianjin, China, in 2010 and 2013, respectively. His research interests include co-optimization of integrated energy systems, electricity markets, microgrid optimal operation, and renewable energy integration.